

ALMA MATER STUDIORUM - UNIVERSITÀ DI BOLOGNA

DIPARTIMENTO DI FISICA

Dottorato di Ricerca in Fisica - XX ciclo

Settore scientifico disciplinare di afferenza: FIS/02

**Perturbative and non perturbative
effects
in the Standard Model and
orbifolded ADS/CFT based theories**

Presentata da:
**Dott. PASQUALE LUCA
IAFELICE**

Supervisore:
Prof. GIOVANNI VENTURI

Co-supervisore:
Dr. GIAN PAOLO VACCA

Coordinatore:
Prof. FABIO ORTOLANI

17 Marzo 2008

Abstract

We study some perturbative and nonperturbative effects in the framework of the Standard Model of particle physics. In particular we consider the time dependence of the Higgs vacuum expectation value given by the dynamics of the Standard Model and study the non-adiabatic production of both bosons and fermions, which is intrinsically non-perturbative. In the Hartree approximation, we analyze the general expressions that describe the dissipative dynamics due to the back-reaction of the produced particles. Then, we solve numerically some relevant cases for the Standard Model phenomenology in the regime of relatively small oscillations of the Higgs vacuum expectation value ($v\bar{v}$). As perturbative effects, we consider the leading logarithmic resummation in small Bjorken x QCD, concentrating ourselves on the N_c dependence of the Green functions associated to reggeized gluons. Here the eigenvalues of the BKP kernel for states of more than three reggeized gluons are unknown in general, contrary to the large N_c limit (planar limit) case where the problem becomes integrable. In this contest we consider a 4-gluon kernel for a finite number of colors and define some simple toy models for the configuration space dynamics, which are directly solvable with group theoretical methods. In particular we study the dependence of the spectrum of these models with respect to the number of colors and make comparisons with the planar limit case. In the final part we move on the study of theories beyond the Standard Model, considering models built on $AdS_5 \otimes S^5/\Gamma$ orbifold compactifications of the type IIB superstring, where Γ is the abelian group Z_n . We present an appealing three family $\mathcal{N} = 0$ SUSY model with $n = 7$ for the order of the orbifolding group. This result in a modified Pati–Salam Model which reduced to the Standard Model after symmetry breaking and has interesting phenomenological consequences for LHC.

Contents

Preface	ix
I Standard Model time dependent Higgs v_{ev}	1
1 Introduction	3
2 Higgs v_{ev} time dependence	5
3 Massive fields in a time dependent background	9
3.1 Fermions in a time dependent Higgs v_{ev}	10
3.1.1 Fermion solutions and physical quantities	13
3.1.2 Band structure	17
3.2 Bosons in a time dependent Higgs v_{ev}	19
3.2.1 Boson occupation number and energy density	23
4 Particle production	24
4.1 Fermion production	24
4.2 Boson production	31
5 Back-reaction	35
5.1 Fermion back-reaction	38
5.2 Boson back-reaction	39
5.3 Fermion and boson back-reaction	41
6 Conclusions	43

II	Small x QCD and multigluon states: A Color toy model	47
7	Introduction	49
8	BKP Kernel	51
9	Color structure	55
10	Toy models	58
10.1	BKP toy model	59
10.2	TOY _{Adj,Fund}	63
10.3	TOY _{AllFund}	65
11	Conclusions	68
	Appendix	69
III	Quiver Gauge Theories from orbifolded AdS/CFT	73
12	Introduction	75
13	A modified Pati-Salam Model	81
13.1	Description of the model	81
13.2	Phenomenology	86
14	Conclusions	91
	Appendices	92
A	Orbifolding	93
A.1	One dimensional Orbifold	93
A.2	Two dimensional Orbifold	95
A.3	Z_3 Orbifold	96
B	Chiral Z_n models	100
B.1	$\mathcal{N} = 1$ models	100
B.2	$\mathcal{N} = 0$ models	101

Bibliography

Preface

The anticipated data in a new energy regime expected from the Large Hadron Collider (LHC), commissioned at the CERN laboratory, makes this an exciting and fertile time for particle phenomenology. Yet, the only tested model is the Standard Model (SM) of elementary particles and their interactions [1, 2]. It combines the $SU(3)$ color gauge theory of the strong interactions (Quantum Chromodynamics - QCD) with the $SU(2) \otimes U(1)$ model of weak and electromagnetic interactions. This model is believed to be free of mathematical inconsistencies. An important point is that the basic interactions are all described by gauge theories, which implies that the form of the couplings of the vector bosons that mediate these interactions are determined by the underlying gauge symmetry.

Despite these attractive features, many insights suggest that the SM is not the ultimate theory of elementary particles. From a purely theoretical point of view [3], one problem relies on the excessive complication and arbitrariness of this model. The strong, weak and electromagnetic interactions are largely independent of each other, as it is illustrated by the fact that the gauge group $G_{SM} = SU(3) \otimes SU(2) \otimes U(1)$ is a direct product of three factors with different gauge coupling constants. Another problem is that the pattern of fermion representations is arbitrary and complicated: there is no fundamental explanation for the repetition of fermion families or for the violation of parity in the weak interactions but not in the strong ones. Another difficulty is that the electric charges are not quantized, that is there are no a priori reasons for the quark and lepton charges to be related by simple factors 3, apart from requiring the quantum consistency, i.e. the cancellation of chiral gauge anomalies. Moreover, even given the groups, the representations and the electric charge assignments, the SM has many free parameters (19 or 26, depending on whether the neutrinos are assumed to be massless), so some observable quantities are completely arbitrary. Yet, the SM does not incorporate gravity, nor it offers an explanation for the empirical ab-

sence of a large cosmological term.

Finally, there is the so called *hierarchy problem*, which is a special case of *naturalness* [4], i.e. a theory should not contain any unexplained very large (or, on the contrary, very small) dimensionless numbers.¹ The adjustment needed to achieve such naturalness violating numbers is called *fine tuning*. This problem can be especially acute in gauge field theories because even after fine tuning at tree level, i.e., the classical lagrangian, the fine tuning may need to be repeated order by order in the loop expansion during the renormalization process and while such a theory can be internally consistent it violates naturalness. When the Standard Model was rendered renormalizable by appending the Higgs mechanism it was soon realized that it fell into trouble with naturalness, specifically through the hierarchy problem. In particular, the scalar propagator has quadratically divergent radiative corrections which imply that a bare Higgs mass M_H^2 will be corrected by an amount Λ^2/M_H^2 where, Λ is the cut-off scale corresponding to new physics. Unlike logarithmic divergences, which can be absorbed in the usual renormalization process, the quadratic divergences create an unacceptable fine tuning: for example, if the cut off is at the conventional Grand Unification scale $\Lambda \sim 10^{16}$ GeV and $M_H \sim 100$ GeV, the degree of fine tuning is one part in 10^{28} .

An obvious consequence is that theory has ventured into speculative areas such as string theory [7], extra dimensions and supersymmetry [8]. Although there is no *direct* evidence from the experiments, these ideas are of great interest and theoretically consistent. Moreover they have solved some of the previously mentioned problems. String Theories was found to describe also gravity and other gauge interactions in a unified way, but with no phenomenological improvement respect to the SM that could be experimentally verified. The Minimally Supersymmetric Standard Model (MSSM), with $\mathcal{N} = 1$ supersymmetry, elegantly solved the hierarchy problem, since quadratic divergences are cancelled between bosons and fermions [9], with only logarithmic divergences surviving, even if it has yet a lot of free parameters. The Yang-Mills theory with extended $\mathcal{N} = 4$ supersymmetry [10], though phenomenologically quite unrealistic as it allows no chiral fermions and all matter fields are in adjoint representations, was found finite to all orders of perturbation theory and conformally invariant. Then Maldacena [11] showed a duality between $\mathcal{N} = 4$ gauge theory and the superstring in ten spacetime dimensions, named ADS/CFT connection. This conjecture is actually one of the main explored area in theoretical physics. Moreover

¹A similar idea was already stressed by Dirac [5, 6].

$\mathcal{N} = 4$ SYM (Super Yang-Mills) theory, an $SU(N)$ gauge theory, is believed to be integrable in the limit $N \rightarrow \infty$ (planar limit). More phenomenologically interesting is that the $\mathcal{N} = 4$ supersymmetry can be broken by orbifolding down to $\mathcal{N} = 0$ theories with no supersymmetry at all [12, 13]. It was conjectured [14] that such nonsupersymmetric orbifolded models can be finite and conformally invariant. This last important result opened the route to the construction of the *conformality* based models [15].

However, all of these new directions must take into account that the Standard Model has been experimentally confirmed and reconfirmed. Starting from this observation, the thesis analyze some of the opening questions related to the Standard Model and to the theories beyond it. The thesis is divided into three self consistent parts, for each we provide an introduction and some final comments.

The first part of the thesis is inspired by the problem of naturalness. In fact, this last, among other things, led to a possible time variation of the fundamental constants of physics. This is also a result from string and extra dimension theories for the phenomenological (low - Standard Model - energy range) constants. So it is natural to ask how this hypothesis is compatible with the mathematical structure of the Standard Model. In a more modern language, we can talk about a particular source for the time variation of the fundamental constants, referring to a time variation in the vacuum expectation value (vev) of the Higgs field, as it is coupled to each massive field of the Model. We study the particular time dependence that comes from the Standard Model Euler-Lagrangian equation for the Higgs sector. The periodicity in time of the founded solution is the starting point for non adiabatic quantum production of particle by parametric resonance, a purely non perturbative effect. The Bogoliubov formalism has been used to analyze the production of particles in this time dependent background. Some results obtained are analytic, especially those for the production of bosons. The back reaction effects have been taken into account numerically solving the system of all the equations of motion coupled (fermion, bosons and Higgs vev) in the Hartree approximation. The resultant phenomenology is studied in detail [16].

The second part of this thesis is a tentative to find a way to grasp some aspects of the problem of *finite number of color* corrections. Another common feature of some unification theories [3] is that they are based on simple or semi-simple $SU(N)$ groups, like, for example, the Georgi-Glashow [17] or the Pati-Salam [18, 19] model. This is true also for string theories, as, for example, the ADS/CFT correspondence connects the type IIB string theory to the $\mathcal{N} = 4$ SYM

theory. It is usual to refer to N as the *number of color* because in QCD the gauge color group has $N = 3$. A lot of simplification in treating these theories and some important results have been obtained taking $N \rightarrow \infty$. In the Regge limit (small Bjorken x) of the QCD [20] this planar limit showed, for the first time, that gauge theories can contain some integrable structures and these can be treated as “non compact” spin chains [21]. Similar structures have been found also in the Bjorken limit and, recently, in $\mathcal{N} = 4$ SYM (see [22] and references therein), even if the connection between this supersymmetric version of QCD ($\mathcal{N} = 4$ SYM) and string theories is believed to be valid also in the non planar limit (in the planar limit there are no string loops and the problem becomes more tractable). In particular, the Regge limit of QCD is characterized by the factorization of the scattering amplitudes in impact factors and Green functions, that depend on the rapidity. Here the resultant degrees of freedom are called reggeized gluons. The physical particles interact through the exchange of color singlet composite objects, Pomeron and Odderons, and the resultant effective vertex seems to define a field theory of these degrees of freedom. The evolution kernels of three or more reggeized gluons as functions of the rapidity, called BKP kernels [23], are known only in the leading log approximation and their eigenvalues can be completely calculated in the planar limit, because this problem is indeed integrable. For finite N the calculation of the spectra of these kernels is yet a very difficult task. In the thesis a great simplification to treat this problem has been considered. Starting from a four-gluon kernel, some simple toy models have been defined [24, 25] and based on the group $SU(2) \otimes SU(N)$, where the compact $SU(2)$ is used to overcome the problems that come from the noncompactness of the conformal group $SL(2, \mathbb{C})$. In some cases these toy models can be treated even in a completely analytic way, using group theoretical and tensorial methods to analyze the spectrum and to calculate the eigenvalues as a function of N .

The planar limit is not only a way to simplify the theories and to perform perturbative calculations, but gives us also the advantage of connecting (supersymmetric) gauge theories to string theories, being this last yet the only candidate for a theory that unifies the four fundamental interactions (strong, weak, electromagnetic and gravity), even if, from a computational point of view, the planar limit only partially simplifies the use of the AdS/CFT correspondence. In particular orbifolded $AdS_5 \times S^5$ is fertile ground for building models which can potentially test string theory. When models are based upon conformal field theory obtained from the large N expansion of the AdS/CFT correspondence, stringy effects can

show up also at scale of few TeV. The guideline of these theories relies on the conformality approach [15]. To build these models, there is a myriad of apparent routes from string theory to regions of parameter space that resemble the Standard Model of particle physics, and it is easy to get lost in the landscape of these possibilities. Perhaps the most sensible alternative to exploring all possible routes is to seek out and explore routes of “minimal length”. While it may be difficult to describe precisely what is meant by minimal length, what is practically usual to do is reaching the SM particle content as quickly as possible. The last part of this thesis present a String Theory inspired model that unified the fundamental interactions [26]. This is a minimal (respect to the order n of the orbifolding group Z_n) nonsupersymmetric model that has SM particles as a subset of its particle content and contain the Pati-Salam group as a subgroup before reaching the SM. The running of the coupling constants predicted by the model is studied and the unification scale is founded. The phenomenology of the model is presented discussing the possibility of a proton decay and candidates for dark matter.

Pasquale Luca Iafelice
Nashville, February 6, 2008

Part I

Standard Model time dependent Higgs VEV

Chapter 1

Introduction

In the Standard Model, several fundamental constants such as the Fermi coupling and the mass of gauge bosons and fermions depend on the vacuum expectation value (v_{ev}) of the Higgs field, because of the well-known mechanism of spontaneous symmetry breaking. The equation of motion of the Higgs field on the other hand allows for (periodic) time-dependent solutions for the Higgs v_{ev} , which can then be viewed as a particular case of varying fundamental constants (for a review, see Ref. [27]). This behaviour differs from the more common cases of adiabatic variations of the fundamental constants and, due to its periodic nature, can lead to efficient (non-adiabatic) particle production.

The issue of the constancy of the constants of physics was (probably) first addressed by P. A. M. Dirac [5, 6] with his “Large Numbers hypothesis”: very large (or small) dimensionless universal constants cannot be pure mathematical numbers and must not occur in the basic laws of physics. He then proposed that they be considered as (typically slowly) variable parameters characterising the state of the Universe and pointed out the possibility of measuring astrophysical quantities to settle this question [28, 29, 30]. More recently, theories such as string theory and models with extra spatial dimensions have also predicted the time-dependence of the phenomenological constants of the low energy regime describing our Universe [7, 31].

The cases we shall consider instead correspond to oscillations of the Higgs v_{ev} with periods (set by the Higgs mass scale) of the order of 10^{-26} s. Such a behaviour can be obtained from the usual dynamics of the spatially homogeneous Higgs field [32]. We therefore begin by considering the classical equation of motion for the time-dependent Higgs v_{ev} (i.e. a classical condensate) in a homoge-

neous patch of space-time and identifying the relevant regimes. Quantum fluctuations of fermion and boson fields of the Standard Model are then analysed on this Higgs background and explicit expressions for the particle production [33], an intrinsically non-perturbative effect, are presented. In particular, we investigate which bosons and fermions are produced more abundantly depending on the Higgs mass which we consider in a physically sound range of values [34]. Further, the back-reaction of particle production [35] is analysed in the Hartree approximation which is well suited to describe such a dissipative effect. Similar methods have been previously employed to study particle production in strong fields [36] and pre- as well as re-heating in Cosmology [37, 38, 39, 40].

According to our findings, particle production induced by the oscillating Higgs can be very efficient. From the phenomenological point of view, if the Higgs were oscillating now, the amplitudes of such oscillations should therefore be extremely small. On the other hand, this mechanism could explain how Higgs kinetic and potential energy have dissipated in the past [38]. Note that we typically consider regimes such that only small oscillations around an absolute minimum are present and the symmetry breaking phase transition is not significantly affected. However, since we solve the complete system of coupled non-linear equations that describe particle production and their back-reaction, one does not expect that the produced particles are thermal [41]. They also turn out to have mostly small momenta and are therefore non-relativistic.

In Chapter 2, we review the solutions of the classical equation of motion for the Higgs $v\bar{v}$ to properly identify the periodicity properties. Fermion modes on such a Higgs background are then studied in Chapter 3, Section 3.1, with a particular emphasis on the introduction of physical quantities and the regions which lead to quantum particle production. The same kind of analysis is then given for the bosons in Section 3.2. Fermion and boson production within the Standard Model are then studied in details in Chapter 4 taking into account the dependence on the Higgs mass. At this stage we neglect the back-reaction. This latter effect, which has to be included to describe consistently the dynamics is then considered in Chapter 5. In this section we analyze phenomena like the dissipation of the Higgs energy and particle production, consistent with total energy conservation. Final comments are given in Chapter 6.

Chapter 2

Higgs $v\bar{e}v$ time dependence

The Higgs sector of the Standard Model Lagrangian we are interested in is given by [42]:

$$\mathcal{L}_H = \partial^\mu H^\dagger \partial_\mu H - \mu^2 H^\dagger H - \frac{1}{2} \lambda (H^\dagger H)^2, \quad (2.1)$$

where H is the complex iso-doublet

$$H = \frac{1}{\sqrt{2}} \exp\left(i \frac{\xi^a \tau^a}{v}\right) [v + h(x)] \begin{pmatrix} 0 \\ 1 \end{pmatrix}, \quad (2.2)$$

τ^a (with $a = 1, 2, 3$) are the $SU(2)_L$ generators, ξ^a and h (with $\langle 0|\xi^a|0\rangle = 0 = \langle 0|h|0\rangle$) are scalar fields which parameterise the fluctuations of H around the vacuum state. We have neglected the couplings with gauge and fermion fields.

We find it useful to introduce two new quantities, M_H and β , defined as

$$M_H = 2 \frac{M}{g} \sqrt{\lambda}, \quad \mu^2 = \beta - \frac{1}{2} M_H^2, \quad (2.3)$$

where g is the $SU(2)_L$ coupling constant and M_H is the “bare” Higgs boson mass (corresponding to constant Higgs $v\bar{e}v$). In the same way, M is the “bare” weak vector boson mass. The parameter β is such that $\langle 0|h|0\rangle = 0$ to all orders in perturbation theory. Since we are going to neglect the loop corrections, we set $\beta = 0$ hereafter. Note also that the potential in the Lagrangian (2.1) yields a partial spontaneous symmetry breaking (SSB). In fact, ground-state configurations are only invariant under $U(1)_{em} \subset SU(2)_L \otimes U(1)_Y$.

The starting point of our work is the assumption that the Higgs field is a *time-dependent* “classical” homogeneous condensate, $v = v(t)$. Working in the unitary

gauge ($\xi^a = 0$), the Lagrangian (2.1) becomes

$$\mathcal{L}_H = \frac{1}{2}\dot{v}^2 + \frac{M_H^2}{4}v^2 - \frac{\lambda}{8}v^4 + \mathcal{L}_{v,h}, \quad (2.4)$$

where a dot denotes the derivative with respect to t and $\mathcal{L}_{v,h}$ is a polynomial in h and its derivatives. We then introduce a dimensionless real scalar field Φ such that

$$v = 2 \frac{M}{g} \Phi, \quad (2.5)$$

and

$$H = \frac{1}{\sqrt{2}} \left[\frac{2M}{g} \Phi(t) + h(x) \right] \begin{pmatrix} 0 \\ 1 \end{pmatrix}. \quad (2.6)$$

in order to study the fluctuations around the constant value $\Phi^2 = 1$, which is at the basis of the SSB mechanism. On neglecting all terms involving h (which will be analysed in Section 5), the Euler-Lagrange equation for Φ becomes

$$\ddot{\Phi} - \frac{M_H^2}{2} \Phi + \frac{M_H^2}{2} \Phi^3 = 0, \quad (2.7)$$

which can be put in dimensionless form by rescaling the time as $\tau \equiv M_H t/2$ (primes will denote derivatives with respect to τ),

$$\Phi'' - 2\Phi(1 - \Phi^2) = 0. \quad (2.8)$$

After a simple integration we obtain

$$\Phi'^2 - 2\Phi^2 + \Phi^4 \equiv \Phi'^2 + V(\Phi) = c, \quad (2.9)$$

where the integration constant $c \in \mathbb{R}$ is a function of the initial conditions. From a physical point of view, c is proportional to the total vacuum energy¹ and $V(\Phi)$ is the potential in which this vacuum is “moving” (see fig. 2.1).

The equation (2.9) can be formally solved by separating variables, which yields

$$\tau - \tau_0 = \pm \int_{\Phi_0}^{\Phi} \frac{d\Phi}{\sqrt{-\Phi^4 + 2\Phi^2 + c}} \equiv \int_{\Phi_0}^{\Phi} f(\Phi) d\Phi. \quad (2.10)$$

¹It is easy to see that the integral over space of the Hamiltonian density obtained from (2.4) gives the total Higgs vacuum energy $E_{\Phi} = M_H c/\lambda$. We shall thus refer to c as the “Higgs vacuum total energy” for brevity.

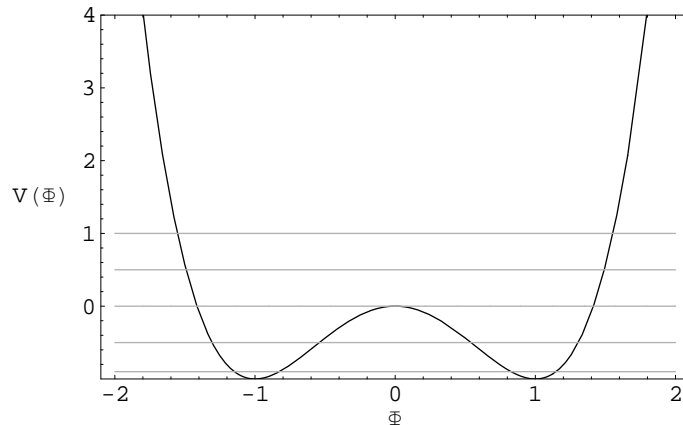


Figure 2.1: The Higgs *vev* potential $V(\Phi) = \Phi^4 - 2\Phi^2$. Straight horizontal lines correspond to $c = -0.9, -0.5, 0.5, 0, 1$, with c proportional to the Higgs vacuum total energy.

Since we are interested in real solutions of Eq. (2.9), we must restrict to the case

$$(-\Phi^4 + 2\Phi^2 + c) > 0, \quad (2.11)$$

which corresponds to positive kinetic energy for Φ (see eq. (2.9)). For any c , the stationary points of $f(\Phi)$ are given by $\Phi = 0, \pm 1$, for which the potential $V(\Phi)$ has a maximum and two minima respectively. Moreover, note that for $c = 0$ and $c = -1$ the integral in Eq. (2.10) is not defined at these points. We shall therefore consider the following cases:

1. $c \leq -1$. Since $c = -1$ corresponds to the absolute minimum in the vacuum total energy, this case is not physically relevant;
2. $-1 < c < 0$. The system exhibits closed trajectories in phase space and a periodic evolution;
3. $c = 0$. The motion is along the separatrix and the system leaves the equilibrium point $\Phi = 0$ with an exponentially growing velocity;
4. $c > 0$. The system again exhibits closed trajectories in phase space but with periods longer than those in case 2.

It can further be shown that the solutions for all four cases can be connected by

analytic continuation². Therefore, in what follows, we shall use the simplest form of such solutions [44] (which corresponds to $c > 0$) for the sake of simplicity, namely

$$\Phi(\tau) = L_m \operatorname{cn}(R_m \tau, m), \quad (2.12)$$

where $L_m \equiv \sqrt{\frac{2m}{2m-1}}$ and $R_m \equiv \sqrt{\frac{2}{2m-1}}$. The parameter m is given by

$$m = \frac{1 + \sqrt{1+c}}{2\sqrt{1+c}}, \quad (2.13)$$

and is a function of the initial conditions because so is the vacuum energy c . The function $\operatorname{cn}(z, m)$ is called Jacobi Elliptic function and has the following properties [45]:

$$\text{periods:} \quad 4\mathbf{K}, \quad 2\mathbf{K} + 2i\mathbf{K}' \quad (2.14)$$

$$\text{zeros:} \quad (2l+1)\mathbf{K} + 2ni\mathbf{K}' \quad (2.15)$$

$$\text{poles:} \quad \beta_{l,n} = 2l\mathbf{K} + (2n+1)i\mathbf{K}', \quad (2.16)$$

where l, n are integers and $\mathbf{K}(m)$ is a special case of the complete elliptic integral of the first kind $F(\theta, m)$,

$$\mathbf{K}(m) = F\left(\frac{\pi}{2}, m\right) \quad \mathbf{K}'(m) = F\left(\frac{\pi}{2}, m'\right), \quad (2.17)$$

with $m' = 1-m$. From (2.14) we deduce that the period along the real (imaginary) axis of the function in Eq. (2.12) is given by

$$T = \begin{cases} 2\sqrt{2}\sqrt{2m-1}F\left(\frac{\pi}{2}, m\right), & \text{for } m < 1 \quad (m > 1) \\ \sqrt{2}\sqrt{2m-1} [F\left(\frac{\pi}{2}, m\right) + iF\left(\frac{\pi}{2}, 1-m\right)], & \text{for } m > 1 \quad (m < 1). \end{cases} \quad (2.18)$$

It is also important to note that the solution (2.12) describes the evolution in time of the Higgs vacuum Φ for every initial conditions (Φ_0, Φ'_0) only after a suitable time *shift* (so that $\Phi'(\tau=0) = 0$).

²These solutions are well known in the literature for the ϕ^4 theory in $(1+1)$ and $(3+1)$ -dimensions [43].

Chapter 3

Massive fields in a time dependent background

In this chapter we describe the theoretical developments needed to study the coupling of fermionic and bosonic fields to a time dependent background (the Higgs vev). Introducing some auxiliary field, for both fermion and boson is possible to recast the equation of motion into an oscillator-type equation, with time dependent coefficients that take into account the time dependence of the Higgs vev. The Bogoliubov formalism used to diagonalize the hamiltonian make transparent the physics of this quantum field theory in a time dependent background and allow to express each phenomenological quantities (occupation numbers, energy density, etc.) as a function of the quantum equations of motion solutions. In this way, is possible to calculate each physical quantity after integrate the equations of motion. In the case of fermion, this integration is very difficult, due to an imaginary term in the frequency, so we must content ourselves with a numerical approach. On the other hand, for the boson, there are a lot of analytical results from the Floquet theory, especially for the limit of small background oscillations that we consider here, and the problem is more tractable.

3.1 Fermions in a time dependent Higgs vev

In the Standard Model the coupling of a generic fermion field ψ to the Higgs scalar field H and gauge fields is described by the Lagrangian density terms [42]

$$\begin{aligned} \mathcal{L}_f = & i\bar{\psi}_L\gamma^\mu \left(\partial_\mu - ig\frac{\vec{\sigma}}{2} \cdot \vec{A}_\mu(x) - ig'\frac{Y_W}{2}B_\mu \right) \psi_L \\ & + i\bar{\psi}_R\gamma^\mu \left(\partial_\mu - ig'\frac{Y_W}{2}B_\mu \right) \psi_R - G (\bar{\psi}_L H \psi_R + \bar{\psi}_R H^\dagger \psi_L), \end{aligned} \quad (3.1)$$

where ψ_L is a *left handed* isospin doublet, ψ_R a *right handed* isospin singlet and G the coupling constant between the Higgs boson and the fermions. Neglecting the gauge fields, in the unitary gauge (2.6), the previous Lagrangian becomes

$$\mathcal{L}_f = i\bar{\psi}\gamma^\mu\partial_\mu\psi - \frac{G}{\sqrt{2}}\frac{2M}{g}\Phi(t)\bar{\psi}\psi - \frac{G}{\sqrt{2}}h(x)\bar{\psi}\psi, \quad (3.2)$$

with $\psi = \psi_L + \psi_R$. Introducing the “mass parameter”¹

$$m_f(t) \equiv \frac{G}{\sqrt{2}}\frac{2M}{g}\Phi(t) = \frac{G}{\sqrt{2}}\frac{M_H}{\sqrt{\lambda}}\Phi(t) \equiv m_f\Phi(t), \quad (3.3)$$

with $\Phi(t)$ given by Eq. (2.12), the equation of motion for ψ is given by

$$\left[i\gamma^\mu\partial_\mu - m_f(t) - \frac{G}{\sqrt{2}}h(x) \right] \psi(x) = 0. \quad (3.4)$$

For our purposes, the last term above can be neglected with respect to the second term proportional to the Higgs condensate and one finally obtains

$$[i\gamma^\mu\partial_\mu - m_f(t)] \psi(\vec{x}, t) = 0 \quad (3.5)$$

which is a Dirac equation with a *time dependent mass*. In a similar manner, one finds that the equation of motion for $\bar{\psi} = \psi^\dagger\gamma^0$ is the Hermitian conjugate of (3.5).

The spinor field is normalized in such a way that $\int d^3x \psi^\dagger(\vec{x}, t)\psi(\vec{x}, t) = 1$ and, in the Heisenberg picture, it becomes a field operator with the usual anticommu-

¹Since there are no stationary states in a time-dependent external field $\Phi(t)$, the mass is strictly speaking ill-defined. We shall however refer to the function $m_f(t)$ as a time dependent mass.

tation rules $\{\psi(\vec{x}, t), \psi^\dagger(\vec{x}', t)\} = \delta(\vec{x} - \vec{x}')$. We can then expand ψ as

$$\psi(x) = \int \frac{d^3k}{(2\pi)^{3/2}} \sum_{s=\pm} e^{i\vec{k}\cdot\vec{x}} \left[U_s(\vec{k}, t) a_s(\vec{k}) + V_s(-\vec{k}, t) b_s^\dagger(-\vec{k}) \right], \quad (3.6)$$

where $s = \pm$ is the helicity,

$$\{a_s(\vec{k}), a_{s'}^\dagger(\vec{k}')\} = \{b_s(\vec{k}), b_{s'}^\dagger(\vec{k}')\} = \delta_{ss'} \delta(\vec{k} - \vec{k}') \quad (3.7)$$

and

$$U_s^\dagger(\vec{k}, t) U_{s'}(\vec{k}, t) = V_s^\dagger(\vec{k}, t) V_{s'}(\vec{k}, t) = \delta_{ss'} \quad (3.8)$$

$$U_s^\dagger(\vec{k}, t) V_{s'}(\vec{k}, t) = V_s^\dagger(\vec{k}, t) U_{s'}(\vec{k}, t) = 0,$$

The vacuum state $|0\rangle$ is as usual defined by the relations

$$a_s(\vec{k})|0\rangle = b_s(\vec{k})|0\rangle = 0. \quad (3.9)$$

With no time dependence in the theory (i.e., for $m_f(t) = m_f$ constant), $U_s(\vec{k})$ and $V_s(\vec{k})$ would be eigenstates of the operator $\vec{\gamma} \cdot \vec{k}$ with eigenvalues m_f and $-m_f$ respectively. The spinors in momentum space $U_s(\vec{k}, t)$ and $V_s(\vec{k}, t)$ satisfy the charge coniugation relation

$$\mathcal{C} \bar{U}_s^T(\vec{k}, t) = V_s(-\vec{k}, t), \quad (3.10)$$

with $\mathcal{C} = i\gamma_0\gamma_2^2$.

It is now convenient to introduce two new scalars defined by

$$\begin{aligned} U_s(\vec{k}, t) &= \left[i\gamma^0 \partial_0 + \vec{\gamma} \cdot \vec{k} + m_f(t) \right] X_k^{(+)}(t) u_s \\ V_s(\vec{k}, t) &= \left[i\gamma^0 \partial_0 - \vec{\gamma} \cdot \vec{k} + m_f(t) \right] X_k^{(-)}(t) v_s, \end{aligned} \quad (3.11)$$

²We are using the gamma matrices

$$\gamma^0 = \left(\begin{array}{c|c} \mathbb{I} & 0 \\ \hline 0 & -\mathbb{I} \end{array} \right), \quad \gamma^j = \left(\begin{array}{c|c} 0 & -\sigma^j \\ \hline \sigma^j & 0 \end{array} \right),$$

where $\sigma^j, j = 1, 2, 3$ are Pauli matrices and \mathbb{I} is the 2×2 identity matrix.

where

$$u_s = \begin{pmatrix} \chi_s \\ 0 \end{pmatrix} \quad v_s = \begin{pmatrix} 0 \\ \eta_s \end{pmatrix}, \quad (3.12)$$

with $\chi_s^\dagger \chi_s = 1$ and $\eta_s = -i\sigma_2 \chi_{-s}$, are eigenvectors of γ^0 with eigenvalues +1 and -1, respectively. Note that $\mathcal{C}\bar{u}_s^T = v_{-s}$ and Eq. (3.10) is thus identically satisfied. With these notations, Eq. (3.5) yields

$$\ddot{X}_k^{(\pm)}(t) + [\Omega_k^2(t) \mp im_f(t)] X_k^{(\pm)}(t) = 0, \quad (3.13)$$

which is of the harmonic oscillator type with the complex and (doubly-)periodic frequency

$$\Omega_k^2(t) \mp im_f(t) \equiv k^2 + m_f^2(t) \mp im_f(t). \quad (3.14)$$

Let us now assume that the Higgs vev remains constant and equal to $\Phi(0)$ for $t \leq 0$. Consequently, the mass $m_f(t)$ will also be constant at negative times and one just has plane waves for $t \leq 0$. The evolution for $t > 0$ is then obtained by imposing the following initial conditions at $t = 0$ ³

$$\begin{cases} X_k^{(\pm)}(0) = \{2\Omega_k(0) [\Omega_k(0) + m_f(0)]\}^{-1/2} \\ \dot{X}_k^{(\pm)}(0) = \mp i \Omega_k(0) X_k^{(\pm)}(0). \end{cases} \quad (3.15)$$

These together with Eq. (3.13) give

$$X_k^{(-)}(t) = \left(X_k^{(+)}(t) \right)^*, \quad (3.16)$$

so that positive and negative energy modes are not independent and we shall then consider mostly the equation for $X_k^{(+)}$ for simplicity.

It can be showed that if $f_1(t)$ and $f_2(t)$ are two arbitrary solutions of Eq. (3.13) with the sign (+) (or, equivalently, with (-)), the quantity

$$I[f_1, f_2] \equiv \Omega_k^2(t) f_1^* f_2 + \dot{f}_1^* \dot{f}_2 + im_f(t) \left(f_1^* \dot{f}_2 - \dot{f}_1^* f_2 \right) \quad (3.17)$$

is a constant of motion and one can then prove the stability of any arbitrary solutions [46]. Finally, note that if $f_1(t) = f_2(t) = X_k^{(+)}(t)$ the relation (3.17) takes the

³We have set the momentum $\vec{k} = (0, 0, k)$.

form

$$\left| \dot{X}_k^{(+)} \right|^2 + \Omega_k^2 \left| X_k^{(+)} \right|^2 + im_f(t) \left(X_k^{(+)*} \dot{X}_k^{(+)} - \dot{X}_k^{(+)*} X_k^{(+)} \right) = 1, \quad (3.18)$$

which is also a consequence of the fact that $U_s(\vec{k}, t)$ and $V_s(\vec{k}, t)$ are evolved by the Hermitian operators $i\gamma^0\partial_0 \mp \vec{\gamma} \cdot \vec{k} - m_f(t)$.

3.1.1 Fermion solutions and physical quantities

The Hamiltonian operator for a fermion field can in general be written as

$$\mathcal{H}(t) = i \int d^3x \psi^\dagger(\vec{x}, t) \dot{\psi}(\vec{x}, t). \quad (3.19)$$

Inserting the expansion (3.6) and using Eq. (3.8), this becomes

$$\begin{aligned} \mathcal{H}(t) = & \int d^3k \sum_s \left\{ \left[iU_s^\dagger(\vec{k}, t) \dot{U}_s(\vec{k}, t) \right] a_s^\dagger(\vec{k}) a_s(\vec{k}) + \left[iV_s^\dagger(-\vec{k}, t) \dot{V}_s(-\vec{k}, t) \right] b_s(-\vec{k}) b_s^\dagger(-\vec{k}) \right. \\ & \left. + \left[iV_s^\dagger(-\vec{k}, t) \dot{U}_s(\vec{k}, t) \right] b_s(-\vec{k}) a_s(\vec{k}) + \left[iU_s^\dagger(\vec{k}, t) \dot{V}_s(-\vec{k}, t) \right] a_s^\dagger(\vec{k}) b_s^\dagger(-\vec{k}) \right\}, \quad (3.20) \end{aligned}$$

where we have integrated on \vec{x} and one of the momenta. Taking into account Eq. (3.11), we end up with

$$\begin{aligned} \mathcal{H}(t) = & \int d^3k \sum_{s=\pm} \Omega_k(t) \left\{ E(k, t) \left[a_s^\dagger(\vec{k}) a_s(\vec{k}) - b_s(-\vec{k}) b_s^\dagger(-\vec{k}) \right] \right. \\ & \left. + F(k, t) b_s(-\vec{k}) a_s(\vec{k}) + F^*(k, t) a_s^\dagger(\vec{k}) b_s^\dagger(-\vec{k}) \right\}, \quad (3.21) \end{aligned}$$

where

$$E(k, t) = \frac{2k^2}{\Omega_k(t)} \text{Im} \left[X_k^{(+)}(t) \dot{X}_k^{(+)*}(t) \right] + \frac{m_f(t)}{\Omega_k(t)}, \quad (3.22)$$

$$F(k, t) \equiv \frac{k}{\Omega_k(t)} \left[(\dot{X}_k^{(+)}(t))^2 + \Omega_k^2(t) (X_k^{(+)}(t))^2 \right]$$

and⁴

$$E^2(k, t) + |F(k, t)|^2 = 1. \quad (3.23)$$

From Eq. (3.22), using (3.15), it is possible to see that $E(k, 0) = 1$ and $F(k, 0) = 0$, therefore $\mathcal{H}(t=0)$ is diagonal. In fact, we have assumed that for $t \leq 0$ the vacuum is constant and there is no explicit time dependence in the theory.

⁴This is a consequence of (3.18).

The Hamiltonian (3.21) can be diagonalized *at every time* using a canonical Bogoliubov transformation [47]. As a matter of fact, the necessary conditions for this kind of diagonalization are ensured by the relations [36]

$$\begin{aligned} iV_s^\dagger(-\vec{k}, t)\dot{V}_s(-\vec{k}, t) &= iU_s^\dagger(\vec{k}, t)\dot{U}_s(\vec{k}, t) = \Omega_k(t)E(k, t) \\ \left[iU_s^\dagger(\vec{k}, t)\dot{V}_s(-\vec{k}, t) \right]^* &= iV_s^\dagger(-\vec{k}, t)\dot{U}_s(\vec{k}, t) = \Omega_k(t)F(k, t). \end{aligned} \quad (3.24)$$

We now introduce *time-dependent* creation and annihilation operators,

$$\begin{pmatrix} \tilde{a}_s(\vec{k}, t) \\ \tilde{b}_s^\dagger(\vec{k}, t) \end{pmatrix} = \begin{bmatrix} \alpha(k, t) & \beta(k, t) \\ -\beta^*(k, t) & \alpha^*(k, t) \end{bmatrix} \begin{pmatrix} a_s(\vec{k}) \\ b_s^\dagger(-\vec{k}) \end{pmatrix} \equiv \mathcal{A}(k, t) \begin{pmatrix} a_s(\vec{k}) \\ b_s^\dagger(-\vec{k}) \end{pmatrix}, \quad (3.25)$$

and the condition that this be a non singular canonical transformation requires that \mathcal{A} is a special unitary matrix,

$$|\alpha(k, t)|^2 + |\beta(k, t)|^2 = 1. \quad (3.26)$$

We have thus shown that $SU(2)$ is the dynamical symmetry group for fermion creation in a homogeneous non stationary scalar field and the time-dependent vacuum $|0\rangle_t$ (see below) is a generalized coherent state built on this group [48].

The hamiltonian also takes the diagonal form

$$\mathcal{H}(t) = \int d^3k \sum_{s=\pm} \Omega_k(t) \left[\tilde{a}_s^\dagger(\vec{k}, t)\tilde{a}_s(\vec{k}, t) - \tilde{b}_s(-\vec{k}, t)\tilde{b}_s^\dagger(-\vec{k}, t) \right], \quad (3.27)$$

if the coefficients of the canonical transformation are such that

$$\begin{aligned} |\beta(k, t)|^2 &= \frac{1 - E(k, t)}{2} \\ \frac{\alpha(k, t)}{\beta(k, t)} &= \frac{F(k, t)}{1 - E(k, t)} = \frac{1 + E(k, t)}{F^*(k, t)}, \end{aligned} \quad (3.28)$$

which are indeed compatible with the condition (3.26) thanks to (3.23).

It is now possible to use the operators \tilde{a} e \tilde{b} to define time dependent Fock spaces, each of them built from the zero (quasi)particle state at the time t defined imposing $\tilde{a}_s(\vec{k}, t)|0_t\rangle = 0$ and $\tilde{b}_s(\vec{k}, t)|0_t\rangle = 0$, which, at $t = 0$, are equal to

$a_s(\vec{k})|0\rangle = 0 = b_s(\vec{k})|0\rangle$. These relations mean that a quantized fermion field interacting with a classical external field $\Phi(t)$ can be represented at every time as a free field, with a corresponding redefinition of the particle concept and vacuum state. Moreover, one can show that diagonalizing the Hamiltonian (3.21) is equivalent to finding exact solutions of the Heisenberg equations of motion and all the matrix elements (expectation values of physical observables) of interest can be written in terms of the coefficients of the Bogoliubov transformation (3.25) [36].

For example, the vacuum expectation value of the (quasi-)particle number operator is given by

$$N_k(t) \equiv \langle 0 | \tilde{a}_s^\dagger(\vec{k}, t) \tilde{a}_s(\vec{k}, t) | 0 \rangle = |\beta(k, t)|^2 \langle 0 | b_s(\vec{k}) b_s^\dagger(\vec{k}) | 0 \rangle = |\beta(k, t)|^2 \delta(\vec{0}), \quad (3.29)$$

where we have used Eqs. (3.25) and (3.9). From the previous relation we see that the number of created (quasi)particle pairs is spin-independent because the homogeneous field Φ is isotropic [49]. If we put the system in a finite volume V , we must replace $\delta(\vec{0})$ in (3.29) with $\delta_{\vec{k}\vec{k}} = 1$. The (quasi)particle density at the time t is thus given by ⁵

$$n(t) = \langle 0 | \frac{1}{V} \sum_{s=\pm} \int \frac{d^3k}{(2\pi)^3} N_k(t) | 0 \rangle = \frac{2}{(2\pi)^3} \int d^3k \langle 0 | N_k(t) | 0 \rangle = \frac{1}{\pi^2} \int dk k^2 |\beta(k, t)|^2 \quad (3.30)$$

which is different from zero whenever the Hamiltonian is not diagonal in terms of the operators a and b . The occupation number of fermions created with a given momentum \vec{k} will be $n_k(t) = |\beta(k, t)|^2$, and the condition (3.26) ensures that the Pauli principle is respected at every time [36, 51].

In order to implement numerical methods, it is useful to cast some of the previous expressions in dimensionless form. We thus introduce the following quantities:

$$\tau \equiv \frac{M_H}{2} t, \quad \kappa \equiv \frac{2k}{M_H}, \quad q \equiv 2 \frac{G^2}{\lambda} = 4 \frac{m_f^2}{M_H^2}, \quad (3.31)$$

where $m_f \equiv m_f(\tau \rightarrow -\infty) = m_f(0)$. On further multiplying by $4/M_H^2$, Eq. (3.13) takes the dimensionless form

$$X_k^{(\pm)''}(\tau) + [\kappa^2 + q \Phi^2(\tau, m) \mp i\sqrt{q} \Phi'(\tau, m)] X_k^{(\pm)}(\tau) = 0. \quad (3.32)$$

⁵Of course, the same result holds for antifermions.

Moreover, if we define the dimensionless frequency

$$\omega_\kappa \equiv \frac{2\Omega_k}{M_H} = \sqrt{\kappa^2 + q\Phi^2}, \quad (3.33)$$

the initial conditions (3.15) become

$$\begin{cases} X_\kappa^{(\pm)}(0) = \{2\omega_\kappa(0)[\omega_\kappa(0) + \sqrt{q}\Phi(0, m)]\}^{-1/2} \\ X_\kappa^{(\pm)'}(0) = \mp i\omega_\kappa(0)X_\kappa^{(\pm)}(0). \end{cases} \quad (3.34)$$

Note that, despite this is not explicitly indicated, the frequency and the initial conditions are also functions of the amplitude m of the elliptic function, that is of the vacuum energy c (see Eq. (2.13)). On using (3.28), (3.22) and (3.31) we finally obtain

$$n_\kappa(\tau) = \frac{1}{2} - \frac{\kappa^2}{\omega_\kappa(\tau)} \text{Im}[X_\kappa(X'_\kappa)^*] - \frac{\sqrt{q}\Phi(\tau, m)}{2\omega_\kappa(\tau)}, \quad (3.35)$$

which gives the occupation number for every mode κ as a function of the solutions $X_\kappa \equiv X_\kappa^{(+)}$ ⁶ of Eq. (3.32). Analogously, the (dimensionless) energy density will be

$$\tilde{\rho}_\psi(\tau) = \frac{1}{2\pi^2} \int d\kappa \kappa^2 \omega_\kappa(\tau) n_\kappa(\tau). \quad (3.36)$$

Note that $n_\kappa(0) = \tilde{\rho}_\psi(0) = 0$ thanks to the initial conditions (3.34).

A very useful result follows from the periodicity of the vacuum⁷, $\Phi(\tau) = \Phi(\tau + T)$, which remarkably simplifies the evaluation of the occupation number and shows, although in an approximate way, its explicit time dependence [46]. If we define

$$\omega_\kappa \equiv \omega_\kappa(\tau \rightarrow -\infty) = \omega_\kappa(0), \quad (3.37)$$

an approximate expression for $n_\kappa(\tau)$ is given by⁸

$$\hat{n}_\kappa(\tau) = \frac{\kappa^2}{\omega_\kappa^2} \frac{\{\text{Im}[X_\kappa^{(1)}(T)]\}^2}{\sin^2(d_\kappa)} \sin^2\left(d_\kappa \frac{\tau}{T}\right) \equiv F_\kappa \sin^2(\nu_\kappa \tau), \quad (3.38)$$

where $X_\kappa^{(1)}(\tau)$ satisfies Eq. (3.32) with initial conditions $X_\kappa^{(1)}(0) = 1$, $X_\kappa^{(1)'}(0) = 0$

⁶This definition is not restrictive since we only need either $X_\kappa^{(+)}$ or $X_\kappa^{(-)}$ to calculate $n_\kappa(\tau)$.

⁷We clearly refer to the period of Φ along the real axis (see Eq. (2.18)).

⁸We shall see in Section 4.1 that Eq. (3.38) is actually exact at $\tau = nT$ for any positive integer n .

and d_κ is such that $\cos(d_\kappa) = \text{Re}[X_\kappa^{(1)}(T)]$. According to Eq. (3.38) the number density of fermions produced depends periodically on τ for all κ . So, on average, this density does not depend on the time during which the external field is turned on. The physical meaning of this result was pointed out by V. S. Popov through a quantum mechanics analogy [46]. Finally observe that in our case the time scale is fixed by the factor $2/M_H$ and if $M_H \sim 10^2$ GeV then $2/M_H \sim 1.3 \cdot 10^{-26}$ s.

3.1.2 Band structure

A non adiabatic quantum effect arises from the explicit time dependence of the frequency in Eq. (3.32), and this leads to the production of particles. When the time dependence is periodic, one usually speaks of *parametric resonance*. It is then clear that the quantity q has the role of a *resonance parameter* due to the fact that the time-dependent terms in Eq. (3.32) are proportional to q .

We are interested in values of q and κ which give solutions of the mode equation associated to particle production, identified by a mean occupation number (see Eq. (3.38))

$$\bar{n}_\kappa \equiv \langle n_\kappa \rangle_\tau = \frac{F_\kappa}{2} \quad (3.39)$$

different from zero. The result is shown in Fig. 3.1 in which every peak corresponds to $\bar{n}_\kappa = 1/2$: note the band structure in the plane (q, κ^2) . The left plot in the upper part of Fig. 3.1 shows the first and second bands while the right plot displays bands from the second to the fourth. Moving along a band, \bar{n}_κ oscillates between 0 and $1/2$. Moreover, the bands get narrower with increasing κ^2 for a given value of q and after several bands they shrink to a negligible width, as we show in Fig. 3.2 with a plot of the mean occupation number as a function of κ^2 for the *bottom* quark.

To obtain the curves in the lower graphs of Fig. 3.1 we have studied the mean occupation number along straight lines $\kappa^2 = \vartheta q$, with ϑ constant. First of all, for $\vartheta \approx 0$ ¹⁰ the peaks are located on the q axis at $q_n(\vartheta \approx 0) = n^2$, with n a positive integer. We then made the ansatz $q_n(\vartheta) = n^2 \Gamma(\vartheta)$, with $\Gamma(0) = 1$, for the position of the peaks q_n along the generic line $\kappa^2 = \vartheta q$. A numerical interpolation starting

⁹We recall that $1 \text{ GeV}^{-1} \sim 6.582 \cdot 10^{-25} \text{ s}$ for $\hbar = c = 1$.

¹⁰Note that if $\vartheta = 0$, $\kappa^2 = 0$ and $\bar{n}_\kappa = 0$ with no production.

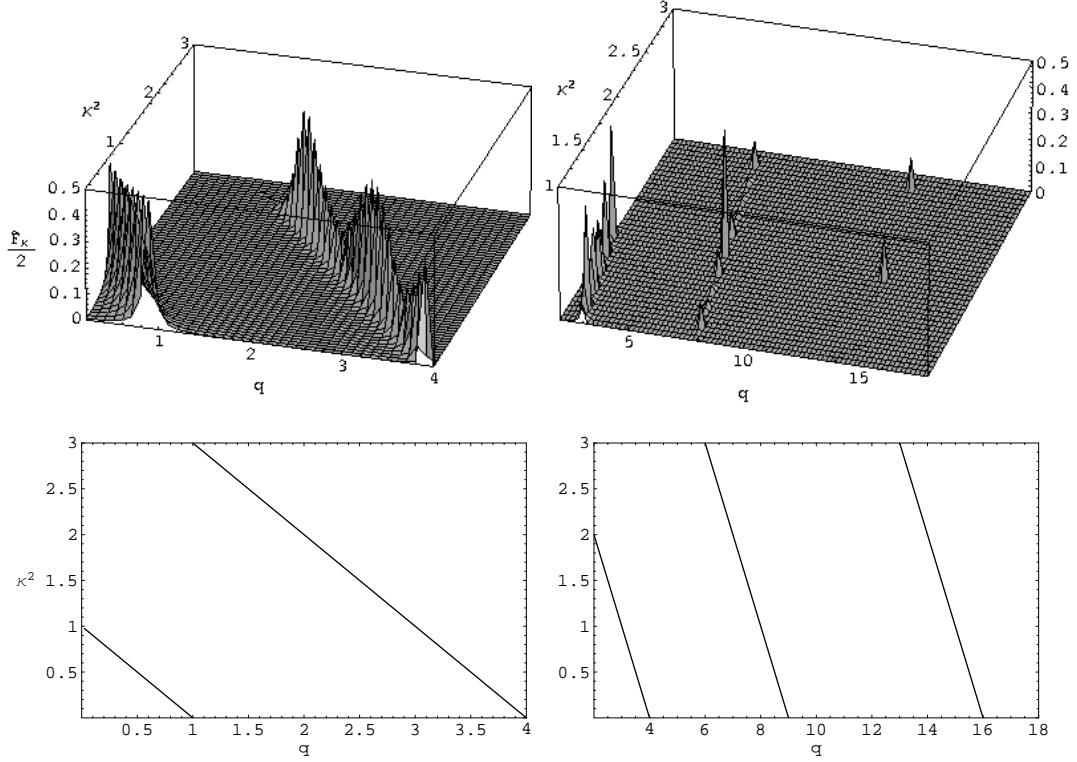


Figure 3.1: Production chart for fermions coupled to the Higgs. Upper graphs show the occupation number as a function of the parameters q and κ^2 . Lower plots show in details the lines in the plane (q, κ^2) along which the mean occupation number takes its maximum values. Note that for $\kappa \simeq 0$ we have $q_n \simeq n^2$.

from the analysis of the first five peaks for different values of ϑ has then yielded

$$\Gamma(\vartheta) = \frac{1}{1 + \vartheta}, \quad (3.40)$$

for which the parametric equation of the lines in Fig. 3.1 are given by

$$\begin{cases} q_n(\vartheta) = \Gamma(\vartheta) n^2 \\ \kappa_n^2(\vartheta) = \vartheta \Gamma(\vartheta) n^2. \end{cases} \quad (3.41)$$

On replacing ϑ from the first into the second equation, we finally find that the production rate must take its maximum values at points in the plane (q, κ^2) that

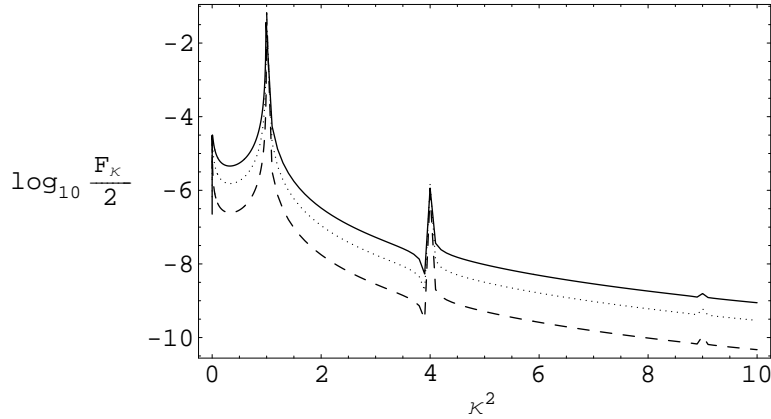


Figure 3.2: Mean occupation number $F_\kappa/2$ as a function of κ^2 for the *bottom* and $M_H = 115$ GeV (solid line), 200 GeV (dotted line), 500 GeV (dashed line). Note that the peaks get narrower with increasing κ^2 . Similar plots are obtained by varying the resonance parameter q at κ^2 fixed as for decreasing q the bandwidth shrinks.

satisfy the relation

$$\kappa_n^2 + q \simeq n^2, \quad (3.42)$$

with n a positive integer. Note that the above relation represents a very good approximation in the regime of small oscillations around the static Standard Model Higgs.

The band structure we just described will lead to a preferred production of non-relativistic particles, that is particles with small momentum compared to their mass. For example, for fermions with a mass smaller than $M_H/2$, the production is mostly driven by the first band ($n = 1$) and Eq. (3.42) yields a typical momentum $k^2 \sim M_H^2/4 - m_f^2$ which is smaller than m_f^2 for the particles we consider in the following. On the other hand, the production of more massive particles will be caused by higher order bands (so that $n^2 - q > 0$) and is normally suppressed.

3.2 Bosons in a time dependent Higgs vev

The Lagrangian which describes the coupling between the Higgs field and the vector bosons is the same as in Eq.(2.1), but with gauge covariant derivatives and

kinetic terms for the gauge fields,

$$\mathcal{L}_{H-B} = D^\mu H^\dagger D_\mu H - \mu^2 H^\dagger H - \frac{\lambda}{2} (H^\dagger H)^2 - \frac{1}{4} F_{\mu\nu}^i F_i^{\mu\nu} - \frac{1}{4} G_{\mu\nu} G^{\mu\nu}, \quad (3.1)$$

where $D_\mu = \partial_\mu - ig\frac{\vec{\sigma}}{2} \cdot \vec{A}_\mu - ig'B_\mu$, $F_{\mu\nu}^i = \partial_\mu A_\nu^i - \partial_\nu A_\mu^i + g\epsilon^{ijk} A_\mu^j A_\nu^k$ and $G_{\mu\nu} = \partial_\mu B_\nu - \partial_\nu B_\mu$. For the electroweak vector bosons we thus have

$$\begin{aligned} \mathcal{L}_{W^\pm, Z_0} = & -\partial_\nu W_\mu^+ \partial^\nu W^{-\mu} - \frac{1}{2} (\partial_\nu Z_\mu)^2 + \frac{g^2}{4M^2} h^2 \left(M^2 W^{+\mu} W_\mu^- + \frac{M_Z^2}{2} Z^\mu Z_\mu \right) + \\ & + \Phi^2 \left(M^2 W^{+\mu} W_\mu^- + \frac{M_Z^2}{2} Z^\mu Z_\mu \right) + \frac{g}{M} \Phi h \left(M^2 W^{+\mu} W_\mu^- + \frac{M_Z^2}{2} Z^\mu Z_\mu \right). \end{aligned} \quad (3.2)$$

Taking the vev with the condition $\langle 0|h|0\rangle = 0$ and neglecting the *back-reaction* of h , the classical equation of motion for Z^μ is given by

$$\partial_\nu \partial^\nu Z^\mu + M_Z^2 \Phi^2(t) Z^\mu = 0. \quad (3.3)$$

The fields W_μ^\pm satisfy the same equation with M_Z replaced by M . We therefore conclude that any component \mathcal{Z} of the vector field Z^μ and any component \mathcal{W} of $W^{\mp\mu}$ satisfy Klein-Gordon equations with mass $M_Z^2(t) \equiv M_Z^2 \Phi^2(t)$ and $M^2(t) \equiv M^2 \Phi^2(t)$ which, after performing a spatial Fourier transform, take the form

$$\ddot{\mathcal{Z}}_k + [k^2 + M_Z^2(t)] \mathcal{Z}_k = 0, \quad (3.4)$$

$$\ddot{\mathcal{W}}_k + [k^2 + M^2(t)] \mathcal{W}_k = 0, \quad (3.5)$$

where $\mathcal{Z}(t) = (2\pi)^{-3/2} \int d^3k e^{i\vec{k}\cdot\vec{x}} \mathcal{Z}_k(t)$ and $\mathcal{W}(t) = (2\pi)^{-3/2} \int d^3k e^{i\vec{k}\cdot\vec{x}} \mathcal{W}_k(t)$. Analogously, from the Lagrangian (2.1) in the unitary gauge (2.6) and keeping only terms up to second order, one obtains the following equation for the Fourier modes of the quantum Higgs field

$$\ddot{h}_k + [k^2 + M_h^2(t)] h_k = 0, \quad (3.6)$$

where

$$M_h^2(t) = M_H^2 \left[\frac{3}{2} \Phi^2(t) - \frac{1}{2} \right]. \quad (3.7)$$

We are interested in the case when the Higgs vev $\Phi(t)$ oscillates near one of its two absolute minima (see Fig. 2.1). We therefore take the limit $m \rightarrow +\infty$ ($c \rightarrow -1$)

in Eq. (2.12) and obtain

$$\Phi(\tau) \simeq 1 - \frac{1}{2m} \sin^2 \tau + O\left(\frac{1}{m^2}\right). \quad (3.8)$$

Moreover, from now on, we shall for simplicity denote with Y_κ any bosonic mode, that is Y_κ can be either \mathcal{L}_κ , \mathcal{W}_κ or h_κ . Eqs. (3.4), (3.5) and (3.6) then become

$$Y_\kappa''(\tau) + \varpi_\kappa^2(\tau) Y_\kappa(\tau) = 0, \quad (3.9)$$

with

$$\varpi_\kappa^2(\tau) = \kappa^2 + q \left(1 - \frac{\sigma_Y}{m} \sin^2 \tau\right), \quad (3.10)$$

where we have neglected terms beyond the first order in $1/m$ and introduced the dimensionless constants

$$\kappa \equiv \frac{2k}{M_H} \quad \text{and} \quad q \equiv 4 \frac{M_Y^2}{M_H^2}, \quad (3.11)$$

with $M_Y = M_Z, M$ or M_H and $\sigma_Y = 1$ for the gauge fields and $3/2$ for the Higgs. Note that Eq. (3.32) for the fermion modes takes the same form as Eq. (3.9) when the imaginary part of the fermion frequency can be neglected and that the period of $\varpi_\kappa(\tau)$ is π .

If we define

$$a \equiv \frac{1}{4} \left[\kappa^2 + q \left(1 - \frac{\sigma_Y}{2m}\right) \right], \quad \epsilon \equiv \frac{q \sigma_Y}{16 m}, \quad (3.12)$$

and change the time to $\eta \equiv 2\tau = M_H t$, we obtain

$$Y_\kappa''(\eta) + (a + 2\epsilon \cos \eta) Y_\kappa(\eta) = 0. \quad (3.13)$$

When the total vacuum energy c is near the minimum value $c = -1$ (for which Φ is constant), $W^{\pm\mu}$, Z^μ and h therefore satisfy a *Mathieu equation*.

The Mathieu equation is a linear differential equation with time periodic coefficients and is described in the general framework of Floquet theory [52]. An important result from this theory is the existence of stable solutions only for particular values of a and ϵ (see Fig. 3.3). For our purposes, the relevant solutions which lead to an efficient particle production in the quantum theory are however

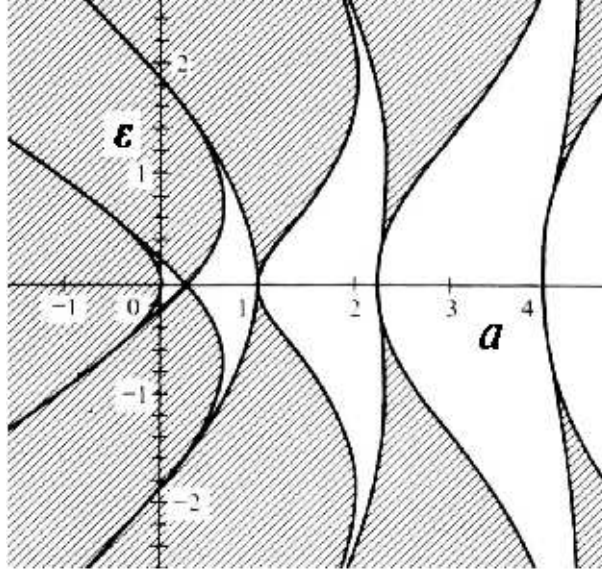


Figure 3.3: Stability regions for the Mathieu equation. Stable solutions have a and ϵ in the unshaded regions. When $\epsilon = 0$, instability bands cross the a -axis at $a_n = n^2/4$, with $n = 0, 1, 2, \dots$

those which show an exponential instability of the form $(\mu_\kappa^{(n)})$ is known as Floquet index or growth factor)

$$Y_\kappa \sim \exp(\mu_\kappa^{(n)}\eta/2) \quad (3.14)$$

and appear within the set of resonance bands of width $\Delta\kappa^{(n)}$ labelled by the integer index n . Using Eq. (3.12) one can then map the stability chart of Fig. 3.3 into the plane (q, κ^2) and finds that the instabilities also correspond to an exponential growth of the occupation number of quantum fluctuations, $n_\kappa \propto \exp(\mu_\kappa^{(n)}\eta)$ (see Eq. (3.18) below), which can be interpreted as strong particle production. Stable solutions also lead to particle production, although with no exponential growth in time, and thus resemble the fermion case [46].

If $c \approx -1$ then $m \gg 1$ and $\epsilon \approx 0$ in Fig 3.3. One then finds $4a \approx n^2$, or

$$\kappa_n^2 + q \left(1 - \frac{\sigma_Y}{2m}\right) = n^2, \quad n = 1, 2, 3, \dots, \quad (3.15)$$

which, for a given q , gives the value of κ^2 around which the n -th resonance peak is centred. Further, the physical constraint $\kappa^2 \geq 0$ implies $q \leq 2n^2m/(2m-1)$, so if $q \lesssim 1$ ($M_H \gtrsim 2M_Y$) all the resonance bands contribute to production, otherwise

at least the first band ($n = 1$) is not available. In particular, the first band is never available for the Higgs particle and its production can therefore be negligible with respect to that of gauge bosons if the Higgs mass is sufficiently large.

3.2.1 Boson occupation number and energy density

The same analytical steps of Section 3.1 allows one to relate relevant physical quantities to the solutions of the equation of motion also in the case of bosons. We again take initial conditions corresponding to positive frequency plane waves for $\tau \leq 0$,

$$\begin{cases} Y_\kappa(0) = [2\varpi_\kappa(0)]^{-1/2} \\ Y'_\kappa(0) = -i\varpi_\kappa(0)Y_\kappa(0). \end{cases} \quad (3.16)$$

The occupation numbers for bosons will then be given by [36]

$$n_\kappa(\tau) = \frac{1}{2\varpi_\kappa} |Y'_\kappa|^2 + \frac{\varpi_\kappa}{2} |Y_\kappa|^2 - \frac{1}{2}, \quad (3.17)$$

where $\varpi_\kappa = \varpi_\kappa(0)$ and note that $n_\kappa(0) = 0$ thanks to eqs. (3.16).

Like for fermions, it is possible to find an analytic approximation for the boson occupation number [36],

$$\hat{n}_\kappa = \sinh^2(\mu_\kappa \tau), \quad (3.18)$$

with the *Floquet index*, or growth factor, μ_κ given by

$$\cosh(\mu_\kappa T) = \text{Re} [Y_\kappa^{(1)}(T)] , \quad (3.19)$$

in which $Y_\kappa^{(1)}$ is the solution of Eq. (3.9) with initial conditions $Y_\kappa^{(1)}(0) = 1, Y_\kappa^{(1)'}(0) = 0$ and $T = \pi$ is the period of $\varpi_\kappa(\tau)$ (the period of the Higgs vacuum). Using this approximate expression, the boson energy density can be written as

$$\tilde{\rho}_B(\tau) = \frac{1}{2\pi^2} \int d\kappa \kappa^2 \varpi_\kappa(\tau) \sinh^2(\mu_\kappa \tau), \quad (3.20)$$

where the tilde on ρ is to remind that this is a dimensionless quantity (like the fermion analogue in Eq. (3.36)).

Chapter 4

Particle production

The time dependence of the vacuum expectation value of the Higgs field, also in the regime of small oscillations considered here, is an efficient source of particles production. This non adiabatic quantum effect will be considered here thinking the Higgs vev as an “infinite sea” of energy, i.e. neglecting every kind of back-reaction due to the produced particles. This approximation will be showed to be valid only in a first stage of the production process and a more complete analysis will be performed in the next chapter.

4.1 Fermion production

We shall now use the numerical solutions to Eq. (3.32) to evaluate the fermion occupation number n_κ in Eq. (3.35) and compare it with its analytical approximation \hat{n}_κ in Eq. (3.38). In order to illustrate the magnitude of the effect, we shall consider three possible values for the Higgs boson mass which result from different experimental lower or upper bounds, namely $M_H = 115$ GeV, 200 GeV and 500 GeV [34]. In this Section, we shall not take into account the back-reaction of the produced fermions which is treated later.

Let us begin with Fig. 4.1, which shows the time evolution of the occupation number n_κ and its enveloping \hat{n}_κ for the *top* quark in the case $M_H = 500$ GeV and two different values of the momentum κ , and Fig. 4.2, which shows the same quantities for the *bottom* quark in the case $M_H = 200$ GeV:

- a) For κ on the (first) resonance band both functions n_κ and \hat{n}_κ for the *top* reach the maximum allowed by the Pauli blocking and are remarkably indistin-

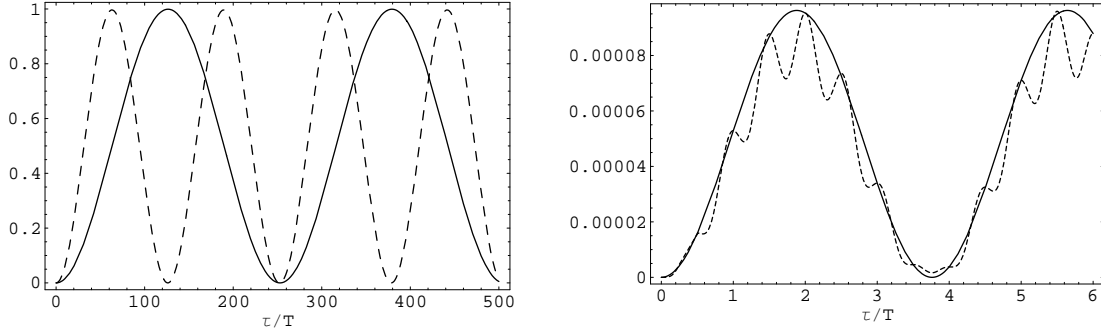


Figure 4.1: Time evolution of the occupation number n_κ and its envelope \hat{n}_κ for the *top* quark and $M_H = 500 \text{ GeV}$. Left graph: $\kappa^2 = 1 - q \simeq 0.51$ on the first resonance band, $c_0 = -1 + 10^{-3}$ (solid line) and $c = -1 + 4 \cdot 10^{-3}$ (dashed line). Note that n_κ and \hat{n}_κ exactly coincide and their period scales as $(c + 1)^{1/2}$. Right graph: $\kappa^2 = q/10 \simeq 4.8 \cdot 10^{-2}$ is outside resonance bands and \hat{n}_κ (solid line) differs from n_κ (dashed line).

guishable (left graph in Fig. 4.1). In fact, their difference remains of the order of 10^{-8} for both values of the initial background energy $c = c(\tau = 0)$ and we do not show it. For the *bottom* (i.e., a smaller value of q at the resonance with respect to the *top*'s) instead, the two functions differ slightly and always remain smaller than one (see Fig. 4.2). In both cases however, from the numerical simulations one can infer a *scaling law* for the period T_κ of the occupation number with respect to the initial vacuum energy c . If c_0 is a reference energy, one has

$$T_\kappa(c) = T_\kappa(c_0) \left(\frac{c_0 + 1}{c + 1} \right)^{n/2}, \quad (4.1)$$

which holds for all values of κ on the n -th resonance band provided c is small enough that only small oscillation of the background Φ are relevant (see case 2 in Section 2). Note also that $T_\kappa \gg T$ for the *top* (we recall that the Higgs vev period is $2T/M_H \sim 10^{-26} \text{ s}$).

- b)** For values of κ not on a resonance band (right graph in Fig. 4.1), the production is of course much damped and the exact occupation number shows relatively high frequency oscillations, with period comparable to the Higgs vev 's, which are modulated by the function \hat{n}_κ with a period usually larger than T . It is therefore clear that the time average over these relatively high

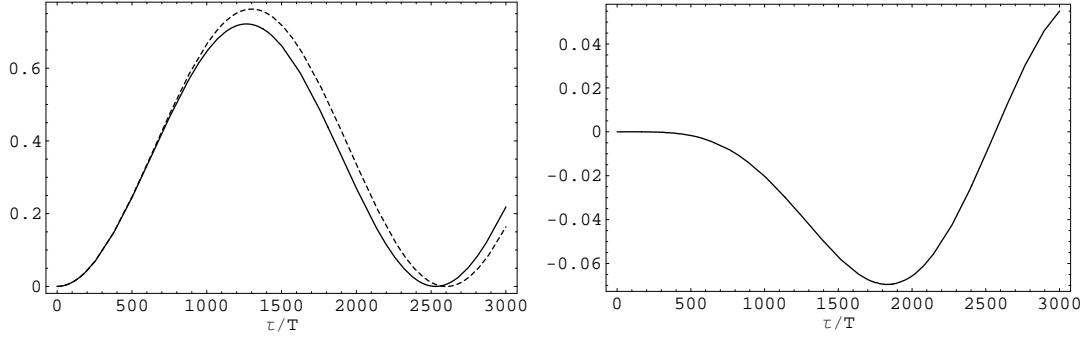


Figure 4.2: Time evolution of the occupation number for the *bottom* quark, $M_H = 200$ GeV, $\kappa^2 = 1 - q \simeq 0.9982$ on the first resonance band and $c_0 = -1 + 10^{-3}$. Left graph: n_κ (dashed line) and its envelope \hat{n}_κ (solid line). Right graph: difference between n_κ and \hat{n}_κ .

frequency oscillations can still be related to the enveloping \hat{n}_κ as

$$\bar{n}_\kappa(\tau) = \langle n_\kappa(\tau) \rangle_\tau \equiv \frac{1}{T} \int_\tau^{\tau+T} d\zeta n_\kappa(\zeta) \simeq \hat{n}_\kappa(\tau), \quad (4.2)$$

where \hat{n}_κ is given in Eq. (3.38).

Note that qualitatively similar results were obtained by Greene and Kofman in Ref. [50], although in a very different context (cosmological models). Some differences are due to the fact that fermion masses of relevance for the latter case are typically much larger than the inflaton's, whereas we consider the fermion masses of the SM (that is, much smaller or of the same order of the Higgs mass). The resonance parameter q is therefore at most of order one in our case but is always much larger in theirs and, consequently, the imaginary part of the frequency is negligible in the cosmological context but could not be neglected in the present treatment.

We emphasize that the fermion occupation number is always periodic in time and the function in Eq. (3.38) *exactly* equals $n_\kappa(pT)$, with p a positive integer, regardless of the fact that κ and q are on a resonance band or not (see Fig. 4.1). This is a general behaviour which still holds for very small values of q , for example $q \sim 10^{-10}$ or $q \sim 10^{-22}$, corresponding to the scales of the electron and neutrino mass ($\lesssim 1$ eV) respectively. These cases are however very difficult to treat numerically because one should integrate for very long times (the period of the function in Eq. (3.38) grows with the inverse of the fermion mass). For this reason we have

chosen to show the occupation number only for quarks like the *top* and *bottom*.

We are now interested in the production probability for a given fermion, *i.e.*, in the occupation number n_κ summed over all κ 's for a given value of q (see Eq. (3.31)). The generally oscillating behaviour of n_κ leads us to estimate this probability in time as the mean number (4.2) summed over all the momenta κ ,

$$\bar{n}_\psi \equiv \langle n_\psi(\tau) \rangle_\tau = \frac{1}{4\pi^3} \int d^3\kappa F_\kappa \langle \sin^2(\nu_\kappa \tau) \rangle_\tau = \frac{1}{4\pi^3} \int d^3\kappa \frac{F_\kappa}{2}. \quad (4.3)$$

As we see from Fig. 3.2, the mean occupation number \bar{n}_κ as a function of κ at fixed q is significantly different from zero only near the values $\kappa^2 = \kappa_n^2$ around which the production peaks are centred. We can therefore estimate \bar{n}_ψ as

$$\bar{n}_\psi \simeq \frac{1}{4\pi^3} \sum_{n=1}^{n_p} \int_{\text{Supp}(P_n)} d^3\kappa \bar{n}_\kappa \simeq \frac{1}{2\pi^2} \sum_{n=1}^{n_p} \sqrt{\kappa_n^2} \Delta\kappa_n^2 \bar{n}_{\kappa_n} \quad (4.4)$$

where $\text{Supp}(P_n)$ is the interval around κ_n^2 in which \bar{n}_κ is significantly large. The effective width of the peak $\Delta\kappa_n^2$ on the n -th band is determined by estimating each integral in the above expression numerically. Further, we found that

$$\Delta\kappa_n^2(c) \simeq \Delta\kappa_n^2(c_0) \left(\frac{c+1}{c_0+1} \right)^{\frac{n}{2}}, \quad (4.5)$$

a scaling behaviour also shared by the bosons (see Section 4.2).

The occupation number in Eq. (4.4) for the *top*, *bottom*, *down* and for the *tau* are shown in Table 4.1 for three different values of the Higgs mass and Higgs total vacuum energy $c_0 = -1 + 10^{-3}$. Note that the production is mostly generated from the first band and, if $q < 1$, the production probability is larger than for $q > 1$ since for the latter case only the bands of order greater than one can contribute. So, recalling that $q = 4m_f^2/M_H^2$, we conclude that in the Standard Model all the fermions except the *top* have a greater production probability for a “light” Higgs. Moreover, within a given band, the production is still strongly affected by the resonance parameter q . On varying q along a given band one observes a change in the value of the momentum κ of the produced particles (see Eq. (3.42)), in the width of the band and, consequently, in the number density of produced particles (see Figs. 3.1 and 3.2). These facts lead to the values of \bar{n}_ψ (as defined in Eq. (4.4) above) presented in Table 4.1. Note finally that the *bottom* is the “dom-

$M_H = 115 \text{ GeV}$			$M_H = 200 \text{ GeV}$		
ψ	\bar{n}_ψ	q	ψ	\bar{n}_ψ	q
t	$\ll 10^{-10}$	9.26	t	$1.6 \cdot 10^{-5}$	3.06
b	$8.7 \cdot 10^{-5}$	$5.46 \cdot 10^{-3}$	b	$5.1 \cdot 10^{-5}$	$1.80 \cdot 10^{-3}$
d	$1.6 \cdot 10^{-7}$	$1.38 \cdot 10^{-8}$	d	$8.2 \cdot 10^{-8}$	$4.54 \cdot 10^{-9}$
τ	$3.9 \cdot 10^{-5}$	$9.54 \cdot 10^{-4}$	τ	$2.4 \cdot 10^{-5}$	$3.16 \cdot 10^{-4}$

$M_H = 500 \text{ GeV}$		
ψ	\bar{n}_ψ	q
t	$4.3 \cdot 10^{-4}$	0.48
b	$2.4 \cdot 10^{-5}$	$2.90 \cdot 10^{-4}$
d	$3.3 \cdot 10^{-8}$	$7.28 \cdot 10^{-10}$
τ	$8.8 \cdot 10^{-6}$	$5.06 \cdot 10^{-5}$

Table 4.1: Production probability of various quarks and of the lepton *tau* for three different values of the Higgs mass and Higgs total vacuum energy $c_0 = -1 + 10^{-3}$.

inant” (with the highest production probability) fermion for $M_H = 115 \text{ GeV}$ and $M_H = 200 \text{ GeV}$, while for $M_H = 500 \text{ GeV}$ the *top* production is more probable.

We remark that the average occupation number \bar{n}_ψ also scales with the energy according to the relation

$$\bar{n}_\psi(c) \simeq n_\psi(c_0) \left(\frac{1+c}{1+c_0} \right)^{\frac{n}{2}} \sim (1+c)^{\frac{n}{2}}, \quad |c+1| \lesssim 10^{-3}, \quad (4.6)$$

where n is the order of the “dominant” peak (the one which contributes most to the production). So if one is interested in the production probabilities at an arbitrary but always very small energy, the values in Table 4.1, calculated for $c_0 = -1 + 10^{-3}$, must be multiplied by the factor $[(1+c)/(1+c_0)]^{\frac{1}{2}}$ if the production is associated with the first band. For example, this is true for the *top* if $M_H > 2 m_{\text{top}}$ and all other fermions for any Higgs mass. Instead, in the region $M_H < 2 m_{\text{top}}$ (of phenomenological interest), the *top* may be produced only starting from the second band and the relevant scale factor is $(1+c)/(1+c_0)$.

Finally, we evaluate the fermion energy density using Eq. (3.36). The integral over κ can be calculated in the same way as in Eq. (4.4) and including just the dominant peak for the production. This approximation is better the lower the Higgs vacuum energy, since the peak amplitude decreases proportionally to this

energy. we thus find

$$\tilde{\rho}_\psi(\tau) = \frac{1}{2\pi^3} \int d^3\kappa \omega_\kappa(\tau) \frac{F_\kappa}{2} \sin^2(\nu_\kappa \tau) \simeq \frac{1}{2\pi^3} \int_{\text{Supp}(P_{dom})} d^3\kappa \omega_\kappa(\tau) \bar{n}_\kappa \sin^2(\nu_\kappa \tau). \quad (4.7)$$

Around the dominant peaks $\bar{\kappa}_n^2$ given by Eq. (3.42) we have

$$\nu_{\bar{\kappa}_n^2} \approx 1, \quad (4.8)$$

and we can therefore write the energy density (4.7) as

$$\tilde{\rho}_\psi(\tau) \simeq \frac{\sin^2(\tau)}{2\pi^3} \int_{\text{Supp}(P_{dom})} d^3\kappa \omega_\kappa(\tau) \bar{n}_\kappa \simeq \frac{\sin^2(\tau)}{\pi^2} \sum_{n=1}^{n_p} \sqrt{\kappa_n^2} \Delta\kappa_n^2 \omega_{\kappa_n}(\tau) \bar{n}_{\kappa_n}, \quad (4.9)$$

which significantly simplifies the evaluation of the integral over κ . One can also find a scaling law for the energy density so obtained, namely

$$\tilde{\rho}_\psi \sim (1+c)^{\frac{n}{2}}, \quad (4.10)$$

with the same prescriptions as for n_ψ .

From Eq (2.4), the vacuum energy in a volume $8/M_H^3$ can be calculated and put in the usual dimensionless form as

$$\tilde{\mathcal{E}}_\Phi \equiv \frac{16}{M_H^4} \mathcal{E}_\Phi = \frac{2}{\lambda} c. \quad (4.11)$$

The Higgs vacuum energy density available for the production is thus given by

$$\Delta\tilde{\mathcal{E}}_\Phi \equiv \tilde{\mathcal{E}}_\Phi - \tilde{\mathcal{E}}_{\Phi=1} = \frac{2}{\lambda} (c+1). \quad (4.12)$$

In the Standard Model λ appears as an arbitrary parameter and there are presently no experimental constraints on it. There are however good reasons to believe that $\lambda < 1$ but we shall consider in all our calculations simply the value $\lambda = 1$. Taking into account the dependence of $\langle \tilde{\rho}_\psi \rangle$ and $\Delta\tilde{\mathcal{E}}_\Phi$ on c , the fraction of total energy absorbed by a given fermion scales as

$$R(c) = \frac{\langle \tilde{\rho}_\psi \rangle}{\Delta\tilde{\mathcal{E}}_\Phi} = R(c_0, \lambda) \left(\frac{1+c_0}{1+c} \right)^{n/2}, \quad R(c_0, \lambda) \equiv \frac{\lambda}{2} (1+c_0)^{-n/2} \langle \tilde{\rho}_\psi(c_0) \rangle \quad (4.13)$$

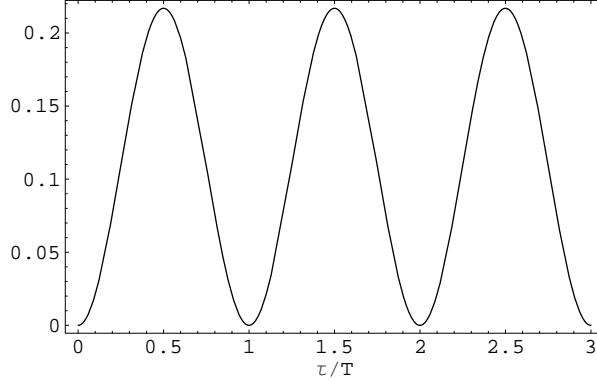


Figure 4.3: Fraction of Higgs vacuum energy R absorbed by the produced top for $M_H = 500 \text{ GeV}$ and $c_0 = -1 + 10^{-3}$.

ψ	R	q	M_H
t	$1.1 \cdot 10^{-1}$	0.48	500 GeV
b	$2.2 \cdot 10^{-2}$	$5.46 \cdot 10^{-3}$	115 GeV
d	$4.0 \cdot 10^{-5}$	$1.38 \cdot 10^{-8}$	115 GeV
τ	$1.0 \cdot 10^{-2}$	$9.54 \cdot 10^{-4}$	115 GeV

Table 4.2: Fraction of Higgs vacuum energy absorbed by various quarks and the tau lepton for the particular Higgs mass (out of the three considered in Table 4.1 with $c_0 = -1 + 10^{-3}$) which gives the highest production rate.

An example of this quantity is plotted in Fig. 4.3. Notably, the maximum value is reached before the end of the first vacuum oscillation.

Using the results shown in the Table 4.1, for each included fermion we have selected the values of the Higgs mass which give the greatest production probability and the corresponding energy densities are shown in Table 4.2 in units of the Higgs vacuum energy density available for the production $\Delta\tilde{\mathcal{E}}_\Phi$. Of course, the physical condition $R < 1$ limits the range of validity of this first approximation where production is not taken to affect the vev oscillation (no back-reaction), breaking energy conservation. For example, the value of R given in Table 4.2 for the top for $c_0 = -1 + 10^{-3}$ can be rescaled down to a minimum energy $c \simeq -1 + 4 \cdot 10^{-5}$, for our choice of λ .

When their energy density becomes comparable with the background energy, the produced fermions are expected to back-react on the Higgs vev , thus affecting its evolution and eventually suppressing the parametric production of particles. We shall see this in detail in Section 5. For now we just note that the different

scaling law for the *top* quark energy density as a function of c (when the Higgs mass is large) implies that back-reaction effects will become important sooner and one should therefore be aware that in this case, for very small Higgs energy oscillations, the *top* energy density produced will be strongly affected by these effects.

4.2 Boson production

In Section 3.2 we reviewed the fact that the equation of motion for a bosonic field admits unstable solutions only for some values of the parameters q and κ . The results of the numeric integration of Eq. (3.9) will be used to evaluate the occupation number for every mode κ_n given in Eq. (3.15). For both Z_0 and W^\pm we have seen that, for a given value of M_H , the first band ($n = 1$) contributes to the production in an extremely dominant way with respect to the others since the Floquet numbers scale with the Higgs vacuum energy according to

$$\mu_\kappa^{(n)}(c) \simeq \left(\frac{1+c}{1+c_0} \right)^{\frac{n}{2}} \mu_\kappa^{(n)}(c_0), \quad (4.1)$$

where we usually take $c_0 = -1 + 10^{-3}$. Therefore, in the following we shall just refer to the first band and then do not describe the Higgs production (see Section 3.2), which could be trivially included. Moreover, motivated by the discussion at the end of Section 3.2, we shall first study the case $M_H \simeq 2 M_{Z^0} = 182 \text{ GeV}$ as the plot in Fig. 4.4 shows that this yields a more efficient production.

Let us note that for the case of production dominated by the second band (*i.e.*, for bosons with mass less than twice the Higgs mass, including the Higgs itself), the relevant Floquet index is much smaller. In particular, a plot similar to that in Fig. 4.4 would display a curve for $\mu_\kappa^{(2)}$, which scales as $(1+c)$ instead of $(1+c)^{1/2}$, with maximum value on the vertical axis of the order of 10^{-2} .

Fig. 4.5 shows the time dependence of the occupation number (3.17) and its enveloping approximation (3.18) for the boson Z^0 with a momentum on the first resonance band, $\kappa^2 = \kappa_1^2 \simeq 0.17$, $M_H = 200 \text{ GeV}$ and $c_0 = -1 + 10^{-3}$. The exact n_κ , whose mean value grows exponentially with time, oscillates and coincides with \hat{n}_κ at the end of each background oscillation.

To evaluate the production probability (*i.e.*, the total occupation number) for a given boson we must integrate the mode occupation number n_κ over a finite

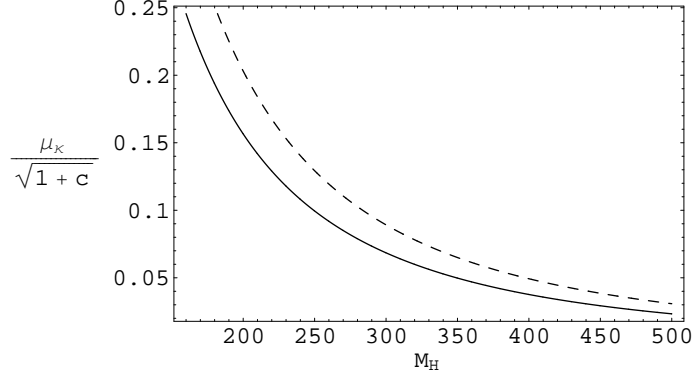


Figure 4.4: Floquet index for the first resonance band $\mu_\kappa^{(1)}$ as a function of the Higgs mass for Z^0 (dashed line) and W^\pm (solid line). In both cases $\mu_\kappa^{(1)}$ is maximum if $M_H \approx 2 M_Y$ and decreases for larger values. A factor $\sqrt{1+c}$ on the vertical axis is used in consideration of Eq. (4.1) with $c_0 = -1 + 10^{-3}$.

volume in momentum space (at fixed q). This very difficult integration is greatly simplified by the fact that the production only arises around the peaks in the (q, κ^2) plane, that is for $\kappa^2 = \kappa_n^2$ given in Eq. (3.15). Moreover, the production from the first instability band is the most relevant, so that the integration can be consistently restricted to an interval around κ_1 (denoted as $Supp(P_1)$, like for fermions),

$$n_B(\tau) = \frac{1}{(2\pi)^3} \int d^3\kappa \hat{n}_\kappa(\tau) \approx \frac{1}{4\pi^2} \int_{Supp(P_1)} d\kappa^2 \sqrt{\kappa^2} \sinh^2(\mu_\kappa\tau) . \quad (4.2)$$

We shall then consider two different time scales. For short times ($\mu_\kappa\tau \ll 1$), the above expression can be approximated as

$$n_B(\tau) \approx \frac{1}{2\pi^2} \int_{Supp(P_1)} d\kappa^2 \sqrt{\kappa^2} (\mu_\kappa\tau)^2 , \quad (4.3)$$

whereas for long times ($\mu_\kappa\tau \gg 1$) we shall use

$$n_B(\tau) \approx \frac{1}{8\pi^2} \int_{Supp(P_1)} d\kappa^2 \sqrt{\kappa^2} e^{2\mu_\kappa\tau} . \quad (4.4)$$

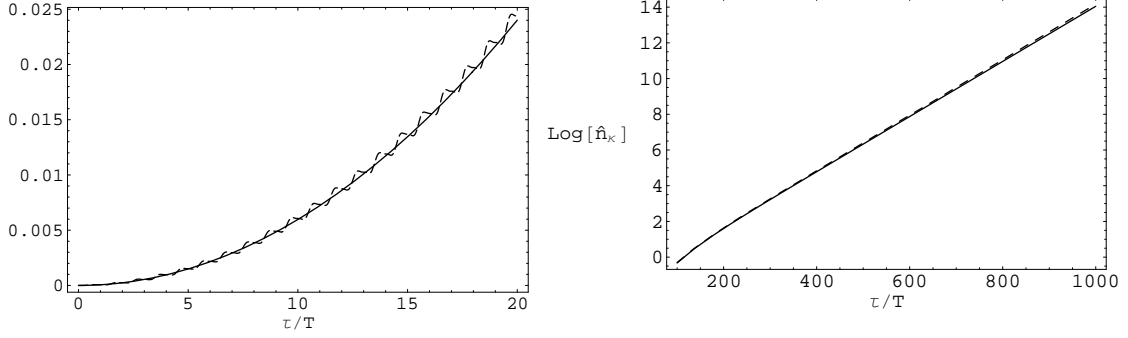


Figure 4.5: Time evolution of the number of produced Z^0 with $\kappa^2 = \kappa_1^2 \simeq 0.17$ for two time ranges, $M_H = 200$ GeV and $c_0 = -1 + 10^{-3}$. Note that \hat{n}_κ (solid line) matches n_κ (dashed line) at the end of each background oscillation.

The Floquet index as a function of κ^2 has a parabolic shape around κ_1 ,

$$\mu_\kappa^{(1)} \approx \mu_{\kappa_1}^{(1)} \left[1 - \left(\frac{\kappa^2 - \kappa_1^2}{\Delta\kappa_1^2/2} \right)^2 \right], \quad (4.5)$$

where $\Delta\kappa_1^2$ denotes the width of the first peak (the same notation we used for the fermions) which scales with the Higgs vacuum total energy exactly according to the same law (4.5) for fermions provided $c \lesssim -1 + 10^{-3}$.

For $\mu_\kappa\tau \ll 1$, the integral in Eq. (4.3) can now be easily estimated and yields

$$n_B(\tau) \approx \frac{(\mu_{\kappa_1}^{(1)})^2}{2\pi^2} N_B \tau^2, \quad (4.6)$$

where $N_B = N_B(\kappa_1, \Delta\kappa_1^2)$ is a rather cumbersome expression which we do not show explicitly since it will not be used in the present paper. For long times, one can likewise estimate the integral in Eq. (4.4) using a *saddle point* approximation and obtain [39]

$$n_B(\tau) \approx \frac{\kappa_1 \Delta\kappa_1^2}{16\pi^2} \sqrt{\frac{\pi}{\mu_{\kappa_1}^{(1)}}} \frac{e^{2\mu_{\kappa_1}^{(1)}\tau}}{\sqrt{2\tau}}. \quad (4.7)$$

The left plot in Fig. 4.6 shows the time dependence of the total number of produced Z^0 following from (4.7) for $M_H = 500$ GeV and $c_0 = -1 + 10^{-3}$. This quantity grows exponentially in time and when the fraction ¹ of Higgs vacuum

¹This fraction is defined in analogy with that for the fermions given in Eq. (4.13).

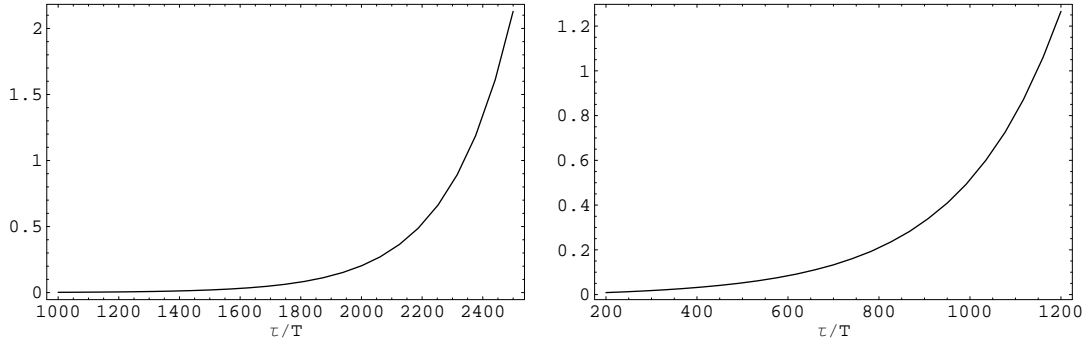


Figure 4.6: Time evolution of the total number of produced Z^0 (left graph) and fraction of the Higgs vacuum energy absorbed by Z^0 (right graph) for $M_H = 500$ GeV and $c_0 = -1 + 10^{-3}$ (in the right plot, fractions larger than unity signal that the back-reaction cannot be neglected).

energy converted into Z^0 approaches unity (see right plot), the back-reaction is expected to become relevant. Indeed, values of that fraction larger than unity do not make sense and actually signal the complete failure of the approximation which neglects the back-reaction. Note that this occurs after about a thousand background oscillations. Recalling the results for the top from Section 4.1, it is clear that, during the first few hundreds of vacuum oscillations the energy transferred to the top is larger than that absorbed by the Z^0 , and it seems that the back-reaction of the latter particles can be neglected at an early stage. The production of Z^0 and their interaction with the time dependent Higgs background take the lead later and, with a good approximation, remain the only processes with significant effects (we shall have more to say on this in the next Chapter).

Chapter 5

Back-reaction

The results presented so far have been obtained by neglecting the back-reaction of the produced fermions and bosons on the evolution of the Higgs vacuum. This is a common approximation, since a more complete treatment of these effects is a very difficult task. We shall therefore begin by considering the simple case of one kind of fermion simply denoted by ψ (which we shall identify with the *top* quark later) and one kind of boson (the Z^0).

The Lagrangian density for our system is given by (see Eqs. (2.4), (3.2) and (3.2) with $v = M_H \Phi / \sqrt{\lambda}$)

$$\mathcal{L}_{BR} = \mathcal{L}_H - \frac{\lambda}{4} \sqrt{q} \bar{\psi} \psi \Phi - \frac{\lambda}{8} q Z^\mu Z_\mu \Phi^2, \quad (5.1)$$

where we have redefined the product $\langle \bar{\psi} \psi \rangle$ to make it dimensionless. The back-reaction effects can be studied to a good degree of accuracy in the Hartree approximation (see Refs. [39, 38] for a discussion on this subject). Let us then consider the vacuum expectation value of the Euler-Lagrange equation for Φ which reads

$$\Phi'' - 2\Phi(1 - \Phi^2) + \frac{\lambda}{4} \sqrt{q} \langle \bar{\psi} \psi \rangle - \frac{\lambda}{4} q \langle Z^\mu Z_\mu \rangle \Phi = 0. \quad (5.2)$$

The product $\langle \bar{\psi} \psi \rangle$ can be rewritten in terms of an integral in momentum space of the Bogoliubov coefficients (previously introduced to diagonalize the Hamiltonian operator for a generic fermion field) using the expansion (3.6). In this way one encounters ultraviolet divergencies and, in order to obtain a finite result, the operator $\bar{\psi} \psi$ must be normal ordered to subtract vacuum quantum fluctuations [38, 39, 54]. Moreover, we shall neglect any other renormalization related,

for example, to perturbative quantum corrections. Note that after a Bogoliubov transformation the vacuum state $|0_\tau\rangle$ is time-dependent and we have a different renormalization at every time. We thus define the (time-dependent) normal ordering of a generic operator as

$$\mathcal{N}_\tau(\mathcal{O}) \equiv \mathcal{O} - \langle 0_\tau | \mathcal{O} | 0_\tau \rangle, \quad (5.3)$$

so that the vev of $\bar{\psi}\psi$ will be given by

$$\begin{aligned} \langle \bar{\psi}\psi \rangle &\equiv \langle 0 | \mathcal{N}_\tau(\bar{\psi}\psi) | 0 \rangle = \langle 0 | \bar{\psi}\psi | 0 \rangle - \langle 0 | (\langle 0_\tau | \bar{\psi}\psi | 0_\tau \rangle) | 0 \rangle \\ &= \langle 0 | \bar{\psi}\psi | 0 \rangle - \langle 0_\tau | \bar{\psi}\psi | 0_\tau \rangle. \end{aligned} \quad (5.4)$$

Using results from Section 3.1, we find

$$\begin{aligned} \langle \bar{\psi}\psi \rangle &= \int \frac{d^3\kappa}{2\pi^3} \kappa^2 \left[|X_\kappa(\tau)|^2 + \frac{\sqrt{q}\Phi(\tau)}{2\omega_\kappa(\tau)} - \frac{1}{2} \right] \\ &= -2n_\psi(\tau) + \int \frac{d^3\kappa}{2\pi^3} \kappa^2 \left[|X_\kappa(\tau)|^2 - \frac{\text{Im}[X_\kappa(\tau)X_\kappa'^*(\tau)]}{2\omega_\kappa(\tau)} \right]. \end{aligned} \quad (5.5)$$

As for the Z^0 , analogous prescriptions to those used for the fermion lead to

$$\langle Z^\mu Z_\mu \rangle = - \int \frac{d^3\kappa}{(2\pi)^3} \left(|Y_\kappa|^2 - \frac{1}{\sqrt{\kappa^2 + q\Phi^2}} \right). \quad (5.6)$$

Note that the two back-reaction terms (5.5) and (5.6) vanish at $\tau = 0$ by virtue of the initial conditions (3.34) and (3.16), as expected. The system of back-reaction equations is thus

$$\begin{cases} \Phi'' - 2\Phi(1 - \Phi^2) + \frac{\lambda}{4}\sqrt{q}\langle \bar{\psi}\psi \rangle - \frac{\lambda}{4}q\langle Z^\mu Z_\mu \rangle\Phi = 0 \\ X_\kappa'' + (\kappa^2 + q\Phi^2 - i\sqrt{q}\Phi')X_\kappa = 0 \\ Y_\kappa'' + (\kappa^2 + q\Phi^2)Y_\kappa = 0. \end{cases} \quad (5.7)$$

The last two terms in the first equation (Higgs-fermion and Higgs-vector coupling terms) depend on λ , that is the strength of the quartic term in the Higgs vev potential. In the Standard Model the coupling λ is not fixed but it is possible

to take $0 < \lambda < 1$ if one considers the Higgs self-interaction as described by a perturbative theory.

For the above system, it is easy to show that the (renormalized) total energy

$$E = M_H \left\{ \frac{c}{\lambda} + \frac{1}{2} \int \frac{d^3\kappa}{(2\pi)^3} \omega_\kappa n_\kappa^{(f)} + \frac{1}{2} \int \frac{d^3\kappa}{(2\pi)^3} \varpi_\kappa n_\kappa^{(B)} \right\}, \quad (5.8)$$

is exactly conserved by virtue of the equations of motion themselves. In the above

$$c(\tau) = [\Phi'(\tau)]^2 - 2\Phi^2(\tau) + \Phi^4(\tau), \quad (5.9)$$

the fermion (boson) occupation number $n_\kappa^{(f)}$ ($n_\kappa^{(B)}$) and frequency ω_κ (ϖ_κ) are given in Eq. (3.35) [Eq. (3.17)] and Eq. (3.33) [Eq. (3.10)], respectively.

The approximate evaluation of the integrals (5.5) and (5.6) by restricting their integrand on the dominant band (see also [39]) is based on the results of Sections 4.1 and 4.2 for fermions and bosons respectively, and proceeds in a similar way. We therefore assume the validity of scaling laws of the form given, for example, in Eqs. (4.5) or (4.6) and Eqs. (4.6) and (4.7). These approximations are not valid for asymptotically long time evolution, when the dissipative dynamics takes over and very little particle production may still take place. In such a case, one may need different computational schemes, and probably a full lattice approach, useful also to describe rescattering phenomena and estimate a possible thermalization phase. Nevertheless, our approximation scheme has the virtue of been simple enough to lead to a system of differential equations of finite order which helps to grasp some aspects of the back-reaction dynamics and gains more and more validity in the limit $\lambda \ll 1$.

In order to make the qualitative features of the system (5.7) clearer, we shall first study separately its behaviour for short and long times. In particular, as we have seen in the two previous Sections, the production of fermions is expected to dominate during the first few hundreds of Higgs background oscillations and in that regime we shall neglect boson production by simply switching its coupling off and set $M_H = 500 \text{ GeV}$ in order to have the maximum *top* production. At larger times the production of bosons overcomes that of fermions (limited by Pauli blocking) and we shall then neglect the fermions and set $M_H = 200 \text{ GeV}$ so as to maximise the Z^0 production. In the last Subsection, we shall finally consider the entire system with both the *top* and Z^0 for $M_H = 500 \text{ GeV}$ in order to show the effect of the fermion back-reaction on the later boson production. This value of

the Higgs mass, although not very likely, is chosen as it is particularly convenient to study the interplay between fermion and boson production.

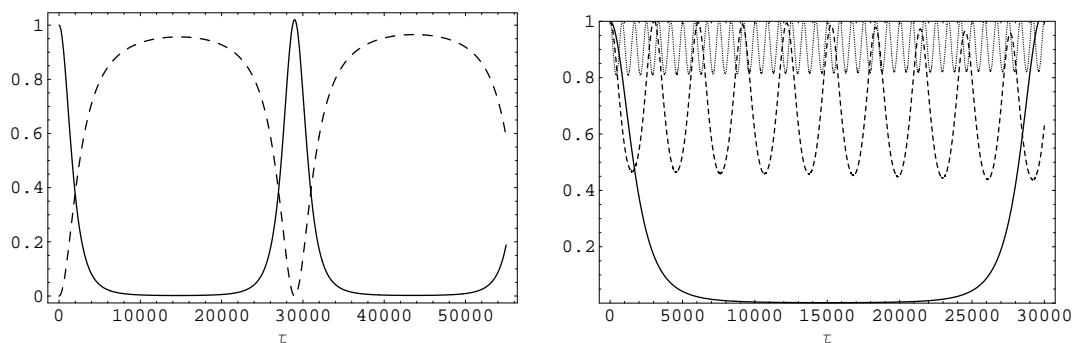


Figure 5.1: *Fermion back-reaction* with $M_H = 500$ GeV. Left plot: Time evolution of the *top* occupation number (dashed line) and Higgs vacuum energy (solid line) for $\lambda = 1$ and initial $c(0) = -1 + 10^{-5}$. Right plot: Comparison of the Higgs total vacuum energy for initial values $c(0) + 1 = 10^{-3}$ (dotted line), 10^{-4} (dashed line) and 10^{-5} (solid line). A normalization factor of $[c(0) + 1]^{-1}$ is used for the Higgs energies.

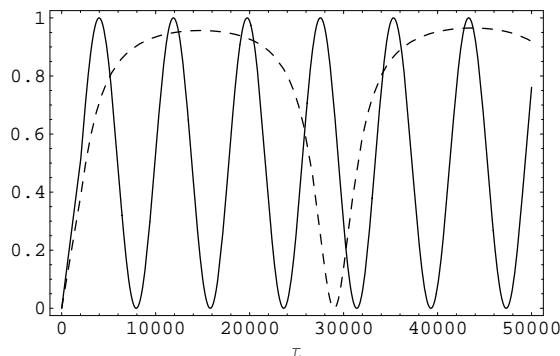


Figure 5.2: *Fermion back-reaction*: comparison of *top* occupation number with (dashed line) and without (solid line) back-reaction for $c(0) = -1 + 10^{-5}$.

5.1 Fermion back-reaction

As we mentioned above, for relatively short times, we at first consider the evolution of the Higgs background and one fermion, namely the *top* quark with $M_H = 500$ GeV.

The left graph in Fig. 5.1 shows the time dependence of the corresponding occupation number for the *top* and Higgs energy densities up to a time $\tau \simeq 3.14 \cdot 10^3$ ($\simeq 10^3 T$, where T is the Higgs period without back-reaction) when the boson back-reaction is expected to take over. The Higgs energy oscillates periodically in time and of course takes its minimum values when the *top*'s occupation number is maximum. The right graph displays how the Higgs energy changes in time for different initial values of c , that is for different total energy (all curves assume $\lambda = 1$). Note that the maximum fraction of Higgs energy converted into the *top* increases for decreasing initial total energy, as one would expect from the Pauli blocking. Fig. 5.2 then compares the *top*'s occupation number with and without back-reaction for $c(0) = -1 + 10^{-5}$. It is clear that the back-reaction in general suppresses the number of produced fermions and this effect is more pronounced for smaller total energy. We also remark that the above numerical solution conserves the total energy with an accuracy better than 1 part in 10^3 .

To conclude this section, we would like to spend a few words about the behaviour of the system with respect to the value of λ . Further numerical analysis shows that the fraction of energy absorbed by the produced fermions is proportional to λ . Moreover, the system of non-linear differential equations (5.7) seems to produce a chaotic behaviour only for $\lambda > 10^6$. In fact for $\lambda \approx 10^6$ the highly non-linear term proportional to $\langle \bar{\psi}\psi \rangle$ becomes of the same order of magnitude as the other terms in the first equation of (5.7). But at this level the approximations used in our equations to evaluate the back-reaction terms should break down.

5.2 Boson back-reaction

From the results of the previous Chapter, we know that the energy density of created bosons is comparable to the initial Higgs energy density after about 10^3 vacuum oscillations (that is, for $\tau \gtrsim 3.14 \cdot 10^3$). The production of bosons then overcomes fermion production (limited by the Pauli principle) and their back-reaction becomes the most relevant phenomenon. We shall therefore neglect the fermion contribution here and just consider the Z^0 and $M_H = 200 \text{ GeV}$ or $M_H = 500 \text{ GeV}$.

Even with the above simplification, it is still very difficult to solve the system (5.7) and we need to employ yet another approximation. Since the integrand in Eq. (5.6) is sharply peaked around the centres of resonance bands, we estimate that integral in the same way we used to obtain the total number of produced

bosons in Eq. (4.7), as we have already anticipated in the general discussion of this Chapter.

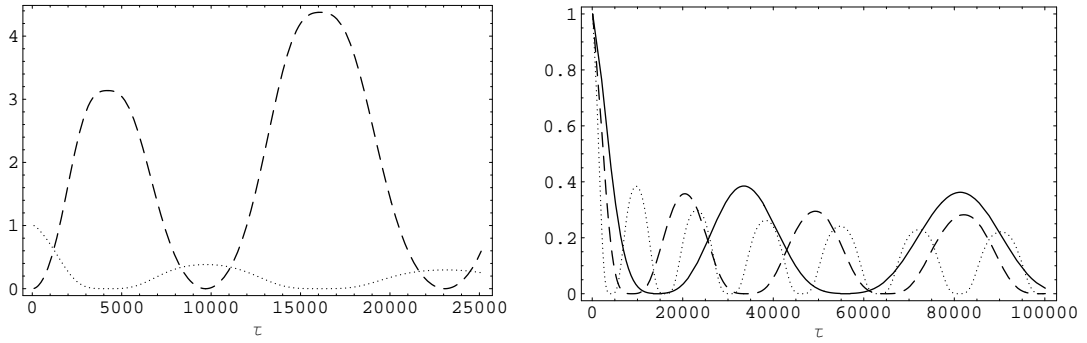


Figure 5.3: *Boson back-reaction* with $M_H = 200$ GeV. Left graph: Z^0 occupation number (dashed line) and Higgs vacuum energy (dotted line) for an initial value of $c(0) + 1 = 10^{-5}$. Right graph: Time variation of the Higgs vacuum energy for initial total energy $c(0) + 1 = 10^{-5}$ (dotted line), 10^{-6} (dashed line) and 10^{-7} (solid line). A normalization factor of $[c(0) + 1]^{-1}$ for the Higgs energies is always used.

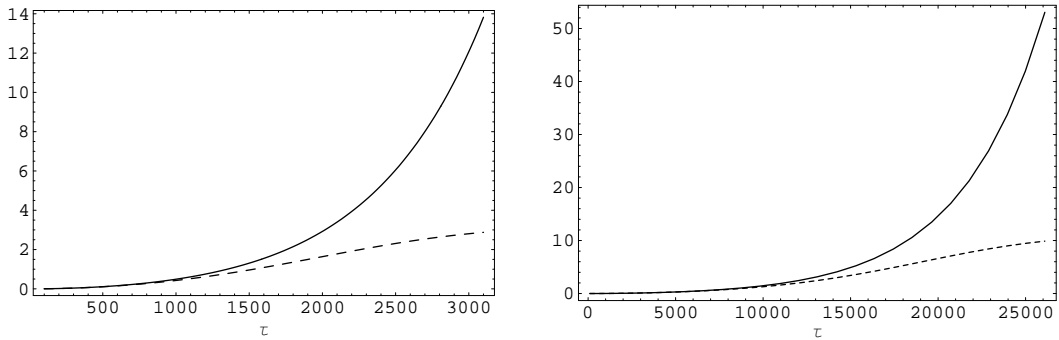


Figure 5.4: *Boson back-reaction*: comparison of Z^0 occupation numbers with (dashed line) and without (solid line) back-reaction for $c(0) = -1 + 10^{-5}$. $M_H = 200$ GeV in left plot and $M_H = 500$ GeV in right plot.

We can now solve numerically the system (5.7) and Fig. 5.3 shows some relevant results. Starting from the left, it is possible to see that the Higgs energy is minimum when the rate of production is maximum. Further, from Fig. 5.4, one sees that the back-reaction strongly suppresses the boson production. The right plot in Fig. 5.3 shows the amount of vacuum energy dissipated by back-reaction effects as a function of the time for three different values of the total (dimensionless) energy (which of course coincides with the initial Higgs energy). An important feature of this plot is that we have a “regeneration” of the vacuum energy,

which now oscillates in time, and the number of peaks in a given time interval is seen to increase (that is, the periods of oscillations become shorter) for increasing total energy. In all cases, the values at the peaks slowly decrease in time and the periods of oscillations stretch. One can therefore conclude that the system will evolve towards a complete dissipation of the Higgs oscillations. This is due to the presence of a dumping term [analogous to $1/\sqrt{\tau}$ in Eq. (4.7)] that appears in the back-reaction term (5.6) after integrating in κ .

5.3 Fermion and boson back-reaction

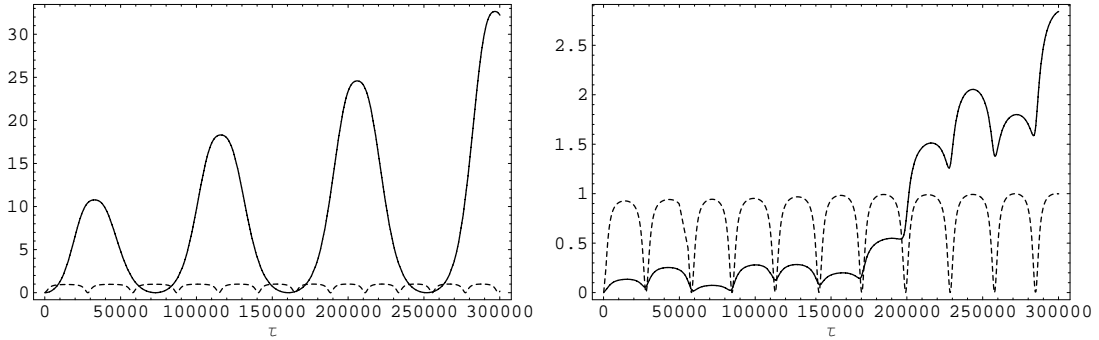


Figure 5.5: Time evolution of the occupation numbers for the *top* (dashed line) and Z^0 (solid line) for $\lambda = 1$, $M_H = 500$ GeV and $c(0) = -1 + 10^{-5}$. Left plot: *Partial back-reaction* from the approximations of Sections 5.1 and 5.2. Right plot: *Full back-reaction* from Section 5.3.

We finally consider the whole system with the *top* and Z^0 described by Eq. (5.7) for $M_H = 500$ GeV. Again, we choose this value of the Higgs mass in order to have both fermion and boson production from the first resonant band. This corresponds to a particularly complicated scenario with large production of both the *top* and Z^0 , whereas a more realistic smaller value of M_H would mostly lead to the production of lighter quarks with smaller effects on the Z^0 at late times.

The coupled dynamics is then described in Fig. 5.5 in which we show on the right the occupation numbers for the *top* and Z^0 . This results has to be compared to the results of back-reaction computed in the “factorized” approximation used in Secs. 5.1 and 5.2 which we report together for convenience on the left, both computed at $M_H = 500$ GeV. We note that the *top* production is not particularly affected, whereas the Z^0 occupation number is suppressed in the sense that it

increases significantly only at later times. The time needed for the production of Z^0 to overtake the top is about one order of magnitude larger than without fermion back-reaction.

As we have already observed, we are able to study the evolution of the system in a window of time far from the asymptotics (presumably with an upper bound in time inversely proportional to λ). Beyond that, the adopted approximations break down and the asymptotic time behaviour of the system should be studied taking into account a more accurate description of the mode production (eventually in a full lattice approach) together with the rescattering contribution of the produced particles.

Chapter 6

Conclusions

We have considered oscillating solutions for the Higgs vev in the context of the Standard Model of particle physics and studied some resulting dissipative effects. In the Standard Model, in fact, the masses of fundamental particles depend on that vev and its oscillations can be viewed as a time-dependent renormalization of the particles' masses which leads to the production of fermion and boson pairs by parametric resonance.

In the first part of this work, the back-reaction of the produced pairs has been totally neglected. In this approximation, particle production by the oscillating Higgs appeared to be very efficient. For fermions, the Pauli blocking constrains their occupation numbers to oscillate in time (see Figs. 4.1) about mean values smaller than one. From the entries given in Table 4.1, one can see that such mean values strongly depend on the resonance parameter q , that is the Higgs and fermion masses [see the definitions (3.31)]. Moreover, the particular form of the governing Dirac equation (3.13) yields a significant probability of producing only those fermions whose momenta lie on well-defined bands in the (q, κ^2) -plane [see Fig. 3.1 and Eq. (3.42)]. Considering the masses of Standard Model particles, this also implies a larger probability of producing fermions with non-relativistic momenta.

As for the bosons, their production is not constrained by any fundamental principles and the governing Mathieu equation (3.13) (in the small oscillation regime) leads to occupation numbers which grow exponentially in time. Analogously to the fermions, the boson production only occurs on narrow bands in the (q, κ^2) -plane [see the definitions (3.11) and Eq. (3.15)].

In our analysis, we have regarded the Higgs mass M_H as an adjustable param-

eter, for the experimental data only place a lower bound on it. Consequently, we have given our results for different possible values of M_H and the initial Higgs energy $c(0)$ [see the definition (2.9) and Eq. (5.9)]. For natural values of these parameters, we have found that a significant fraction of the initial vacuum energy can be transferred to the fermions before a complete background oscillation (whose period we denoted as T , see Fig. 4.3). The Pauli blocking then prevents the fermion production from increasing further. The bosons, on the other hand, grow exponentially in time but absorb a significant fraction of the Higgs vacuum energy only after about a thousand oscillations (see Fig. 4.6). This feature seems to suggest that it is possible to analyse the back-reaction of fermions and bosons separately.

In particular, we have studied the system of one fermion (the *top* quark) and one boson (the Z^0) coupled to the Higgs field Φ in the Hartree approximation [see Eq. (5.7)]. For such a system, the total energy (5.8) is conserved and, for $0 \leq \tau \lesssim 10^3 T$, the back-reaction of the produced Z^0 has been neglected. To make the problem more tractable, and avoid a complicated study of the system on a lattice of Fourier modes, we have adopted another approximation which might breakdown at asymptotic times. We have thus found that the fermion production is in general mildly suppressed by the back-reaction (see Figs. 5.1 and 5.2). At later times ($\tau \gtrsim 10^3 T$), the back-reaction of the produced *top* has been neglected and, in the same framework of approximations, we have found that the production of Z^0 is more strongly suppressed by the back-reaction (see Figs. 5.3 and 5.4).

The study of the system where both fermion and boson backreaction effects are included has shown a slower boson production, which takes over almost an order of magnitude later in time, against the naive expectation of some kind of factorization in the production events. We however remark that we have chosen a value of the Higgs mass $M_H = 500 \text{ GeV}$ which corresponds to a large production of the *top* in order to study its effect on the production of the Z^0 . For a more realistic (presumably smaller) value of M_H , one should instead consider the quarks and leptons with the higher production rates (as shown in Table 4.1).

Future investigations, apart from being focused on more appropriate values of the Higgs mass as, for example, an awaited discovery at LHC would provide, should address aspects which we have found beyond our possibility because of the approximation schemes adopted. In particular, one should investigate the production and dissipative dynamics in the late (asymptotic) times of the evo-

lution and evaluate the rescattering phenomena associated with the produced particles. Keeping in mind that we are mainly considering a possible “starting” regime of very small Higgs oscillations, the rescattering could lead to a thermal background characterized by a very low temperature.

We conclude by noting that, although suppressed when the back-reaction is properly included in the analysis, particle production by parametric resonance with an oscillating Higgs field remains a remarkable effect with phenomenological relevance and could be an (indirect) way of testing the time-dependence of the constants of the Standard Model.

Part II

Small x QCD and multigluon states: A Color toy model

Chapter 7

Introduction

In quantum field theory and statistical mechanics the $1/N$ (or large N) expansion [55] is a well known and extensively used perturbative framework whenever the theories under investigation present an internal symmetry typically related to groups like $SO(N)$ or $SU(N)$.

Quantum Chromodynamics is one of the theories mostly studied under this approximation even if, as a physical gauge theory, it is characterized by a gauge group $SU(N_c)$ where the number of colors N_c is just 3. Recently, thanks to the renewed interest induced by the ADS/CFT correspondence, the $\mathcal{N} = 4$ SYM theory in the infinity color (planar) limit has been intensively studied and several important results achieved.

The fact that the planar $\mathcal{N} = 4$ SYM is expected by the theoretical community to be solvable and that it is dual to a superstring sigma model has led several theorists to look for hints, in the absence of any supersymmetry, for the existence of a possible dynamical system dual to planar QCD sharing with it some integrability properties. The starting point are the integrable structures unveiled many years ago at one loop in standard perturbation theory and some hints of possible integrability at two loops in the planar limit.

The first evidence of an integrable structure at one loop in QCD was found by L.N. Lipatov [21] in the framework of the Regge limit of scattering amplitudes, whose behavior may be conveniently described by systems of interacting reggeized gluons, as we shall briefly review in the next chapter. The integrable dynamics, associated to the evolution in rapidity of such a system, appears when one is taking the large N_c approximation, which makes the BKP kernel [23] to resemble the structure of an Heisenberg XXX spin chain, but for a non compact

$SL(2, \mathbb{C})$ “spin”.

Going beyond the large N_c approximation, even in the lowest orders in perturbation theory in the coupling constant, is a formidable task and it is very difficult also to try to estimate the error one faces when computing quantities for infinite N_c (planar limit) instead of at $N_c = 3$.

It is the purpose of this part of the thesis to introduce some finite toy models, which shares the same color structure of the BKP systems, and which can be studied to determine the dependence of the spectrum on the number of colors N_c . They are characterized by a configuration space which is no more the transverse plane but a finite vector space associated to irreducible representations of the $SU(2)$ group so that one may use group theoretical methods to analyse some of these models.

This is of course not providing any concrete answer for the question related to the real QCD problem, but nevertheless can be of some help. Moreover some toy models may be interesting by themselves as dynamical systems.

We start in the next chapter with a short review of the properties of the system of interacting reggeized gluons in the Leading Logarithmic Approximation. In chapter 9 we consider the color structure for the four reggeized gluon system and describe how to use a convenient basis for it. In chapter 10 we construct some finite toy models which are studied in some details in separate sections.

Chapter 8

BKP Kernel

Let us start by giving a brief overview of the kernels which encode the evolution in rapidity of systems of interacting reggeized gluons in the leading logarithmic approximation (LLA). The reggeized gluons provide a convenient perturbative description of part of the QCD degrees of freedom in the Regge limit (also known as the small x limit) and appeared in the investigations of the leading dependence of the total cross sections on the center of mass energy in the LLA, which is associated to the so called BFKL (perturbative) pomeron [20]. In the simplest form, the BFKL pomeron turns out to be a composite state of two interacting reggeized gluons “living” in the transverse configuration plane in the colorless configuration. The construction of the kernel reflects the property that in the Regge limit the scattering amplitude factorizes in the impact factors, which determine the coupling of the external particles to the t -channel reggeized gluons, and in a Green’s function, which exponentiates the kernel and contains the rapidity dependence of their composite state. Such a dependence can be analyzed in terms of the spectral properties of the kernel and in particular one is interested in the eigenvalues and eigenstates associated to the leading behavior. Because of this the spectral problem is often formulated in quantum mechanical terms with the kernel being the “Hamiltonian” and its eigenvalues the “energies”.

In the case of a colorless exchange the Hamiltonian is infrared finite and in LLA is constructed summing the perturbative contributions of different Feynman diagrams: in particular the virtual ones (reggeized gluon trajectories) ω and the real ones (associated to an effective real gluon emission vertex) V . One writes formally $H = \omega_1 + \omega_2 + \vec{T}_1 \vec{T}_2 V_{12}$ where \vec{T}_i are the generators of the color group in adjoint representation. In the colorless case one has $\vec{T}_1 \vec{T}_2 = -N_c$ and finally one

obtains:

$$H_{12} = \ln |p_1|^2 + \ln |p_2|^2 + \frac{1}{p_1 p_2^*} \ln |\rho_{12}|^2 p_1 p_2^* + \frac{1}{p_1^* p_2} \ln |\rho_{12}|^2 p_1^* p_2 - 4\Psi(1), \quad (8.1)$$

where $\Psi(x) = d \ln \Gamma(x)/dx$, a factor $\bar{\alpha}_s = \alpha_s N_c/\pi$ has been omitted and the gluon holomorphic momenta and coordinates have been introduced.

The gauge invariance gives the freedom to choose a description within the Möbius space [56, 57], wherein the functions describing the positions of the two reggeized gluons in the transverse plane are zero in the coincidence limit. In this space the BFKL hamiltonian has the property of the holomorphic separability ($H_{12} = h_{12} + \bar{h}_{12}$). Moreover a remarkable property is its invariance under the Möbius group, whose generators for the holomorphic sector in the Möbius space for the principal series of unitary representations are given by:

$$M_r^3 = \rho_r \partial_r, \quad M_r^+ = \partial_r, \quad M_r^- = -\rho_r^2 \partial_r. \quad (8.2)$$

The associated Casimir operator for two gluons is

$$M^2 = |\vec{M}|^2 = -\rho_{12}^2 \partial_1 \partial_2, \quad (8.3)$$

where $\vec{M} = \sum_{r=1}^2 \vec{M}_r$ and $\vec{M}_r \equiv (M_r^+, M_r^-, M_r^3)$. Due to this symmetry the holomorphic and antiholomorphic parts of the Hamiltonian can be written explicitly in terms of the Casimir operator: indeed one has, after defining formally $J(J-1) = M^2$,

$$h_{12} = \psi(J) + \psi(1-J) - 2\psi(1). \quad (8.4)$$

Labelled by the conformal weights $h = \frac{1+n}{2} + i\nu$, $\bar{h} = \frac{1-n}{2} + i\nu$, where n is the conformal spin and $d = 1 - 2i\nu$ is the anomalous dimension of the operator $O_{h,\bar{h}}(\rho_0)$ describing the compound state [58], the eigenstates and eigenvalues of the full hamiltonian in eq. (8.1), $H_{12} E_{h,\bar{h}} = 2\chi_h E_{h,\bar{h}}$, are respectively given by:

$$E_{h,\bar{h}}(\rho_{10}, \rho_{20}) \equiv \langle \rho | h \rangle = \left(\frac{\rho_{12}}{\rho_{10} \rho_{20}} \right)^h \left(\frac{\rho_{12}^*}{\rho_{10}^* \rho_{20}^*} \right)^{\bar{h}}, \quad (8.5)$$

and

$$\chi_h \equiv \chi(\nu, n) = \psi \left(\frac{1+|n|}{2} + i\nu \right) + \psi \left(\frac{1+|n|}{2} - i\nu \right) - 2\psi(1). \quad (8.6)$$

The leading eigenvalue, at the point $n = \nu = 0$, has a value $\chi_{max} = 4 \ln 2 \approx$

2.77259, responsible for the rise of the total cross section as $s^{\bar{\alpha}_s \chi_{max}}$, which corresponds to a strong violation of unitarity.

Let us now consider the evolution in rapidity of composite states of more than 2 reggeized gluons [23]. The BKP Hamiltonian in LLA acting on a colorless state can be written in terms of the BFKL pomeron Hamiltonian and has the form (see [21])

$$H_n = -\frac{1}{N_c} \sum_{1 \leq k < l \leq n} \vec{T}_k \vec{T}_l H_{kl}. \quad (8.7)$$

This Hamiltonian is conformal invariant but cannot be solved in general. Nevertheless the case of three reggeized gluons, where the color structure trivially factorizes, is solvable [21] and different families of solutions were found [59, 60]. Physically these states are associated to the so called odderon exchange [61] and in particular the family of solutions given in [60] corresponds to eigenvalues up to zero (intercept up to one) and are the leading one in the high energy limit. Moreover they have a non null coupling to photon-meson impact factors [62].

The case of more than three reggeized gluon is in general not solvable, but if one considers the color cylindrical topology taking the large N_c limit, the resulting Hamiltonian

$$H_n^\infty = \frac{1}{2} [H_{12} + H_{23} + \dots + H_{n1}] = h_n + \bar{h}_n \quad (8.8)$$

is integrable, i.e. there exists a set of other $n - 1$ operators q_r , which commute with it and are in involution. They are given, in coordinate representation, by

$$q_r = \sum_{i_1 < i_2 < \dots < i_r} \rho_{i_1 i_2} \rho_{i_2 i_3} \dots \rho_{i_r i_1} p_{i_1} p_{i_2} \dots p_{i_r}, \quad (8.9)$$

together with similar relations for the antiholomorphic sector. In particular, $q_2 = M^2$ is the Casimir of the Möbius group. This is the first case where integrability was found within the context of gauge theories analyzing the Green's function in some kinematical limit. This integrable model is a non compact generalization of the Heisenberg XXX spin chains [21, 63, 64, 65] and has been intensively studied with different techniques in the last decade [66, 67, 68, 69, 70, 71].

Here we remind the result for the highest eigenvalue of a system of four reggeized gluons in the planar, one cylinder topology (1CT), case:

$$H_4^\infty \psi_4 = 2E_4^{1CT} \psi_4.$$

The maximum value found, for zero conformal spin, is

$$E_4^{1\text{CT}} = 0.67416. \quad (8.10)$$

In general for an arbitrary number n of reggeized gluon in the cylindrical topology the leading eigenvalues have been found to be positive for even n and negative for odd n and asymptotically behaving as $1/n$ [68, 69].

An important question, unfortunately very hard to answer is: what are the eigenvalues at finite $N_c = 3$ and what is in general their dependence in N_c ? One may be tempted to apply variational or perturbative techniques to the spectral problem, which nevertheless appears to be quite involved. In any case a first step consists to analyze the color structure, which simplifies a bit in the case of four reggeized gluon in a total colorless state.

Chapter 9

Color structure

We consider the BKP kernel H_4 for four gluons, given in eq. (8.7). This is an operator acting on 4-gluon states, which may be represented as functions of the transverse plane coordinates $\{\rho_i\}$ and of the gluon colors $\{a_1 a_2 a_3 a_4\}$, written as $v(\{\rho_i\})^{a_1 a_2 a_3 a_4}$. Let us concentrate here on the color space.

It is convenient, due to the fact that the four gluons are in a total color singlet state, to write the color vector $v^{a_1 a_2 a_3 a_4}$ in terms of the color state of a two gluon subchannel. Let us therefore start from the resolution of unity for a state of two $SU(N_c)$ particles in terms of the projectors $P[R_i]_{a_1 a_2}^{a'_1 a'_2}$ onto irreducible representations:

$$1 = P_1 + P_{8_A} + P_{8_S} + P_{10+\bar{10}} + P_{27} + P_0 = \sum_i P[R_i], \quad (9.1)$$

where $Tr P[R_i] = d_i$ is the dimension of the corresponding representation. Let us note that we have chosen to consider a unique subspace for the direct sum of the two spaces corresponding to 10 and $\bar{10}$ representations. This is convenient for our purposes and we shall therefore consider just 6 different projectors to span the color space of two gluons.

If we consider gluons (1, 2) to be the reference channel we introduce as the base for the color vector space the set $\{P[R_i]_{a_1 a_2}^{a_3 a_4}\}$ of projectors and write

$$v^{a_1 a_2 a_3 a_4} = \sum_i v^i (P[R_i]_{a_1 a_2}^{a_3 a_4}) \quad \text{or} \quad v = \sum_i v^i P_{12}[R_i]. \quad (9.2)$$

Note that one could have also chosen other reference channels corresponding to a description in terms of projection onto irreducible representations of other gluon subsystems. Having chosen a color basis, the next step is to write the BKP kernel

with respect to it. We can slightly simplify the expression for the kernel since for a colorless state we have $\sum_i \vec{T}_i v = 0$ which implies that $\vec{T}_1 \vec{T}_2 v = \vec{T}_3 \vec{T}_4 v$ (an similarly for the other permutations of the indices). Therefore one may write:

$$H_4 = -\frac{1}{N_c} \left[\vec{T}_1 \vec{T}_2 (H_{12} + H_{34}) + \vec{T}_1 \vec{T}_3 (H_{13} + H_{24}) + \vec{T}_1 \vec{T}_4 (H_{14} + H_{23}) \right]. \quad (9.3)$$

Let us now write explicitly the action of the color operators $\vec{T}_i \vec{T}_j = \sum_a T_i^a T_j^a$ which are associated to the interaction between the gluons labelled i and j . We start from the simple ‘‘diagonal channel’’ for which we have the relation $\vec{T}_i \vec{T}_j = -\sum_k a_k P_{ij}[R_k]$ with coefficients $a_k = (N_c, \frac{N_c}{2}, \frac{N_c}{2}, 0, -1, 1)$. Consequently we can write in the $(1, 2)$ reference base

$$\left(\vec{T}_1 \vec{T}_2 v \right)^j = -a_j v^j = -(A v)^j, \quad (9.4)$$

where $A = \text{diag}(a_k)$. The action on v of the $\vec{T}_1 \vec{T}_3$ and $\vec{T}_1 \vec{T}_4$ operators is less trivial and is constructed in terms of the $6j$ symbols of the adjoint representation of $SU(N_c)$ group. We shall give few details in the appendix A and write directly the results, in terms of the symmetric (after a similarity transformation) matrix operators:

$$\left(\vec{T}_1 \vec{T}_3 v \right)^j = -\sum_i \left(\sum_k C_k^j a_k C_i^k \right) v^i = -(C A C v)^j \quad (9.5)$$

and

$$\left(\vec{T}_1 \vec{T}_4 v \right)^j = -\sum_i \left(\sum_k s_j C_k^j a_k C_i^k s_i \right) v^i = -(S C A C S v)^j. \quad (9.6)$$

The matrix C is the crossing matrix build on the $6j$ symbols and $S = \text{diag}(s_j)$ is constructed on the parities $s_j = \pm 1$ of the different representations R_j .

We can therefore write the general BKP kernel for a four gluon state, given in eq. (9.3), as

$$H_4 = \frac{1}{N_c} [A (H_{12} + H_{34}) + C A C (H_{13} + H_{24}) + S C A C S (H_{14} + H_{23})] \quad (9.7)$$

One can check that if we make trivial the transverse space dynamics, replacing the H_{ij} operators by a unit operators, the general BKP kernel in eq. (8.7) becomes $H_n = \frac{n}{2} \hat{1}$ and indeed one can verify that $A + C A C + S C A C S = N_c \hat{1}$.

Let us make few considerations on the large N_c limit approximation. As we

have already discussed, in the Regge limit one faces the factorization of an amplitude in impact factors and a Green's function which exponentiates the kernel. The topologies resulting from the large N_c limit depend on the impact factor structure. In particular one expects the realization of two cases: the one and two cylinder topologies. The former corresponds to the case, well studied, of the integrable kernel, Heisenberg XXX spin chain-like. This is encoded in the relation: $\vec{T}_i \vec{T}_j \rightarrow -\frac{N_c}{2} \delta_{i+1,j}$ which leads to $H_4 = \frac{1}{2} (H_{12} + H_{23} + H_{34} + H_{41})$ and is characterized by eigenvalues corresponding to an intercept less than a pomeron. The latter case instead is expected to have a leading intercept, corresponding to an energy dependence given by two pomeron exchange. Consequently one expects at finite N_c a contribution with an energy dependence even stronger. In the two cylinder topology the color structure is associated to two singlets ($\delta_{a_1 a_2} \delta_{a_3 a_4}$, together with the other two possible permutations). Such a structure is indeed present in the analysis, within the framework of extended generalized LLA, of unitarity corrections to the BFKL pomeron exchange [72] and diffractive dissociation in DIS (Deep Inelastic Scattering) [73], where the perturbative triple pomeron vertex (see also [74]) was discovered and showed to couple exactly to the four gluon BKP kernel.

It is therefore of great importance to understand how much the picture derived in the planar $N_c = \infty$ case is far from the real situation with $N_c = 3$. One clearly expects for example that the first corrections to the eigenvalues of the BKP kernel are proportional to $1/N_c^2$, but what is unknown is the multiplicative coefficient as well as the higher order terms.

Chapter 10

Toy models

In this chapter we shall consider a family of models, different from the BKP system, which nevertheless share several features with it and can be used to judge how the large N_c approximation might be more or less satisfactory. Moreover these systems may be considered interesting by themselves as quantum dynamical systems.

A state of n reggeized gluons undergoing the BKP evolution, described by the kernel in eq. (8.7), belongs to a vector space of functions on a domain given by the tensor product of the color space $\mathfrak{8}^n$ and the configuration space \mathbb{R}^{2n} , associated to the position or momenta in the transverse plane, of the n gluons. Indeed the BKP kernel is built as a sum of product of color ($\vec{T}_k \vec{T}_l$) and of configuration (H_{kl}) operators; the latter, on the Möbius space, can be written in terms of the Casimir of the Möbius group, i.e. in terms of the scalar product of the generators of the non compact spin group $SL(2, \mathbb{C})$: $H_{kl} = H_{kl}(\vec{M}_k \cdot \vec{M}_l)$.

We are therefore led to consider a class of toy models where the BKP configuration space \mathbb{R}^{2n} is substituted by the space V_s^n where V_s is the finite space spanned by spin states belonging to the irreducible representation of $SU(2)$ with spin s . In particular we shall consider quantum systems with an Hamiltonian fitting the following structure:

$$\mathcal{H}_n = -\frac{1}{N_c} \sum_{1 \leq k < l \leq n} \vec{T}_k \vec{T}_l f(\vec{S}_k \vec{S}_l), \quad (10.1)$$

where \vec{S}_i are the elements of the $SU(2)$ algebra associated to the particle i in any chosen representation and f is a generic function. A particular toy model is therefore specified by giving the spin s of each particle (“gluons”) and the function f . In the following we shall consider two specific cases for the 4 particle system (case

a) and b)). Moreover in order to have another check of our approach we shall also consider the model defined in case c).

- a) A spin $s = 1$ model in a global singlet state v ($\sum_i \vec{S}_i v = 0$). If f is the identity map than the “spin” configuration dynamics is very similar to the one of the color sector. In order to have a system which behaves similarly to the BKP case we first put a constraint on the two particle operators, which describe the basic interaction. In particular we consider the family of functions

$$f_\alpha(x) = 2\text{Re} \left[\psi \left(\frac{1}{2} + \sqrt{-\alpha(4 + 2x)} \right) \right] - 2\psi(1). \quad (10.2)$$

Remembering that for conformal spin $n = 0$ the BFKL Hamiltonian is given by $H_{kl} = 2\text{Re} \left[\psi \left(\frac{1}{2} + \sqrt{\frac{1}{4} + (\vec{M}_k + \vec{M}_l)^2} \right) \right] - 2\psi(1)$, one immediately recognizes that the f_α is associated to the substitution $\frac{1}{4} + L_{ij}^2 \rightarrow -\alpha S_{ij}^2$ which assures to have the same leading eigenvalue for any α , since both expressions have the value zero as upper bound. The parameter α will be chosen in order to constrain the full 4-particle Hamiltonian (10.1) to have the same leading eigenvalue as the QCD BKP system in the large N_c limit (at zero conformal spin). In this system, the **BKP toy model**, we shall investigate finite N_c effects.

- b) A system $\text{TOY}_{\text{Adj, Fund}}$ with f the identity function and spin $s = 1/2$. Such a system in the large N_c limit in the case of one cylinder topology becomes the well known Heisenberg XXX spin chain system, which is integrable. We shall perform some check on the N_c dependence again for the 4-particle case.
- c) A model where the 4 particle belong to the fundamental representation of $SU(2)$ for both the “color” and the “spin”, so that we can perform a comparison with standard results from the spectroscopy of isospin-spin systems.

10.1 BKP toy model

In order to explicitly study this finite system, described by the Hamiltonian in eq. (10.1) acting on vector states with dimension $(8 \times 3)^4$ and singlet under both

$SU(3)_C$ and $SU(2)_{spin\ conf}$, it is convenient to choose the color decomposition in 2-particle subchannel irreducible representations described in chapter 9 and adopt a similar approach also on the “spin” degrees of freedom. After that, one is left with the problem of diagonalizing an Hamiltonian which is a matrix 18×18 , that is addressable with any computer. Without the singlet restriction on the spin part the problem in general is much more complicated to be easily solved and may be addressed in future investigations.

Let us therefore proceed by introducing for 2 spin 1 particle states the resolution of unity $1 = Q_1 + Q_3 + Q_5 = \sum_i Q[R_i]$ which let us write $\vec{S}_i \vec{S}_j = -\sum_k b_k Q_{ij}[R_k]$, with $b_k = (2, 1, -1)$ (c.f. with a_k : first, second and second last terms). It is therefore straightforward to write from a power series representation ($Q_{ij}[R_k]$ are projectors):

$$f(\vec{S}_i \vec{S}_j) = \sum_k f(-b_k) Q_{ij}[R_k] \quad (10.3)$$

and using the corresponding crossing matrices D and the parity matrix S' one obtains relations very similar to the one reported in eqs. (9.4)-(9.6), which read:

$$\left(f \left(\vec{S}_1 \vec{S}_2 \right) v \right)^j = f(-b_j) v^j = (B v)^j, \quad (10.4)$$

$$\left(f \left(\vec{T}_1 \vec{T}_3 \right) v \right)^j = \sum_i \left(\sum_k D_k^j f(-b_k) D_i^k \right) v^i = (DB D v)^j \quad (10.5)$$

and

$$\left(f \left(\vec{T}_1 \vec{T}_4 \right) v \right)^j = \sum_i \left(\sum_k s'_j D_k^j f(-b_k) D_i^k s'_i \right) v^i = (S' DB DS' v)^j. \quad (10.6)$$

From the above results for the two particle representation basis, we can write the explicit form of the Hamiltonian for this toy model, going beyond the one given in eq. (9.7). Indeed we obtain

$$\mathcal{H}_{4\alpha} = \frac{2}{N_c} (A \otimes B + CAC \otimes DB D + SCACS \otimes S' DB DS') \quad (10.7)$$

which contains a dependence on N_c and on the parameter α through the function f_α given in eq. (10.2).

Let us note that in the large N_c limit one faces for the Hamiltonian two possible cases: the one cylinder topology (1CT) which corresponds to the simpler

Hamiltonian

$$\mathcal{H}_{4a}^{1CT} = -\frac{1}{N_c} \left[-\frac{N_c}{2} \sum_i f(\vec{S}_i \vec{S}_{i+1}) \right] = B + S' DBDS' \quad (10.8)$$

and the two cylinder topology (2CT) corresponding to the even simpler Hamiltonian

$$\mathcal{H}_{4a}^{2CT} = -\frac{1}{N_c} \left[-N_c f(\vec{S}_1 \vec{S}_2) - N_c f(\vec{S}_3 \vec{S}_4) \right] = 2B. \quad (10.9)$$

Let us remark that while in the case of $N_c > 3$ we consider a basis for the vector states made of $P[R_i]Q[R_j]$ with 18 elements since in the color sector there is also the P_0 projector, the case $N_c = 3$ is characterized by a basis of 15 elements.

As already anticipated, in order to study a toy model resembling the spectrum of the BKP system of 4 gluons, we require that, in the large N_c limit in the one cylinder topology, the leading eigenvalue must be the same as the one found for the corresponding integrable BKP system, whose value was given in eq. (8.10). This fact fixes the value of the parameter $\alpha = 2.80665$. We are therefore left with an Hamiltonian which is just a function of the number of colors N_c .

Let us now consider its spectrum for the cases $N_c = 3$ and $N_c = \infty$. Here we report the values followed by their multiplicities.

$$\left(\begin{array}{c} N_c = 3 \\ \mathbf{7.04193} \quad (\times 1) \\ \mathbf{5.51899} \quad (\times 2) \\ \underline{1.12269} \quad (\times 2) \\ -3.89328 \quad (\times 2) \\ -4.04744 \quad (\times 1) \\ -4.27838 \quad (\times 1) \\ -7.81242 \quad (\times 1) \\ -9.18576 \quad (\times 2) \\ -12.6743 \quad (\times 2) \\ -14.1005 \quad (\times 1) \end{array} \right) \rightarrow \left(\begin{array}{c} N_c = \infty \\ \mathbf{5.54518} \quad (\times 3) \text{ 2CT} \\ \underline{0.67416} \quad (\times 3) \text{ 1CT} \\ -4.27838 \quad (\times 3) \text{ 1CT} \\ -7.81242 \quad (\times 3) \text{ 2CT} \\ -8.67983 \quad (\times 3) \text{ 1CT} \\ -10.0168 \quad (\times 3) \text{ 2CT} \end{array} \right)$$

Note that for $N_c = 3$ there are 15 eigenvalues while they are 18 for any other value of N_c . For the case $N_c = \infty$ we specify also the topology they belong to.

We track the flow from $N_c = 3$ to $N_c = \infty$: the first three highest eigenvalues (in bold) are moving to the same leading value (in bold) which corresponds to

two BFKL pomeron exchange (in two cylinder topology). The fourth and fifth highest eigenvalues (underlined) are instead moving to the leading eigenvalues of the one cylinder topology case (which are three instead of two because of the larger basis for $N_c > 3$). With very good approximation one finds that the N_c dependence of the leading eigenvalue E_0 is given by

$$E_0(N_c) = E_0(\infty) \left(1 + \frac{2.465}{N_c^2} \right). \quad (10.10)$$

One can see that for this toy model the large N_c approximation corresponds to an error of about 27%, an error which is not negligible because the coefficient of the leading correction to the asymptotic value, proportional to $1/N_c^2$, is a large number.

It is also easy to investigate the color-configuration space mixing which is encoded in the eigenvectors. Fixing $N_c = 3$, from numerical investigations we find that the leading eigenvector v_0 and the two closest subleading v_1 and v_2 have the following components:

$$v_0 \simeq \begin{pmatrix} 0.590 & P_1 Q_1 \\ 0.085 & P_1 Q_5 \\ 0.344 & P_{8A} Q_3 \\ 0.199 & P_{8S} Q_1 \\ 0.199 & P_{8S} Q_5 \\ 0.293 & P_{10+\bar{10}} Q_3 \\ 0.179 & P_{27} Q_1 \\ 0.574 & P_{27} Q_5 \end{pmatrix}, \quad v_1 \simeq \begin{pmatrix} 0.166 & P_1 Q_3 \\ 0.342 & P_{8A} Q_1 \\ 0.317 & P_{8A} Q_5 \\ 0.385 & P_{8S} Q_3 \\ 0.267 & P_{10+\bar{10}} Q_1 \\ 0.598 & P_{10+\bar{10}} Q_5 \\ 0.421 & P_{27} Q_3 \end{pmatrix}, \quad v_2 \simeq \begin{pmatrix} -0.775 & P_1 Q_1 \\ 0.002 & P_1 Q_5 \\ 0.008 & P_{8A} Q_3 \\ 0.123 & P_{8S} Q_1 \\ 0.114 & P_{8S} Q_5 \\ 0.268 & P_{10+\bar{10}} Q_3 \\ 0.151 & P_{27} Q_1 \\ 0.525 & P_{27} Q_5 \end{pmatrix}.$$

As one can see, the eigenvector v_0 , corresponding to the highest eigenvalue, is even, while the two fold degenerate next larger eigenvalue has eigenstates of both parities (v_1 odd and v_2 even).

In the large N_c limit case, the eigenvectors of the three fold degenerate leading eigenvalue of the 2 cylinder topology are:

$$w_0^{(2CT)} \simeq \begin{pmatrix} 1 & P_1 Q_1 \end{pmatrix} \quad w_1^{(2CT)} \simeq \begin{pmatrix} \frac{1}{3} & P_{10+10} Q_1 \\ \frac{\sqrt{5}}{3} & P_{10+10} Q_5 \\ \frac{1}{\sqrt{6}} & P_{27} Q_3 \\ \frac{1}{\sqrt{6}} & P_0 Q_3 \end{pmatrix} \quad w_2^{(2CT)} \simeq \begin{pmatrix} \frac{1}{\sqrt{3}} & P_{10+10} Q_3 \\ \frac{1}{3\sqrt{2}} & P_{27} Q_1 \\ \frac{\sqrt{5}}{3\sqrt{2}} & P_{27} Q_5 \\ \frac{1}{3\sqrt{2}} & P_0 Q_1 \\ \frac{1}{3\sqrt{2}} & P_0 Q_5 \end{pmatrix}.$$

Again also in this system we can track the same parity properties, which are invariant under the flow in N_c .

Similarly one may investigate the states associated to the one cylinder topology at $N_c = \infty$ and their corresponding partners at finite N_c . For brevity we just report here the two most relevant states in the N_c infinity limit:

$$w_0^{(1CT)} \simeq \begin{pmatrix} z_1 & P_{8A} Q_1 \\ z_3 & P_{8S} Q_3 \\ z_5 & P_{8A} Q_5 \end{pmatrix} \quad w_1^{(1CT)} \simeq \begin{pmatrix} z_1 & P_{8S} Q_1 \\ z_3 & P_{8A} Q_3 \\ z_5 & P_{8S} Q_5 \end{pmatrix} \quad w_2^{(1CT)} \simeq \begin{pmatrix} 0.245 & (P_0 Q_1 - P_{27} Q_1) \\ 0.663 & (P_0 Q_5 - P_{27} Q_5) \end{pmatrix}$$

where $z_1 \simeq 0.815$, $z_3 \simeq 0.405$ and $z_5 \simeq 0.415$. We stress that $w_2^{(1CT)}$ has no counterpart at $N_c = 3$.

10.2 TOY_{Adj,Fund}

We now move to study the toy model of case **b**) at the beginning of this chapter, again to see how the large N_c approximation works. It is described by the Hamiltonian

$$\mathcal{H}_{Adj,Fund} = -\frac{1}{N_c} \sum_{1 \leq k < l \leq n} \vec{T}_k \vec{T}_l \frac{\vec{\sigma}_k}{2} \frac{\vec{\sigma}_l}{2}, \quad (10.11)$$

acting on spin singlet states. Again we consider the large N_c limit. The one cylinder topology is associated to the well known Heisenberg XXX spin chain with Hamiltonian

$$\mathcal{H}_{Adj,Fund}^{1CT} = \frac{1}{2} \sum_{i=1}^n \frac{\vec{\sigma}_i}{2} \frac{\vec{\sigma}_{i+1}}{2}, \quad (10.12)$$

which we shall now consider for the case of $n = 4$ particle. In this case at large N_c we have, as before, also the two cylinder topology associated to the Hamiltonian

$$\mathcal{H}_{Adj,Fund}^{2CT} = 2 \frac{\vec{\sigma}_1}{2} \frac{\vec{\sigma}_2}{2}. \quad (10.13)$$

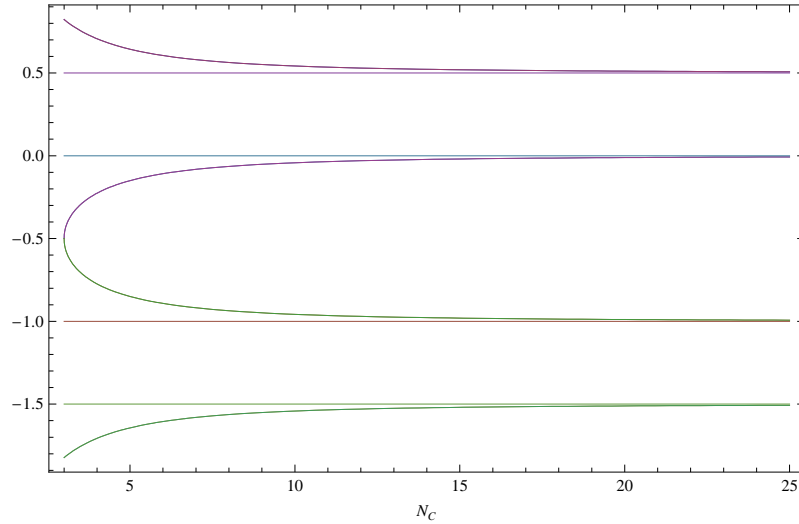


Figure 10.1: N_c dependence of the eigenvalues of the model $\text{TOY}_{\text{Adj,Fund}}$.

The spectrum for the one cylinder topology case is well known from Bethe Ansatz methods [75] and for total zero spin of a 4-particle spin chain the possible eigenvalues are 0 and -1 (see table II in [76] for $J = -1/2$ in their notation). The two cylinder topology is characterized by the eigenvalues $+1/2$ and $-3/2$.

At finite N_c we rewrite the Hamiltonian in a similar way to the BKP toy model case (see eq. (10.7) where the B and D matrices are defined for f the identity map and for the group $SU(2)$ in fundamental representation). At $N_c = 3$ it corresponds to a 10×10 matrix while for $N_c > 3$ it is given by a 12×12 matrix. The leading eigenvalue as function of N_c can be easily computed

$$E_0(N_c) = \frac{\sqrt{10N_c^2 + 36 + 6\sqrt{N_c^4 + 36N_c^2 + 36}} - 2N_c}{4N_c} \quad (10.14)$$

and indeed goes to the value $1/2$ in the large N_c limit. Let us note that if one considers the planar approximation (in the 2CT configuration), the leading eigenvalue would be underestimated with a relative error of $(E_0(3) - E_0(\infty)) / E_0(3) \simeq 40\%$ w.r.t. the case $N_c = 3$. In Fig. 10.1 we report the N_c dependence of all the eigenvalues in the range $3 \leq N_c \leq 25$.

Similar models, but in a higher spin representation, can be constructed in order to maintain the integrability in the large N_c limit. One simply needs to con-

sider for any irreducible representation s of the particles the function f to be a corresponding specific polynomial as described in [75].

10.3 TOY_{AllFund}

This section is devoted to check in one specific case that our approach gives result in agreement with other methods widely used in spectroscopy.

We start by considering a system of n particles in the bifundamental representation of $SU(N_c) \times SU(2)$, characterized by an Hamiltonian (10.1) (with f the identity function)

$$\mathcal{H}_n = -\frac{1}{N_c} \sum_{1 \leq k < l \leq n} \vec{T}_k \vec{T}_l \vec{S}_k \vec{S}_l, \quad (10.15)$$

which can be written in terms of the quadratic Casimir operators of $SU(N_c)$, $SU(2)$ and $SU(2N_c) \supset SU(N_c) \times SU(2)$ (see [82]).

Indeed the tensor products of $\vec{T}_k \vec{S}_l$ are amongs the generators of $SU(2N_c)$, so it is useful to introduce the entire algebras for this group

$$\alpha_k = \begin{cases} \frac{1}{\sqrt{N_c}} S_l & k = 1, 2, 3 = l \\ \frac{1}{\sqrt{2s+1}} T_a & k = 4, \dots, N_c^2 + 2; a = 1, \dots, N_c^2 - 1 \\ \sqrt{2} T_k S_l & k = N_c^2 + 3, \dots, 4N_c^2 - 1; l = 1, 2, 3 \end{cases} \quad (10.16)$$

with the normalization $Tr(\alpha_k \alpha_{k'}) = 1/2 \delta_{kk'}$. The Hamiltonian for this system can be rewritten as

$$\mathcal{H}_{AllFund} = -\frac{1}{4N_c} \left[\mathcal{C}_{2N_c} - \frac{1}{N_c} \mathcal{C}_{N_c} - \frac{1}{2s+1} \mathcal{C}_2 - 2n \frac{N_c^2 - 1}{2N_c} s(s+1) \right], \quad (10.17)$$

where the quadratic Casimir operators \mathcal{C}_n are defined as in [82] and $s = 1/2$. Note that all the operators introduced above depend on the irreducible representation of the symmetry group to which they refer to.

We are interested in the real representations so we set $N_c = 2$ and consider the case of only four particles. The symmetry group of the model becomes $SU(2) \otimes SU(2) \subset SU(4)$ and eq. (10.17), written for the four particle in a global singlet state, takes the form

$$\mathcal{H}_{AllFund} = -\frac{1}{8} \left[\mathcal{C}_4(\mathcal{R}) - \frac{9}{2} \right]. \quad (10.18)$$

$SU(2) \otimes SU(2)$	$SU(4)$	$(\mu_1, \mu_2, \mu_3) \equiv \mathcal{R}_{SU(4)}$
$\mathbf{1} \otimes \mathbf{1}$	1, 20, 35	$(0, 0, 0)(0, 2, 0)(4, 0, 0)$
$\mathbf{1} \otimes \mathbf{3}$	15, 45	$(1, 0, 1)(2, 1, 0)$
$\mathbf{1} \otimes \mathbf{5}$	20	$(0, 2, 0)$
$\mathbf{3} \otimes \mathbf{3}$	15, 20, 35, 45	$(1, 0, 1)(0, 2, 0)(4, 0, 0)(2, 1, 0)$
$\mathbf{3} \otimes \mathbf{5}$	45	$(2, 1, 0)$

Table 10.1: Correspondence between *irreps* of $SU(4)$ and $SU(2) \otimes SU(2)$

In order to find its spectrum the next step consists in analyzing the irreducible representation content of each symmetry group of the model. So, for four particles with spin $1/2$, one has (we specify also the multiplicity)

$$\mathbf{2} \otimes \mathbf{2} \otimes \mathbf{2} \otimes \mathbf{2} = 2(\mathbf{1}) + 3(\mathbf{3}) + \mathbf{5}, \quad (10.19)$$

and in the $SU(4)$ case

$$\mathbf{4} \otimes \mathbf{4} \otimes \mathbf{4} \otimes \mathbf{4} = \mathbf{1} + 3(\mathbf{15}) + 2(\mathbf{20}) + \mathbf{35} + 3(\mathbf{45}). \quad (10.20)$$

Then we need to study the $SU(2) \otimes SU(2)$ content of these $SU(4)$ *irrep*. This can be done using the results of [83] and in particular the entries of table 1, where the values in the third column are Dynkin indices.

So for particles in a total singlet state ($\mathbf{1} \otimes \mathbf{1}$) the Hamiltonian in eq. (10.18) admits four eigenvalues, each for a different *irrep* of $SU(4)$, with a 2-fold degenerate eigenvalue corresponded to $\mathbf{20}_{SU(4)}$ (see eq. (10.20)):

$$\begin{cases} -\frac{15}{16}, & \text{for } \textit{irrep} \mathbf{35} \\ -\frac{3}{16} \quad (2x), & \text{for } \textit{irrep} \mathbf{20} \\ +\frac{9}{16}, & \text{for } \textit{irrep} \mathbf{1} \end{cases} \quad (10.21)$$

and these are in perfect agreement with the spectrum evaluated with the method used previously throughout the paper (we take advantage from the formulas of [84] for the eigenvalues of a quadratic Casimir operator as functions of the Dynkin indices).

As a final remark we want to emphasize that the method of writing the Hamiltonian in terms of the Casimirs can be applied to systems with any number of particles (at the price, increasing their number, of a growing complexity in the in-

duced irreducible representations) and moreover the analysis may not be restricted to singlet subspaces. Unfortunately it is not clear how to define a method for interacting particle not in the bifundamental representation.

Chapter 11

Conclusions

We have introduced a family of dynamical models describing interacting particles with color and spin degrees of freedom. The main motivation was to study within this framework how much the large N_c approximation is significant when one is trying to extract the spectrum of these quantum systems.

Indeed in some relevant physical cases the only results available are restricted to the case with a planar structure resulting from the large N_c approximation, when integrability arises and gives the possibility to exactly solve the problem. These facts are seen when considering QCD scattering amplitudes in the Regge limit and LLA approximation, characterized by the BKP dynamics.

We have focused our study on the case of four particles and considered in details three toy models. One toy model (case **c**) at the beginning of chapter 10) was used to test our computational method based on group theory, since one is able to make a direct comparison with results already known from other methods used in spectroscopy.

The first model presented (case **a**), chapter 10) is aimed to mimic to some extent the behavior of the 4 gluon BKP kernel, since we have forced it to have in the large N_c limit the same leading eigenvalues of the BKP system for both one and two cylinder topologies. We were able to compute the different eigenvalues of this toy model as function of N_c and we have found that the leading one at $N_c = 3$ present corrections of almost 30% w.r.t. the planar approximation, which one may understand in terms of a large coefficient in the $1/N_c^2$ correction term. The mixing in color-spin configuration structure has been also studied.

Another model (case **b**) chapter 10) was considered since in the large N_c limit it gives rise to the one cylinder topology Heisenberg XXX spin chain which is

integrable. For the spin $1/2$ case we have found at finite $N_c = 3$ corrections to the leading eigenvalue of about 40%.

We remark that our analysis is restricted to study the toy model Hamiltonians on the space of states which are singlet with respect to the $SU(2)$ “spin” configurations. Although this choice was dictated by technical reasons, we believe it will be significant to extend this investigation to all the other possible states.

These kind of models and possibly more general ones appear to be interesting also by themselves and we feel that they deserve more studies in order to see, for example, if some remnant from integrability can be traced back at finite N_c .

transformation to work with a symmetric crossing matrix. For this purpose it is sufficient to introduce the matrix $\Delta = \text{diag}(d_i)$ and define the new symmetric matrix $C \rightarrow \Delta^{-\frac{1}{2}}C\Delta^{\frac{1}{2}}$ which acts on the vectors with components $v^i \rightarrow (\Delta^{-\frac{1}{2}}v)^i$.

Part III

Quiver Gauge Theories from orbifolded AdS/CFT

Chapter 12

Introduction

Quiver gauge theories possess a gauge group which is generically a product of $U(N_i)$ factors with matter fields in bifundamental representations. They have been studied in the physics literature since the 1980s for composite model building, but recently they have attracted much attention because of their natural appearance in the duality between superstrings and gauge theories [85]. There are two important reasons why quiver gauge theories are suitable for particle physics model building. First, while an $SU(N)$ gauge theory is typically anomalous for arbitrary choice of fermions, it is not the case if the fermions lie on a quiver. Furthermore the fermions in a quiver arrange themselves in bifundamental representations of the product gauge group and this agrees with the fact that all known fundamental fermions are in bifundamental, fundamental, or singlet representations of the underlying gauge group.

The study of quiver gauge theories goes back to the earliest days of gauge theories and the Standard Model. Other notable early examples are the Pati-Salam model [19, 86] and the trinification model [87]. Starting from $AdS_5 \times S^5$ we have an highly supersymmetric ($\mathcal{N} = 4$ supersymmetries) gauge theory with a single $SU(N)$ gauge group and with matter in adjoint representations. This theory is well known to be conformally invariant [88], but to make the theory more interesting from a phenomenological point of view, we must break SUSY and generate a quiver gauge theory. In order to do this there are several options open to us. Orbifolds [89, 90, 91, 92], conifolds [93, 94, 95, 96, 97], and orientifolds [98, 99, 100, 101, 102, 103] have all played a part in building quiver gauge theories. Since our focus is quiver gauge theories via orbifolding of $AdS_5 \times S^5$, we will not discuss the other options in detail. In building models from orbifolded $AdS_5 \times S^5$,

it is often convenient to break the quiver gauge group to the trinification group $SU^3(3)$ or to the Pati-Salam group $SU(4) \otimes SU(2) \otimes SU(2)$, but there are again other possibilities, including more complicated intermediate groups like the quartification symmetry $SU^4(3)$ [104] that treats quarks and leptons on an equal footing. It is important to note that although the duality with superstrings is a significant guide to such model building, and it is desirable to have a string dual to give more confidence in consistency, we shall focus on the gauge theory description in the approach to particle phenomenology, as there are perfectly good quiver gauge theories that have yet to be derived from string duality.

Back to the $\mathcal{N} = 4$ SYM, by replacing the manifold S^5 by an orbifold (see Appendix A for a geometrical and group theoretical illustration of some simple orbifolding) S^5/Γ one arrives at a theory with less supersymmetries corresponding to $\mathcal{N} = 2, 1$ or 0 , depending [12] on whether: (i) $\Gamma \subset SU(2)$, (ii) $\Gamma \subset SU(3)$ but not in $SU(2)$, or (iii) $\Gamma \subset SU(4)$ but not in $SU(3)$ respectively. Here Γ is in all case a finite group embedded in the isometry $SU(4) \sim O(6)$ of S^5 in the three-dimensional complex space $\mathcal{C}_3 \sim \mathcal{R}_6$.¹

The most general abelian Γ (it is also possible to consider non abelian cases [15]) is made up of the basic units Z_n , the order n cyclic groups formed from the n th roots of unity. Let us define $\alpha = \exp(2\pi i/n)$ and specify the embedding of $\Gamma = Z_n$ giving three integers a_1, a_2, a_3 as

$$\mathcal{C}_3 : (X_1, X_2, X_3) \xrightarrow{Z_n} (\alpha^{a_1} X_1, \alpha^{a_2} X_2, \alpha^{a_3} X_3) \quad (12.1)$$

so that the discrete group Z_n identifies n points in \mathcal{C}_3 . The N converging D3-branes meet on all n copies, giving a gauge group $U(N)^n$ [85]. The matter (spin 1/2 and spin 0 fields) which survives is invariant under a product of a gauge transformation (from the quiver group) and a Z_n transformation.

There is a convenient way to find the matter and interactions using an associated “quiver” or “moose” diagram. It consist of one node for each irreducible representation of Γ (i.e. n nodes if $\Gamma = Z_n$) and fermionic and bosonic arrows connecting the nodes according to how the four- and six-dimensional representations of Γ (inherited from $SU(4)$) act on each irreducible representation, i.e. depending on the values of the integers a_1, a_2, a_3 . To each bosonic/fermionic arrows from node i to node $i + a_k$ we associate a bifundamental (N_i, \bar{N}_{i+a_k}) scalar/Weyl fermion (for

¹Although $O(6)$ and $SU(4)$ have the same local structure, i.e. Lie algebra, globally $O(6)$ is doubly-covered by $SU(4)$ and this distinction is important to study the consistency conditions for AdS/CFT embeddings [105].

$i = i + a_k$, i.e. $a_k = 0$, this correspond to an adjoint representation). A line direct away from a node corresponds to a set of scalar or Weyl fermions transforming as the fundamental representation of the gauge group, while a line direct towards a node corresponds to a set of scalar or Weyl fermions transforming as the complex conjugate of the fundamental representation (antifundamental). There is a Yukawa coupling for each triangle on the quiver, consisting of two fermionic arrows and a bosonic arrow, and quartic scalar interactions for each square on the quiver, consisting of four bosonic arrows. The resulting gauge theory is chiral, i.e. the fermions are all left handed, if and only if Γ is a complex subgroup of $SU(4)$, i.e. if $\mathbf{4}$ and $\bar{\mathbf{4}}$ of $SU(4)$ are inequivalent representations of Γ .

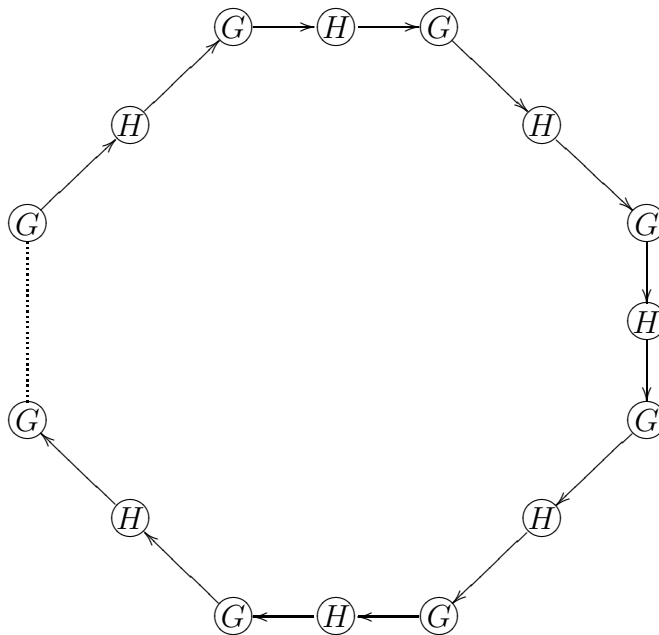


Figure 12.1: A $G^m \times H^m$ quiver diagram. In our case $G = H = SU(N)$ and $2m = n$. Each side of this polygon describes fermions (or scalars) transforming under the three gauge groups associated with this side, $G_i \times H_i \times G_{i+1}$, as $(N, \bar{N}, 1)$.

We remark that here and in the follow we designate *fermions* the representation $\mathbf{4}$ of the underlying R -symmetry group and *scalars* the representation $\mathbf{6}$. It could appear strange at a first look since is usual to associate this names to representations of the Lorentz group, but here we are constructing models starting from the orbifolding of $\mathcal{N} = 4$ SYM, so we can backtrace there to find an explanation [88].

For a general quiver the scalar representation contains the bifundamental scalars $\sum_{k=1}^3 \sum_{i=1}^n (N_i, \bar{N}_{i+a_k})$.

In the case of fermions, the first thing to do is to construct the fundamental representation of the R -parity $SU(4)$. Starting from the set $\{a_1, a_2, a_3\}$, we can write the embedding as $4 = (\alpha^{A_1}, \alpha^{A_2}, \alpha^{A_3}, \alpha^{A_4})$, with

$$\begin{aligned} A_1 &= \frac{1}{2}(a_1 + a_2 + a_3) \\ A_2 &= \frac{1}{2}(a_1 - a_2 - a_3) \\ A_3 &= \frac{1}{2}(-a_1 + a_2 - a_3) \\ A_4 &= \frac{1}{2}(-a_1 - a_2 + a_3) \end{aligned} \tag{12.2}$$

Notice that specifying the four component of A_μ is equivalent to fixing the three a_k , because the constraint: $\sum_\mu A_\mu = 0 \pmod{n}$ [105]. In general the fermion representations contains the bifundamentals $\sum_{\mu=1}^4 \sum_{i=1}^n (N_i, \bar{N}_{i+a_k})$.

We introduce the shorthand notation of write the fundamental representation as $4 = (A_1, A_2, A_3, A_4)$. Consider now the 6 of $SU(4)$, which is the antisymmetric part of (4×4) . In the shorthand notation, this can be written as $6 = (A_1 + A_4, A_2 + A_4, A_3 + A_4, A_1 + A_2, A_2 + A_3, A_3 + A_1)$. For example, a $\mathcal{N} = 0$ quiver gauge field theory based on an orbifolding with Z_n have the 4 of $SU(4)$ defined by four nonvanishing integers A_μ satisfying $A_1 + A_2 + A_3 + A_4 = 0 \pmod{n}$. This is a necessary and sufficient condition for a consistent abelian orbifolding to $\mathcal{N} = 0$.

Our goal will be to examine how the framework of quiver gauge theories can accommodate, as a sub theory, the Standard Model. This requires that the SM gauge group and the three families of quarks and leptons with their correct quantum numbers must be accommodated. In such model building a stringent requirement is that the scalar sector, prescribed by the quiver construction, can, by acquiring vacuum expectation values, break the symmetry spontaneously to the desired sub theory. This is unlike most other model building where one chooses the representations for the scalars to accomplish this goal. We remark that here the representations for the scalars are dictated by the orbifold construction.

One useful guideline in the symmetry breaking is that to break a semi-simple $SU(N)^n$ gauge group to its $SU(N)$ diagonal subgroup requires at least $(n - 1)$ bifundamental scalars connected to one another, such that each of the n $SU(N)$ factors is linked to all of the others. It would be insufficient if the bifundamental

scalars fragment into disconnected subsets.

We shall describe later on a novel abelian orbifold that leads to the accommodation of the Standard Model in the unified group $SU(4)^7$ [26].

Recently, it has been given a complete classification [107, 108] of all $\mathcal{N} = 0$ and $\mathcal{N} = 1$ SUSY models that come from orbifolding $AdS_5 \otimes S^5$ with an abelian group Γ of order less than 12, where Γ embeds irreducibly in the $SU(4)$ isometry or in an $SU(3)$ subgroup of the $SU(4)$ isometry, respectively. This means that, to achieve $\mathcal{N} = 0$, $rep(\Gamma) \rightarrow 4$ of $SU(4)$ must be embedded as $4 = (\mathbf{r})$, where \mathbf{r} is a nontrivial four dimensional representation of Γ ; for $\mathcal{N} = 1$, $rep(\Gamma) \rightarrow 4$ of $SU(4)$ must be embedded as $4 = (\mathbf{1}, \mathbf{r})$, where $\mathbf{1}$ is the trivial singlet of Γ and \mathbf{r} is nontrivial.

We want to focus on non-supersymmetric theories. One motivation for studying the nonSUSY case is that the need for supersymmetry is less clear in conformal field theories (in 1998 Frampton [14] conjectured that such nonsupersymmetric orbifolded models can be conformally invariant) as: (1) the hierarchy problem is absent or ameliorated, (2) the difficulties involved in breaking the remaining $\mathcal{N} = 1$ SUSY can be avoided if the orbifolding already results in $\mathcal{N} = 0$ SUSY, and (3) many of the positive effects of SUSY are still present in the theory, although just hidden.

For $\mathcal{N} = 0$ the fermions are given by $\sum_i \mathbf{4} \otimes R_i$ and the scalars by $\sum_i \mathbf{6} \otimes R_i$ where the set R_i runs over all the irreps of Γ . For Γ abelian, for example $\Gamma = Z_n$, the irreps are all one dimensional and as a consequence of the choice of N in the $1/N$ expansion, the gauge group is $SU^n(N)$ [13]. Moreover we remark that chiral models require the $\mathbf{4}$ to be complex, while the $\mathbf{6}$ must be real for a proper embedding of nonsupersymmetric models.

With this background at hand, we are able to build nonSUSY chiral models. We choose² $N = 4$ throughout, in such a way that our model will proceed to the SM via Pati-Salam group.

In following chapter, starting from the classification of Kephart and Pas (2004) (see Appendix B for a summary of their results), we illustrate our search for a minimal (respect to the order of $\Gamma = Z_n$) nonSUSY model (for a SUSY version see [109]) that have SM particles as a subset of its particle content. To do this we have used symmetry breaking paths that contain the Pati-Salam (PS) group as a subgroup before reaching the SM. The minimal model of this type has symmetry group $SU^7(4)$, hence orbifolding group is Z_7 , as we will discuss.

The running of the coupling constants predicted by the model depends strongly

²In general what choice of N leads to the “optimal” model is still an open question [15].

on the scalar content. In fact, since there are scalars in addition to the usual SM Higgs sector, they can contribute to the running of the beta functions. After a presentation of the model and of the SSB chain that leads to the SM particle content, we show that, with the use of a judicious choice of the scalar sector, unification can be achieved at the very low scale $M_{GUT} \sim 5$ TeV. We then conclude with a few comments on the phenomenology of the model including proton decay constraints and dark matter.

Chapter 13

A modified Pati-Salam Model

In this chapter we consider a model built on $AdS_5 \otimes S^5/\Gamma$ orbifold compactifications of the type *IIB* superstring, where Γ is the abelian group Z_7 . This result in an attractive three family $\mathcal{N} = 0$ SUSY model, that is a modified Pati-Salam Model which reduced to the Standard Model after symmetry breaking of the initial quiver gauge group $SU(4)^7$. Moreover it is *anomaly free* because the SM fermions come from representation of the initial $SU(4)^7$ group that lie on a quiver and it is interesting from a phenomenological point of view due to an unification scale in the LHC energy regime.

13.1 Description of the model

We have systematically gone through all chiral models with $\Gamma = Z_n$ (see Appendix B for a review). All fail to have a PS type intermediate stage until $n = 7$. Hence after considerable exploration, we are lead to choose $\Gamma = Z_7$ and $N = 4$ with orbifold group embedding $4 = (\alpha, \alpha, \alpha^2, \alpha^3)$, so $6 = (\alpha^2, \alpha^3, \alpha^3, \alpha^4, \alpha^4, \alpha^5)$. This yield an $\mathcal{N} = 0$ SUSY model based on the gauge group $SU(4)^7$. The particle spectrum of the unbroken theory at the string scale is given by the fermion states

$$2[(4\bar{4}11111)_F + \dots] + [(41\bar{4}1111)_F + \dots] + [(411\bar{4}111)_F + \dots] \quad (13.1)$$

and scalars (a proper embedding, i.e. $6 = \bar{6}$, led to an extra factor 2)

$$2[(41\bar{4}1111)_S + \dots] + 4[(411\bar{4}111)_S + \dots] + \\ + 4[(4111\bar{4}11)_S + \dots] + 2[(41111\bar{4}1)_S + \dots] \quad (13.2)$$

of $SU(4)^7$, as result from the associated quiver diagrams of Fig 13.1 and where the dots mean cyclic permutations (due to the Z_7 case that we are considering, there are seven states between square brackets).

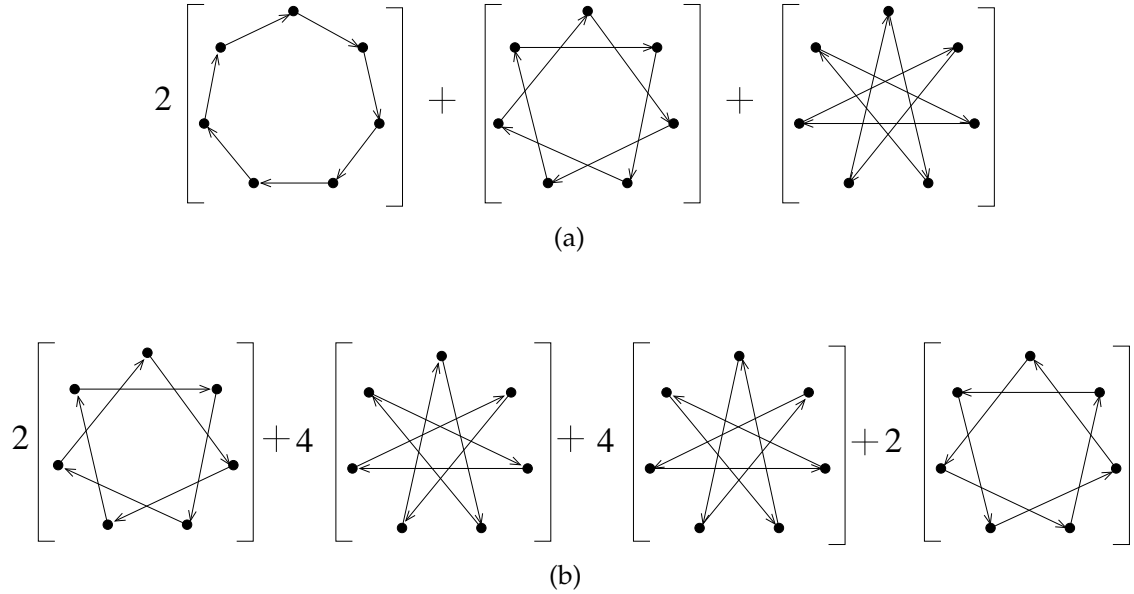


Figure 13.1: Fermion **(a)** and scalar **(b)** quiver diagram for the model M_{1123}^7 (see appendix B for this notation). There are seven nodes as the quiver gauge group is $SU(4) \otimes \dots \otimes SU(4)$ seven times. A line direct away from a node corresponds to a set of scalar or Weyl fermions transforming as the fundamental representation of the gauge group, while a line direct towards a node corresponds to a set of scalar or Weyl fermions transforming as the complex conjugate of the fundamental representation (antifundamental). Notice that, in the scalar case, the third diagram is the hermitian conjugate (h.c.) of the second and the last is the h.c. of the first, since the only thing different among them is the direction of the arrows.

The quiver gauge group $SU(4)^7$ is broken down to $SU(4)^3$ via diagonal subgroups by sequentially assigning vacuum expectation values (VEVs) to

$$\begin{aligned}
 &(14\bar{1}\bar{4}111)_S, \\
 &(114\bar{4}\bar{1}1)_S, \\
 &(114\bar{4}1)_S, \\
 &(114\bar{4})_S.
 \end{aligned}$$

The rule to break the symmetry (diagonally) is given by [112]

$$SU(N) \times SU(N) \rightarrow SU(N)_D, \quad (N, \bar{N}) \rightarrow 1 + (N^2 - 1) = 1 + \text{adj}, \quad (13.3)$$

where, in our case, $N = 4$. Notice that in this “diagonal symmetry breaking” the number of generators is not conserved: we start from an $SU(N) \times SU(N)$ group with $(N^2 - 1) + (N^2 - 1)$ generators to go into a diagonal subgroup $SU(N)_D$ with only $N^2 - 1$ generators. This is encoded in the fact that at each step of the symmetry breaking chain we generate an $N^2 - 1$ representation plus a singlet for each couple of broken representation $(\dots N \dots \bar{N} \dots)$, but, in the breaking of the scalar states, only one of this adjoint representation survives. We remark that when we break the symmetry, some of the particles get a mass. These particles can be integrated out in an effective theory, as they are heavy compared to the masses of the Standard Model particles. No degrees of freedom are lost, but some are too heavy to excite. Moreover notice that the bosons are not present in the initial model but they arise after a diagonal breaking on the scalar states. For this reason, in what follow, the bosons are part of the scalar content.

This procedure leaves **chiral fermions** in the following bifundamental representations of $SU(4)^3$:

$$3 [(4\bar{4}1) + (14\bar{4}) + (\bar{4}14)]_F \quad (13.4)$$

and scalars

$$\begin{aligned} 4 [(4\bar{4}1) + h.c.]_S + 8 [(41\bar{4}) + h.c.]_S + 16 [(14\bar{4}) + h.c.]_S \\ 21 [(1, 1, 15)]_S + 3(1, 15, 1)_S \\ 28 [(111)]_S. \end{aligned} \quad (13.5)$$

We can check the degrees of freedom in our results. For example, the sum of scalar degrees of freedom (*sdof*) in (13.2) (i.e. at the level of $SU(4)^7$) is $12 \times [16 \times 7] = 1344$, while now we have $sdof_{SU(4)^3} = 1284$, with a difference of 60 that is 4×15 due to the above considerations about the diagonal symmetry breaking, being 15 the *dof* associated to an adjoint representation.

We continue the chain of spontaneous symmetry breaking toward the Pati–Salam model. From now on we will use symmetry breaking that preserve the number of *dof* that we have at this level, i.e. when the symmetry group is $SU(4)^3$.

We consider a VEV for the scalar state ($4\bar{4}1$) of the form

$$\begin{pmatrix} 1 & 0 & 0 & 0 \\ 0 & 1 & 0 & 0 \\ 0 & 0 & 1 & 0 \\ 0 & 0 & 0 & -3 \end{pmatrix},$$

up to an extra factor and addition of unity matrix. Notice that the dimension of the matrix reflect the dimension of the representation that we are breaking (i.e. 4 and $\bar{4}$) and that this form leaves a 3×3 block invariant. The diagonal entries are chosen fixing the normalization of the $U(1)$ charges (the values putted below as underscripts of each state) by the branching rules [112]:

$$SU(4) \rightarrow SU(3) \times U(1), \quad 4 \rightarrow 1_1 + 3_{-1/3}, \quad (13.6)$$

together with $\bar{4} \rightarrow 1_{-1} + \bar{3}_{1/3}$ for the antifundamental representation of $SU(4)$. This breaks the first two $SU(4)$ and the symmetry group became $SU(3) \otimes SU(3) \otimes SU(4) \otimes U(1)_A$ (see [110, 111] for a detailed study of the phenomenology of this model without $U(1)_A$ charge), with the $U(1)_A$ charge calculated simply summing the charges that comes from each $SU(4) \rightarrow SU(3) \times U(1)$ breaking. Among the other states we have also three $U(1)_A$ neutral $(3\bar{3}1)_0$ scalars.

Finally the break of $SU(3)$ into $SU(2) \times U(1)$, with $3 \rightarrow 1_1 + 2_{-1/2}$ ($\bar{3} \rightarrow 1_{-1} + 2_{1/2}$), is obtained giving a VEV of the form

$$\begin{pmatrix} 1 & 0 & 0 \\ 0 & 1 & 0 \\ 0 & 0 & -2 \end{pmatrix},$$

with the same prescriptions as above, to one of these $(3\bar{3}1)_0$ scalars. In this way we arrive at the gauge symmetry group

$$SU(2)_L \otimes SU(2)_R \otimes SU(4)_C \otimes U(1)_A \otimes U(1)_B$$

that resemble the Pati-Salam model group $SU(2)_L \otimes SU(2)_R \otimes SU(4)_C$. We have add to each group an underscript: *R-Right*, *L-Left*, *C-Color*, for a reason that we will clarify in the follow. At this stage the scalars content is given by Table 13.1.

In order to reach the Standard Model we must go on with the symmetry break-

Scalars of $SU(2)_L \otimes SU(2)_R \otimes SU(4)_C \otimes U(1)_A \otimes U(1)_B$	
$24 [(11\bar{4})_{1,0} + (11\bar{4})_{-1/3,1} + h.c.]$	$8 [(21\bar{4})_{-1/3,-1/2} + h.c.]$
$16 [(12\bar{4})_{-1/3,-1/2} + h.c.]$	$21 [(1, 1, 15)_{0,0}]$
$8(221)_{0,0} + 3 [(211)_{-4/3,-1/2} + h.c.]$	$3 [(211)_{0,-3/2} + h.c.]$
$6 [(121)_{4/3,1/2} + h.c.]$	$6 [(121)_{0,-3/2} + h.c.]$
$9 [(111)_{4/3,-1} + h.c.]$	$48 [(111)_{0,0}] + 3(131)_{0,0}$

Table 13.1: Scalars of the generalized Pati-Salam model.

ing considering

$$\begin{aligned} SU(4)_C &\rightarrow SU(3)_C \times U(1)_X, \\ SU(2)_R &\rightarrow U(1)_Z. \end{aligned}$$

This can be accomplished by giving a VEV to a scalar in the $(12\bar{4})_{-1/3,-1/2}$ representation, which leads to the group $SU(2)_L \times SU(3)_C$ and three $U(1)$ factors. More precisely this would result in four $U(1)$ factors, but one linear combination is broken due to the non-zero $U(1)$ charges of $(12\bar{4})_{-1/3,-1/2}$, so we can't combine the charge as above simply summing them. For this reason we write these four charge as superscripts in order to fix the normalization later.

Under the group structure $SU(2)_L \times SU(3)_C \times U(1)_X \times U(1)_Z \times U(1)_A \times U(1)_B$, the scalar state $(12\bar{4})_{-1/3,-1/2}$ decomposes as

$$(1\bar{3})_{1/3,1,-1/3,-1/2} + (11)_{-1,1,-1/3,-1/2} + (1\bar{3})_{1/3,-1,-1/3,-1/2} + (11)_{-1,-1,-1/3,-1/2},$$

and similarly for another scalar representation of the same semi-simple group

$$(11\bar{4})_{-1/3,1} \longrightarrow (1\bar{3})_{1/3,0,-1/3,1} + (11)_{-1,0,-1/3,1}.$$

Therefore giving a VEV also to $(11)_{-1,1,-1/3,-1/2}$, $(11)_{-1,0,-1/3,1}$ and the additional scalar $(11)_{0,0,4/3,-1}$, can break $SU(2)_L \times SU(2)_R \times SU(4)_C \times U(1)_A \times U(1)_B$ directly down to $SU(2)_L \times SU(3)_C$ along with a single $U(1)$ formed by a linear combina-

tion of four $U(1)$ factors.

Since we are breaking three combinations of four $U(1)$ charges we must ensure that there exists a normalization pattern that will result in the remaining $U(1)$ being the usual hypercharge of the Standard Model. Starting from the well know Gell Mann-Nishima relation $Q = T_3 + Y$, with Q being the electric charge, T_3 the third isospin component and Y the hypercharge, we can choose a suitable normalization of the charges A, B, X and Z . To this aim we can impose, for example, that the hypercharge Y of the scalar states $(11)_{-1,1,-1/3,-1/2}$, $(11)_{-1,0,-1/3,1}$, $(11)_{0,0,4/3,-1}$ and $(11)_{-1,1,-1/3,-1/2}$ must be zero. The result is a system of four equations that led to a linear combination of the charges in the form

$$xX + zZ + aA + bB = Y, \quad x = \frac{1}{4}, \quad z = \frac{1}{2}, \quad a = \frac{1}{4}, \quad b = \frac{1}{3}. \quad (13.7)$$

So far we have completed the path of symmetry breaking reaching the Standard Model gauge group $U(1)_Y \otimes SU(2)_L \otimes SU(3)_C$. The fermion content from Eq. (13.4) becomes the three chiral families of the Standard Model (see Table 13.3) plus the following vectorlike states: eight adjoints of $SU(3)_C$ and one adjoint of $SU(2)_L$. Moreover there are numerous right handed neutrinos. The scalar content is given in Table 13.2.

Scalars of $U(1)_Y \otimes SU(2)_L \otimes SU(3)_C$	
8 $[(23)_{1/6} + h.c.]$	84 $[(\bar{1}\bar{3})_{1/3} + h.c.]$
16 $[(13)_{2/3} + h.c.]$	22 $[(21)_{1/2} + h.c.]$
31 $[(11)_{-1} + h.c.]$	21 $[(18)_0]$
237 $(11)_0$	

Table 13.2: Scalars at the Standard Model level.

13.2 Phenomenology

In the previous section, the symmetry breaking of the initial $SU(4)^7$ towards to $SU(4)_L \otimes SU(4)_R \otimes SU(4)_C$ gauge group was performed by allowing the states

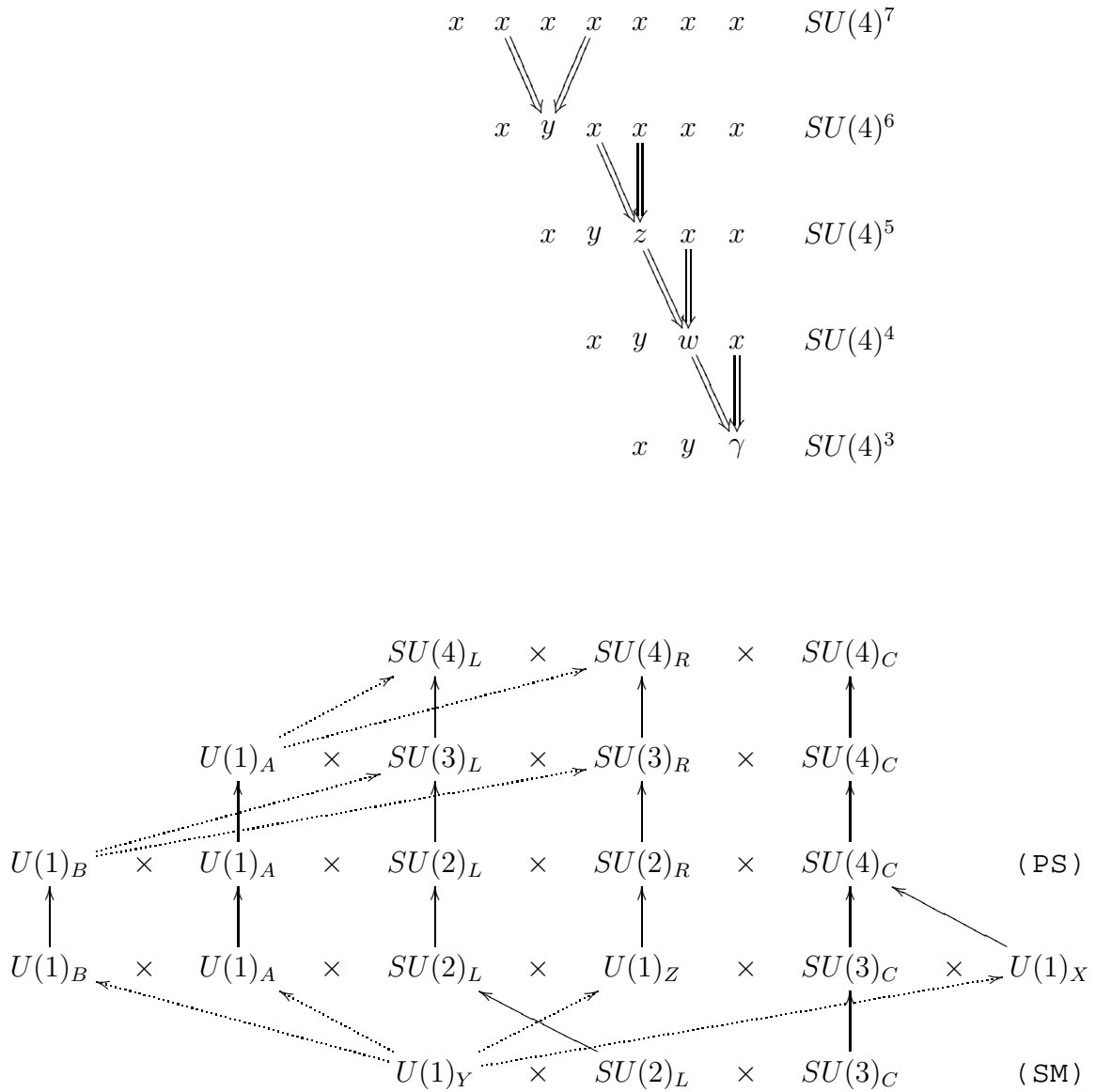


Figure 13.2: Symmetry Breaking “tree”. The break of the initial quiver gauge group $SU(4)^7$ is obtained by diagonal symmetry breaking (upper part of the diagram). The resulting $SU(4)^3$ group is then broken until we reach the Standard Model gauge group, as pictured in the lower part of the diagram where the continuous arrows mean a complete embedding, while the dotted arrows refer to a partial embedding.

SM Fermions	
$3 [(23)_{1/6}]$	$3 [(\bar{1}\bar{3})_{1/3}]$
$3 [(13)_{-2/3}]$	$3 [(21)_{-1/2}]$

Table 13.3: Chiral (left handed) families of the Standard Model

$(141\bar{4}111)_S$, $(114\bar{4}11)_S$, $(114\bar{4}1)_S$, $(114\bar{4})_S$ to obtain VEVs. This makes clear that $SU(4)_L$, $SU(4)_R$ and $SU(4)_C$ are embedded in diagonal subgroups $SU(4)^p$, $SU(4)^q$ and $SU(4)^r$ of $SU(4)^7$, respectively. We then embed all of $SU(2)_L$ in $SU(4)_L$, but for $U(1)_Y$ the embedding is slightly more complicated. In fact we need to go back to Eq. (13.7) to read the fraction of $U(1)_Y$ embedded in each of the $U(1)_{X,Z,A,B}$ factors. Moreover we embed all of $U(1)_X$ in $SU(4)_C$, all of $U(1)_Z$ in $SU(4)_R$, $1/2$ of $U(1)_{A,B}$ in $SU(4)_L$ and the other $1/2$ in $SU(4)_R$. This path is showed in Fig 13.2. Finally, recalling that in GUTs is usual to normalize the coupling constants in such a way that [115] $\alpha_1 = 5/3\alpha_Y$, the ratio α_2/α_1 turns out to be

$$\frac{\alpha_2}{\alpha_1} = \frac{3}{5} \frac{\alpha_2}{\alpha_Y} = \frac{3}{5} \left[\frac{\frac{1}{4}r + \frac{1}{2}q + \frac{1}{4} \left(\frac{p+q}{2} \right) + \frac{1}{3} \left(\frac{p+q}{2} \right)}{p} \right]$$

and $\sin^2 \theta_W$ satisfies (see [115] and references therein)

$$\sin^2 \theta_W(M_{GUT}) = \frac{3}{3 + 5 \left(\frac{\alpha_2}{\alpha_1} \right)} = \frac{24p}{6r + 31p + 19q}. \quad (13.8)$$

In our model $n = 7$, $r = 4$, $p = 1$ and $q = 2$ gives

$$\sin^2 \theta_W(M_{GUT}) = 8/31 \simeq 0.26,$$

very close to the measured value $\sin^2 \theta_W(M_Z) \simeq 0.23$. This means that our model will unify at an energy scale not so far from the electroweak one. The unification scale M_{GUT} is such that

$$\frac{\alpha_3(M_{GUT})}{\alpha_2(M_{GUT})} = \frac{r}{p} = 4 \quad (13.9)$$

together with

$$\frac{\alpha_2(M_{GUT})}{\alpha_1(M_{GUT})} = \frac{36r + 7p + 19q}{5 \cdot 24p} = \frac{69}{40}. \quad (13.10)$$

To find the unification energy scale we consider the renormalization-group evolution of the gauge couplings in leading order as given by

$$\alpha_i(Q) = \frac{1}{\alpha_i(Q')^{-1} + \frac{b_i}{2\pi} \ln\left(\frac{Q}{Q'}\right)}, \quad (13.11)$$

where b_i are the one-loop contributions to the beta function coefficients that are given in general by [113]

$$b_i = \frac{11}{3}C_2(G) - \frac{4\kappa}{3}S_2(F) - \frac{1}{6}S_2(S) \quad (13.12)$$

Here n_F is the number of chiral families, $C_2(G)$ is the quadratic Casimir invariant for the gauge group G and $S_2(F)$ and $S_2(S)$ are the Dynkin indices for the fermion and scalar representations F and S respectively, and κ is $\frac{1}{2}$ for Weyl fermions and 1 for Dirac fermions, see also [114, 112, 115]. For the case at hand

$$b_3 = 11 - \frac{4}{3}n_F, \quad (13.13)$$

$$b_2 = \frac{22}{3} - \frac{4}{3}n_F - \frac{1}{6}N_{SD}, \quad (13.14)$$

$$b_1 = -\frac{4}{3}n_F - \frac{1}{10} \sum_{i=1}^{N_{SR}} d_i q_i^2. \quad (13.15)$$

In b_2 , N_{SD} is the number of real scalar doublets, and in b_1 the sum runs over the scalar representation with $U(1)$ charges q_i of dimensions d_i .

The experimental input values of the gauge couplings are [53]

$$\alpha_1(M_Z) = 0.0169, \quad \alpha_2(M_Z) = 0.0338, \quad \alpha_3(M_Z) = 0.118. \quad (13.16)$$

We can choose the number of light scalar representations, evaluate N_{SD} and the sum in the equations (13.11) to match ratio between the coupling constant at the GUT scale. Of course this choice is not dictated by mass scale cutoff, since we don't know the masses of the scalar predicted by our model. To do this we would define a scalar potential to break the symmetry and give mass to each particle,

as in the SM Higgs mechanism. Unfortunately this task is very difficult also in models much simpler than the one presented here [116]. As an example, this procedure leads to an unification scale $M_{GUT} = 5.0 \cdot 10^3$ GeV, for the choice of a single Higgs doublet plus 24 complex color triplet scalars of hypercharge 1/3. The evolution of the couplings from the weak to the unification scale is shown in Fig. 13.3.

Changing the choice of light scalars adjusts the unification scale, but given the experimental input at low energy and the requirement of unification at a higher scale, we necessarily need many scalars to be light below the unification scale. Increasing the triplet scalar masses (they would probably already have been detected, at least indirectly, if they were at the weak scale) to a few hundred GeV would likewise increase the unification scale to the 6 TeV range. Using extra vectorlike fermions instead of scalars can achieve similar results and with fewer particles, since fermions contribute more strongly to the β functions.

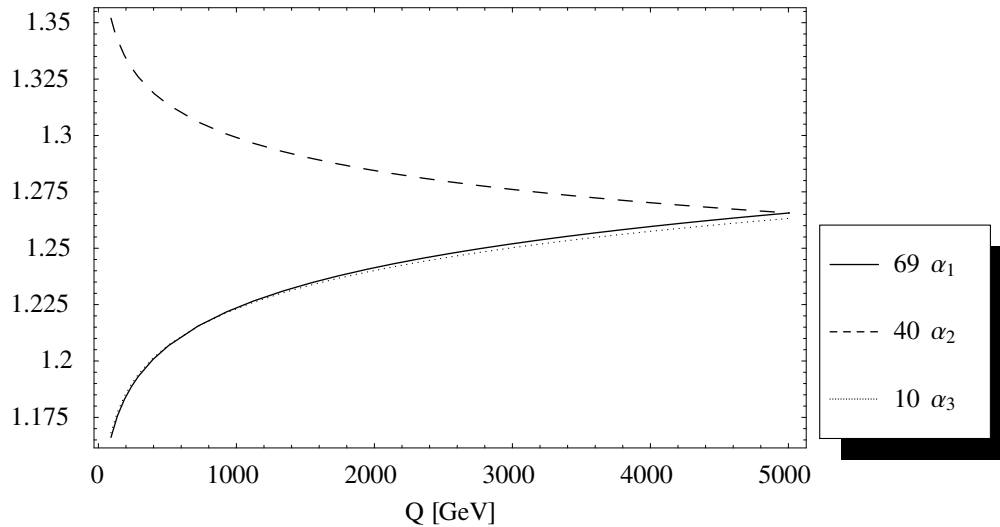


Figure 13.3: Gauge coupling unification in the Modified Pati-Salam model. The curves has been rescaled as $69\alpha_1(Q)$, $40\alpha_2(Q)$ and $10\alpha_3(Q)$ in such a way that their ratio match to one at the unification scale. The plot is for values of Q from M_Z to M_{GUT} .

Chapter 14

Conclusions

We have shown that it is possible to find a non-supersymmetric, “minimal”, Pati-Salam type model based on the *AdS/CFT* orbifold compactifications of type *IIB* string theory on $AdS_5 \otimes S^5/Z_7$. The model is a quiver gauge theory based on the semi-simple group $SU(4)^7$. Since the particles lie on a quiver there are no problem with the naturalness and the model is anomaly free. The path of symmetry breaking that leads to the Standard Model gauge group proceeds through a modified (there are also two $U(1)$ groups) Pati-Salam group. It start with a series of diagonal symmetry breaking that reduce the initial symmetry group to $SU(4)^3$, where we achieve unification. From this level on, giving a VEVs to some cleverly chosed scalars generate, among the other, four $U(1)$ groups. The corresponding charges are renormalized by imposing VEVs to charged singlet scalar representations, in such a way that all the states at the SM level have the correct hypercharge under the remaining $U(1)_Y$ group. The type of fields arising in such a model are constrained by the orbifold group, yet we have shown that there exists the proper scalar content to allow spontaneous symmetry breaking to the Standard Model, as well as provide the usual Higgs sector of the Standard Model. At the unification scale, this model contains bifundamental fermion and scalar representations of the gauge group $SU(4)^7$, where the one loop, and perhaps higher loop β functions vanish, and conformality is partially, or fully restored. To achieve low scale unification, we require scalar content beyond what is found in the Standard Model Higgs sector. Conversely, the existence of such particles may be an indicator of low scale unification. (Similar results hold for extra vectorlike fermions.) The model contains three families of chiral fermions with Standard Model charge assignments, but with no other chiral fermions at low en-

ergy. There are a sufficient number of right handed neutral singlet fermions at intermediate or higher mass to provide neutrino see saw masses. The value of $\sin^2 \theta_W$ at the unification scale depend on how $SU(2)_L$ and $U(1)_Y$ of the SM are embedded in the diagonal subgroups of the initial symmetry group $SU(4)^7$. In our case we found $\sin^2 \theta_W(M_{GUT}) \simeq 0.26$, while the value at the electroweak scale is $\sin^2 \theta_W(M_Z) \simeq 0.23$. The little difference between these values is a strong signal of a “low” unification scale for the model at hand. In fact proton decay is avoided as the model unifies into a modified Pati-Salam model at the intermediate scale $M_{GUT} = 5$ TeV. Generically, the unification is lowered by keeping more scalars light (similar results would hold if we replaced them with vectorlike fermions). Since our model is not supersymmetric, there is no natural LSP dark matter candidate, but one can still expect other options to be available, e.g., axionic dark matter, although we will not explore these possibility here.

Appendix A

Orbifolding

This appendix is devoted to discuss some group theoretical and geometrical aspects of the orbifolds. We will begin with the simplest example, i.e. the one dimensional orbifold. Then we will move to the two dimensional case and finally we will described a six dimensional construction related to the group Z_3 . This last case is especially important as it explain some of the notations introduced in chapter 12 talking about the cyclic group Z_n and its embedding in $SU(4) \sim O(6)$, the isometry of S^5 . A more detailed discussion can be found in [117].

A.1 One dimensional Orbifold

Let \mathbb{R} be the real number line. Define a one-dimensional lattice Λ with lattice spacing $a \in \mathbb{R}$:

$$\Lambda = \{na \mid n \in \mathbb{Z}\} \tag{A.1}$$

where \mathbb{Z} is the set of integers. The elements $l \in \Lambda$ will be referred to as lattice vectors. We construct a *torus* by identifying points on the line with each other if they are related under addition by a lattice vector:

$$x \simeq x + l, \quad x \in \mathbb{R}, \quad l \in \Lambda \tag{A.2}$$

This generates a torus whose fundamental domain can be chosen as $[0, a)$. That is, any other point in \mathbb{R} maps into this domain by the identification made in (A.2); \mathbb{R} is the covering space for the torus. Moreover Eq. (A.2) states that points which are related to each other by a lattice vector translation are equivalent to each other. The discrete group of translations defined by the lattice is referred to as the *lattice*

group and is often also denoted Λ . This group is an invariance or isometry group of \mathbb{R} .

The onedimensional torus is *homeomorphic* (topologically equivalent) to a circle, so while the torus \mathbb{T} is compact the real number line \mathbb{R} is non-compact. We notate this construction

$$\mathbb{T} = \mathbb{R}/\Lambda \quad (\text{A.3})$$

This notations leads to a brief description of the torus construction: we “divide out” or “mod out” the lattice group Λ from the space \mathbb{R} . The lattice group affords an equivalence relation r_Λ (eq. (A.2)), which partitions the real number line into a set of equivalence classes, i.e. into sets of elements which are all equivalent to each other. The set of equivalence classes is called the quotient set or quotient space determined by r_Λ and is denoted by \mathbb{R}/r_Λ or, in shorthand notation, \mathbb{R}/Λ , as in (A.3). Since \mathbb{R} and Λ are groups \mathbb{R}/Λ is a coset space. Each element in the fundamental domain $[0, a)$ is in one-to-one correspondence with an equivalence class contained in \mathbb{R}/Λ . Given $x \in [0, a)$ we can reach (generate) every element in the equivalence class corresponding to x by the action of the lattice group Λ on x .

Now we are ready to study a first example of orbifolding. A *toroidal orbifold* can be constructed from a torus by supplementing (A.2) with other equivalence relations. A twist operator is used to define each equivalence relation. For the toroidal orbifolds considered here, the twist must be an automorphism of the lattice used in constructing the torus. An automorphism α of a lattice Λ is a transformation which maps lattice vectors into lattice vectors:

$$\alpha : l \rightarrow \alpha l \in \Lambda, \quad \forall l \in \Lambda \quad (\text{A.4})$$

Twist operators are most often generators of a discrete rotation group on the compact manifold which is to be “twisted” into an orbifold, typically a torus. But in the simplified one-dimensional case presented here, rotation is not well defined. So we take the twist operator to be the parity operator P :

$$Px = -x, \quad \forall x \in \mathbb{R} \quad (\text{A.5})$$

Using (A.1) it is easy to prove that the parity operation is an automorphism of the lattice, i.e. it satisfies (A.4).

The equivalence relation generated by P is

$$x \simeq Px, \quad \forall x \in \mathbb{R} \tag{A.6}$$

Notice that from the definition (A.5) we have $P^2 = 1$. Thus, P realizes the cyclic group of order two

$$Z_2 = \{1, P\}. \tag{A.7}$$

The group generated by the twist operators is known as the *point group* of the orbifold. So the orbifold described here is the quotient space \mathbb{T}/Z_2 and the *point group* of the orbifold is Z_2 .

We have so far constructed the one-dimensional orbifold in a two step process, imposing the equivalence (A.2) and then equivalence (A.6). In Figure A.1 we

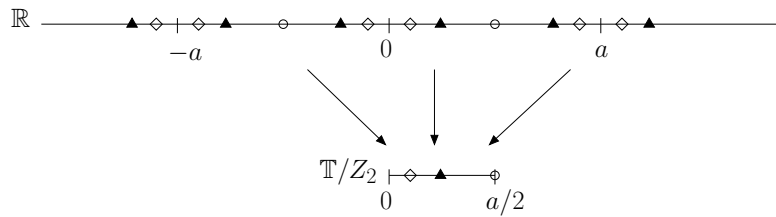


Figure A.1: The orbifold \mathbb{T}/Z_2 and its embedding into the covering space \mathbb{R} . Points marked with the same symbol are equivalent.

illustrate the orbifold. All points marked with the same letter are equivalent. Notice that in the fundamental domain $[0, a)$ of the torus we now have pairs of points which are equivalent, except for the *fixed points* $x = 0$ and $x = a/2$. On the other hand, the fundamental domain of the orbifold is $[0, a/2]$, since every other point in \mathbb{R} may be mapped into this interval.

A.2 Two dimensional Orbifold

As a generalization of the one dimensional orbifold, we consider the two-dimensional real manifold \mathbb{R}^2 and “mod out” by a lattice:

$$\Lambda_2 = \{m^1 e_1 + m^2 e_2 \mid m^1, m^2 \in \mathbb{Z}\} \tag{A.8}$$

where e_1 and e_2 are linearly independent elements of \mathbb{R}^2 . These basis vectors characterize the shape and size of the lattice via

$$\sqrt{e_1 \cdot e_1} = a_1, \quad \sqrt{e_2 \cdot e_2} = a_2, \quad e_1 \cdot e_2 = a_1 a_2 \cos \alpha. \quad (\text{A.9})$$

The torus described by $\mathbb{T}^2 = \mathbb{R}^2/\Lambda$ is obtained by imposing the equivalence relation

$$x \simeq x + l, \quad \forall x \in \mathbb{R}^2, l \in \Lambda_2. \quad (\text{A.10})$$

We again define the twist operator to be the parity operation $Px = -x$ and impose the identification

$$x \simeq Px, \quad \forall x \in \mathbb{T}^2 \quad (\text{A.11})$$

to construct the orbifold \mathbb{T}^2/Z_2 .

We notice that P is equivalent to a rotation by angle π . Thus, the point group is a discrete subgroup of the full rotation group $O(2)$ of the real manifold \mathbb{R}^2 ; this is the usual circumstance in toroidal orbifolds, and we will see this in the six-dimensional Z_3 case considered in the next Section.

It is easy to check that (A.11) is an automorphism of the lattice (A.8). As discussed in the one-dimensional case of Section A.1, this is a necessary condition for the consistency of the orbifold construction.

A.3 Z_3 Orbifold

The six-dimensional Z_3 orbifold may be constructed from a six-dimensional Euclidean space \mathbb{R}^6 . We define basis vectors e_1, \dots, e_6 satisfying

$$e_i^2 = e_{i+1}^2 = 2R_i^2, \quad e_i \cdot e_{i+1} = -1R_i^2, \quad i = 1, 3, 5 \quad (\text{A.12})$$

such that each $x \in \mathbb{R}^6$ can be written as

$$x = \sum_{i=1}^6 x^i e_i, \quad x^i \in \mathbb{R}, \quad \forall i = 1, \dots, 6. \quad (\text{A.13})$$

Notice that $x^i \neq x \cdot e_i$ since the root basis is a skew basis consisting of elements which do not have unit norm. Each of the three pairs $\{e_i, e_{i+1}\}$ ($i = 1, 3, 5$) define a two-dimensional subspace which is referred to below as the “ i th complex plane”. The i th such pair also defines a two-dimensional $SU(3)$ root lattice, obtained from

the set of all linear combinations of the form $n_i e_i + n_{i+1} e_{i+1}$, with $n_i, n_{i+1} \in \mathbb{Z}$. Taking together all six basis vectors e_1, \dots, e_6 , we obtain the $SU(3)^3$ root lattice $\Lambda_{SU(3)^3}$:

$$\Lambda_{SU(3)^3} = \left\{ \sum_{i=1}^6 l^i e_i \mid l^i \in \mathbb{Z} \right\}. \quad (\text{A.14})$$

Notice that the radii R_i and the angles in the scalar products $e_i \cdot e_{i+1}$ of eq. (A.12) are not fixed. These free parameters determine the size and shape of the unit cell of the lattice $\Lambda_{SU(3)^3}$. The lattice group is formed of translations in \mathbb{R}^6 by elements of $\Lambda_{SU(3)^3}$,

$$x \rightarrow x + l, \quad l \in \Lambda_{SU(3)^3}, \quad \forall x \in \mathbb{R}^6. \quad (\text{A.15})$$

Thus we obtain the six-dimensional torus $\mathbb{T}^6 = \mathbb{R}^6 / \Lambda_{SU(3)^3}$. The twist operator α is in this case a simultaneous $2\pi/3$ rotation of each of the three complex planes. Its action on the basis vectors is defined as

$$\alpha \cdot e_i = e_{i+1} \quad \alpha \cdot e_{i+1} = -e_i - e_{i+1}, \quad i = 1, 3, 5, \quad (\text{A.16})$$

so that $\alpha^3 = 1$. Using (A.16) is simple to see that each $x \in \mathbb{R}^6$ transforms according to

$$\alpha \cdot x = \sum_{i=1,3,5} [-x^{i+1} e_i + (x^i - x^{i+1}) e_{i+1}], \quad (\text{A.17})$$

or, in terms of the components by $x \rightarrow \alpha \cdot x = x'$ with

$$x^i \rightarrow (x')^i = -x^{i+1}, \quad x^{i+1} \rightarrow (x')^{i+1} = x^i - x^{i+1}, \quad i = 1, 3, 5. \quad (\text{A.18})$$

Eq. (A.18) leads to a matrix representation of the twist operator:

$$M(\alpha) = \text{diag}[m(\alpha), m(\alpha), m(\alpha)], \quad m(\alpha) = \begin{pmatrix} 0 & -1 \\ 1 & -1 \end{pmatrix}. \quad (\text{A.19})$$

Notice that the difference between the coefficients in (A.16) versus (A.18) is a consequence of the fact that the root basis is a skew basis.

The twist operator α generates the orbifold point group,

$$Z_3 = \{1, \alpha, \alpha^2\} \quad (\text{A.20})$$

and it can be seen from eq. A.16 that the twist operator maps any element of

$\Lambda_{SU(3)^3}$ into $\Lambda_{SU(3)^3}$ (i.e. is an *automorphism*). The orbifold so far construct is denoted \mathbb{T}^6/Z_3 .

A suitable fundamental domain for the orbifold, projected into any one of the three complex planes, is depicted in Figure A.2. Sewing of open boundaries to

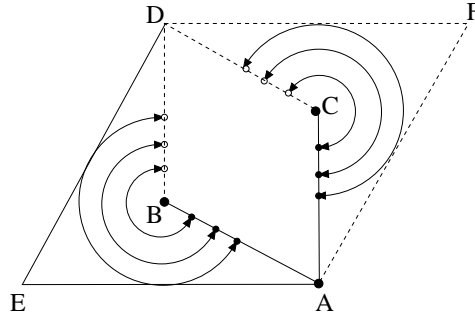


Figure A.2: The parallelogram \overline{BACD} depicts the two-dimensional Z_3 orbifold. We shown how it sits within the $SU(3)$ root torus (the larger parallelogram). We have set $E = 0$, $A = 1$, $D = e^{i\pi/3}$, $F = A + D$, $B = F/3$ and $C = 2F/3$. Open points along the open boundary (dashed) are identified (in the figure, by arrows) with closed points along the closed boundary (solid), forming a three-cornered “pillow”. The fixed points are at A , B and C . We can also view the parallelogram \overline{BACD} as the projection of the six-dimensional Z_3 orbifold into one of the three complex planes. Similarly, the larger parallelogram can be viewed as the projection of the $SU(3)^3$ root torus in one of the three complex planes.

closed boundaries is suggested by the arrows. Whereas the two-dimensional Z_2 orbifold of Section A.2 could be pictured as a four-cornered “pillow”, we now obtain for the Z_3 orbifold a three-cornered “pillow”. Since the orbifold is six-dimensional, we actually have three such pillow spaces associated with the projection of the orbifold into each of the three complex planes.

The interpretation of the figure is more transparent if we introduce a *complex basis*. This is defined in terms of the components x^i appearing in (A.13) according to

$$z^i \equiv x^i + e^{2\pi i/3} x^{i+1}, \quad \bar{z}^i \equiv x^i + e^{-2\pi i/3} x^{i+1}, \quad i = 1, 3, 5 \quad (\text{A.21})$$

This definition is motivated by supposing that in the i th complex plane e_i lies along the real axis while from (A.12) we see that e_{i+1} lies at 120 degrees ($2\pi/3$ rad) counterclockwise from the real axis. This picture is of course the origin of the usage of “complex plane” for each of the three pairs $\{e_i, e_{i+1}\}$ ($i = 1, 3, 5$).

Whithout enter in the details, it is possible to show that the twist operator acts

on z^i as a pure phase rotation:

$$z^i \xrightarrow{\alpha} e^{2\pi i/3} z^i, \quad \bar{z}^i \xrightarrow{\alpha} e^{-2\pi i/3} \bar{z}^i, \quad i = 1, 3, 5. \quad (\text{A.22})$$

In the complex basis a matrix realization of the twist operator is given by

$$M_c(\alpha) = \text{diag}(e^{2\pi i/3}, e^{2\pi i/3}, e^{2\pi i/3}) \quad (\text{A.23})$$

when acting on (z^1, z^2, z^3) and by the complex conjugate $[M_c(\alpha)]^*$ when acting on vectors in the conjugate representation space $(\bar{z}^1, \bar{z}^2, \bar{z}^3)$. It is this decomposition into irreducible representations, i.e. no mixing between z^i and \bar{z}^i , in contrast to the mixing between x^i and x^{i+1} in (A.19), which eases the use of complex basis. Moreover the (A.23) makes clear the Z_3 nature of the point group: it is the generator of the center of $SU(3)$ in the fundamental representation. This is the reason why we called the lattice in (A.14) $\Lambda_{SU(3)^3}$.

In an abuse of notation we shall often write $\alpha = e^{2\pi i/3}$, so that (A.23) becomes

$$M_c(\alpha) = \text{diag}(\alpha, \alpha, \alpha). \quad (\text{A.24})$$

Appendix B

Chiral Z_n models

In this appendix we partially review the classification of Kephart and Pas [107, 108], presenting the supersymmetric and nonsupersymmetric chiral models that comes from an abelian orbifolds of AdS/CFT.

We begin to notice that if the orbifolding group is $\Gamma = Z_n$ the initial $\mathcal{N} = 0$ orbifold model (before any symmetry breaking) is completely fixed (recall we always are taking N , the “color number”, fixed) by the choice of n and the embedding $\mathbf{4} = (\alpha^i, \alpha^j, \alpha^k, \alpha^l)$, so we define these models by M_{ijkl}^n . The conjugate models $M_{n-i, n-j, n-k, n-l}^n$ contain the same information, so we need not study them separately.

In the case of $\mathcal{N} = 1$ model, to preserve the supersymmetry we must keep exactly one invariant spinor under the joint action of the finite symmetry Γ and the quiver gauge group, i.e. $SU(N)^n$, with $n = o(\Gamma)$, if Γ is abelian. This implies that one component of the $\mathbf{4}$ of $SU(4)$ is the trivial singlet representation of Γ , so we can write the embedding $\mathbf{4} = (\mathbf{1}, \alpha^i, \alpha^j, \alpha^k)$ and define the models as M_{ijk}^n .

B.1 $\mathcal{N} = 1$ models

To tabulate the possible models for each value of n , we first show that a proper embedding [105] (i.e., $\mathbf{6} = \bar{\mathbf{6}}$) for $\mathbf{4} = (\mathbf{1}, \alpha^i, \alpha^j, \alpha^k)$ results when $i + j + k = n$. To do this we use the fact that the conjugate model has $i \rightarrow i' = n - i, j \rightarrow j' = n - j$ and $k \rightarrow k' = n - k$. Summing we find $i' + j' + k' = 3n - (i + j + k) = 2n$. But from $\mathbf{6} = (\mathbf{4} \otimes \mathbf{4})_{antisym}$ we find $\mathbf{6} = (\alpha^i, \alpha^j, \alpha^k, \alpha^{j+k}, \alpha^{i+k}, \alpha^{i+j})$, but $i + j = n - k = k'$. Likewise $i + k = j'$ and $j + k = i'$ so $\mathbf{6} = (\alpha^i, \alpha^j, \alpha^k, \alpha^{i'}, \alpha^{j'}, \alpha^{k'})$ and this is $\bar{\mathbf{6}}$ up to an automorphism which is sufficient to provide a proper embedding (or to

provide real scalars in the non-SUSY models).

Models with $i + j + k = n$ are called *partition models* and are always chiral, with *total chirality* (number of chiral states) $\chi = 3N^2n$ except in the case where n is even and one of i, j , or k is equal to $n/2$, where $\chi = 2N^2n$.¹ This immediately gives us a lower bound on the number of chiral models at fixed n : it is the number of partitions of n into three non-negative integers.

There is another class of models with $i' = k, j' = 2j$ and total chirality $\chi = N^2n$ (for example M_{336}^9). Moreover there are a few other sporadically occurring cases like M_{124}^6 , which typically have reduced total chirality, $\chi < 3N^2n$. Such *nonpartition* - i.e. neither partition nor double partition - models can fail other more subtle constraints on consistent embedding [105], but they are also important because they have vanishing anomaly coefficients and vanishing one loop β functions, so are still of phenomenological interest from the gauge theory model building perspective.

B.2 $\mathcal{N} = 0$ models

To list all the possible nonsupersymmetric chiral model we can proceed as in the previous section, with the only difference that now a proper embedding for $\mathbf{4} = (\alpha^i, \alpha^j, \alpha^k, \alpha^l)$ is possible only if $i + j + k + l = n$. The resulting models are showed in Table B.1.

Notice that the first allowed $\Gamma = Z_2$ and Z_3 orbifolds have only real representations and therefore will not yield chiral models. So the simplest example of a nonSUSY chiral model is for $\Gamma = Z_4$ with the choice $\mathbf{4} = (\alpha, \alpha, \alpha, \alpha)$, where $\alpha = \exp(\pi i/2)$. In this model we have $\mathbf{6} = (\alpha^2, \alpha^2, \alpha^2, \alpha^2, \alpha^2, \alpha^2)$. With $N = 4$ this yields an $SU(4)^4$ model with the fermion content

$$4[(4\bar{4}11) + (14\bar{4}1) + (114\bar{4}) + (\bar{4}114)]$$

and scalar content

$$6[(41\bar{4}1) + (141\bar{4}) + (\bar{4}141) + (1\bar{4}14)]$$

as can be read off from the associate quiver diagrams showed in Fig. B.1. In fact each node correspond to one $SU(4)$ group, so we have four nodes. A

¹No more than one of i, j , and k can be $n/2$ since they sum to n and are all positive.

n	4	χ/N^2	comments
4	$(\alpha, \alpha, \alpha, \alpha)$	16	$i + j + k + l = 4$; 1 model ($i = j = k = l$)
4	$(\alpha, \alpha, \alpha, \alpha^3)^*$	8	nonpartition model
5	$(\alpha^i, \alpha^j, \alpha^k, \alpha^l)$	20	$i + j + k + l = 5$; 1 part. model
6	$(\alpha^i, \alpha^j, \alpha^k, \alpha^l)$	≤ 24	2 part. models
6	$(\alpha, \alpha, \alpha^3, \alpha^5)^*$	6	nonpartition model
6	$(\alpha, \alpha^2, \alpha^3, \alpha^5)^*$	6	nonpartition model
6	$(\alpha, \alpha^3, \alpha^4, \alpha^4)$	24	$i + j + k + l = 12$ (double partition model)
7	$(\alpha^i, \alpha^j, \alpha^k, \alpha^l)$	28	3 part. models
8	$(\alpha^i, \alpha^j, \alpha^k, \alpha^l)$	≤ 32	5 part. models
8	$(\alpha, \alpha^2, \alpha^3, \alpha^6)^*$	16	nonpartition model
8	$(\alpha^2, \alpha^2, \alpha^2, \alpha^6)^*$	16	analog of Z_4 ($\alpha, \alpha, \alpha, \alpha^3$) model
8	$(\alpha, \alpha^4, \alpha^5, \alpha^6)$	32	double part. model
9	$(\alpha^i, \alpha^j, \alpha^k, \alpha^l)$	36	3 part. models
9	$(\alpha, \alpha^3, \alpha^4, \alpha^7)^*$	36	nonpartition model
9	$(\alpha, \alpha^4, \alpha^6, \alpha^7)^*$	36	double part. model

Table B.1: Chiral nonsupersymmetric Z_n orbifold models with $n \leq 9$. The nonpartition models are marked with an asterick (*).

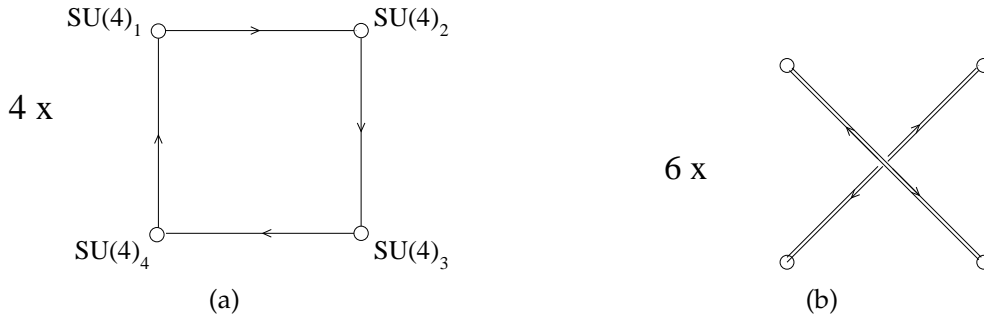


Figure B.1: Fermion (a) and scalar (b) quiver diagram for the model M_{1111}^4 .

line direct away from one node correspond to a fundamental representation for the corresponding group and to an antifundamental representation for the group related to the node where the line ended (i.e. directed toward this node). For example the arrow from the $SU(4)_1$ node to the $SU(4)_2$ node in the fermion quiver diagram of Fig. B.1(a) led to the $(4_1 \bar{4}_2 1_3 1_4)$ representation of the quiver gauge group $SU(4)_1 \otimes SU(4)_2 \otimes SU(4)_3 \otimes SU(4)_4$. As all the $SU(4)$ are the same, we can drop the underscript and, applying the same rules to the other arrows in

Fig B.1, we arrive at the fermion and scalar content presented above. Notice that to draw the quiver diagrams we have used the rules given in chapter 12 with $(a_1, a_2, a_3) = (2, 2, -2)$, as result solving the system (12.2) with $A_\mu = (1, 1, 1, 1)$.

Bibliography

- [1] S. L. Glashow and M. Gell-Mann, *Annals Phys.* **15** (1961) 437.
- [2] S. Weinberg, *Phys. Rev.* **28**, 4482 (1973); S. Glashow, *Nucl. Phys.* **22**, 579 (1961); J. C. Ward and A. Salam, *Phys. Lett.* **13**, 168 (1964); S. Weinberg, *Phys. Rev. Lett.* **19**, 1264 (1967); S. Weinberg, *Rev. Mod. Phys.* **52**, 515 (1980); A. Salam, *Rev. Mod. Phys.* **52**, 525 (1980); S. L. Glashow, *Rev. Mod. Phys.* **52**, 539 (1980).
- [3] P. Langacker, *Phys. Rept.* **72**, 185 (1981).
- [4] K. G. Wilson, *Phys. Rev. D* **3** (1971) 1818.
- [5] P. A. M. Dirac, *Nature (London)*, **139**, 323 (1937); *Proc. Roy. Soc. London A***165**, 198 (1938).
- [6] P. A. M. Dirac, *Proc. Roy. Soc. London A***338**, 439 (1974); *Proc. Roy. Soc. London A***365**, 19 (1979).
- [7] T. R. Taylor and G. Veneziano, *Phys. Lett.* **B 213**, 450 (1988).
- [8] J. Wess and B. Zumino, *Nucl. Phys. B* **70**, 39 (1974).
- [9] S. R. Coleman and J. Mandula, *Phys. Rev.* **159**, 1251 (1967).
- [10] F. Gliozzi, J. Scherk and D. I. Olive, *Phys. Lett. B* **65** (1976) 282; *Nucl. Phys. B* **122** (1977) 253.
- [11] J. M. Maldacena, *Adv. Theor. Math. Phys.* **2**, 231 (1998) [*Int. J. Theor. Phys.* **38**, 1113 (1999)] [arXiv:hep-th/9711200].
- [12] S. Kachru and E. Silverstein, *Phys. Rev. Lett.* **80**, 4855 (1998) [arXiv:hep-th/9802183].

-
- [13] A. E. Lawrence, N. Nekrasov and C. Vafa, Nucl. Phys. B **533**, 199 (1998) [arXiv:hep-th/9803015].
- [14] P. H. Frampton, Phys. Rev. D **60** (1999) 041901 [arXiv:hep-th/9812117].
- [15] P. H. Frampton and T. W. Kephart, Phys. Rept. **454**, 203 (2008) arXiv:0706.4259 [hep-ph].
- [16] R. Casadio, P. L. Iafelice and G. P. Vacca, Nucl. Phys. B **783**, 1 (2007) [arXiv:hep-th/0702175].
- [17] H. Georgi and S. L. Glashow, Phys. Rev. Lett. **28** (1972) 1494.
- [18] J. C. Pati and A. Salam, Phys. Rev. D **8** (1973) 1240.
- [19] J. C. Pati and A. Salam, Phys. Rev. D **10** (1974) 275.
- [20] E. A. Kuraev, L. N. Lipatov and V. S. Fadin, Sov. JETP **44** (1976) 443; *ibid.* **45** (1977) 199; Ya. Ya. Balitskii and L.N. Lipatov, Sov. J. Nucl. Phys. **28**, (1978) 822.
- [21] L.N. Lipatov, *Phys. Lett.* **B309** (1993) 394
- [22] N. Beisert, Phys. Rept. **405** (2005) 1 [arXiv:hep-th/0407277].
- [23] J. Bartels, *Nucl. Phys.* **B175** (1980) 365; J. Kwiecinski and M. Praszalowicz, *Phys. Lett.* **B94** (1980) 413; T. Jaroszewicz, *Acta Phys. Polon.* **B11** (1980) 965.
- [24] G. P. Vacca and P. L. Iafelice, arXiv:0710.0352 [hep-th].
- [25] P. L. Iafelice and G. P. Vacca, Eur. Phys. J. C **52**, 581 (2007) [arXiv:0709.0655 [hep-th]].
- [26] J. B. Dent, P. L. Iafelice and T. W. Kephart, arXiv:0802.0180 [hep-ph].
- [27] J.-P. Uzan, Rev. Mod. Phys. **75**, 403 (2003).
- [28] J. Kujat, R. J. Scherrer, Phys. Rev. D **62**, 023510 (2000).
- [29] S. Hannestad, Phys. Rev. D **60**, 023515 (1999).
- [30] M. Kaplinghat, R. J. Scherrer e M. S. Turner, Phys. Rev. D **60**, 023516 (1999).

- [31] E. Witten, *Phys. Lett.* **B 149**, 351 (1984).
- [32] G. Passarino, "Are constants constant?," [hep-ph/0108254].
- [33] V. M. Mostepanenko, V. M. Frolov and V. A. Shelyuto, *Yad. Fiz.* **37** (1983) 1261; A. D. Dolgov and D. P. Kirilova, *Sov. J. Nucl. Phys.* **51** (1990) 172 [*Yad. Fiz.* **51** (1990) 273].
- [34] F. Cerutti, in *Proc. of the 16th Rencontres de Physique de la Vallee d'Aoste: Results and Perspectives in Particle Physics*, La Thuile, Valle d'Aosta, Italia, 3 – 9 Marzo 2002; CERN - ALEPH - PUB - 2002 - 003. [hep-ex/0205095];
U. Baur et al., *Summary Report of the Precision Measurement Working Group at Snowmass 2001* [hep-ph/0202001];
Yu. F. Pirogov, O. V. Zenin, *Eur. Phys. J.* **C10**, 629 (1999);
U. Mahanta, "New physics, precision electroweak data and an upper bound on Higgs mass," [hep-ph/0009096].
- [35] J. Baacke, K. Heitmann and C. Patzold, *Phys. Rev. D* **58** (1998) 125013.
- [36] V. M. Mostepanenko, A. A. Grib, V. M. Mamayev, *Vacuum Quantum Effects in Strong Fields*, Friedmann Laboratory Publishing, San Pietroburgo (1994).
- [37] L. Kofman, A. Linde and A. A. Starobinsky, *Phys. Rev. Lett.* **73**, 3195 (1994).
- [38] D. Boyanovsky, H. J. de Vega, R. Holman, D. S. Lee and A. Singh, *Phys. Rev. D* **51**, 4419 (1995).
- [39] L. Kofman, A. Linde and A. A. Starobinsky, *Phys. Rev. D* **56**, 3258 (1997).
- [40] J. Garcia-Bellido, S. Mollerach and E. Roulet, *JHEP* **0002** (2000) 034;
P. B. Greene, L. Kofman, A. Linde and A. A. Starobinsky, *Phys. Rev. D* **56**, 6175 (1997); P. B. Greene and L. Kofman, *Phys. Lett. B* **448** (1999) 6; D. Boyanovsky, H. J. de Vega, R. Holman and J. F. J. Salgado, *Phys. Rev. D* **54** (1996) 7570.
- [41] D. Boyanovsky, M. D'Attanasio, H. J. de Vega, R. Holman and D. S. Lee, *Phys. Rev. D* **52** (1995) 6805.
- [42] D. Bardin and C. Passarino, *The Standard Model in the making: Precision study of the electroweak interaction*, Oxford UK, Clarendon (1999).

- [43] J. A. Espichan Carrillo, A. J. Maia and V. M. Mostepanenko, *Int. J. Mod. Phys. A* **15** (2000) 2645.
- [44] I. S. Gradshteyn, I. H. Ryzhik, *Table of Integrals, Series and Products*, Academic Press, New York (1980). E. T. Whittaker, G. N. Watson, *A course of modern analysis*, Cambridge Univ. Press (1978).
- [45] R. Erdelyi et al. , *Higher Transcendental Functions vol. 2*, Bateman Manuscript Project, McGraw–Hill (1953);
H. Abramowitz, I. Stegun, *Handbook of mathematical functions*, Dover (1970).
- [46] V. M. Mostepanenko, V. M. Frolov, *Sov. J. Nucl. Phys.* **19**, 451 (1974).
- [47] N. N. Bogoliubov, *Lectures on Quantum Statistics*, Kiev: Radjanska Shkola (1949).
- [48] A. M. Perelomov, *Theor. and Math. Phys.* **16**, 852 (1973);
A. M. Perelomov, *Theor. and Math. Phys.* **19**, 368 (1974).
- [49] V. S. Popov, M. S. Marinov, *Sov. J. Nucl. Phys.* **16**, 449 (1973).
- [50] P. B. Greene, L. Kofman, *Phys. Rev. D* **62**, 123512 (2000) (hep-ph/0003018).
- [51] M. Peloso and L. Sorbo, *JHEP* **5**, 16 (2000).
- [52] C. M. Bender, S. A. Orszag, *Advanced Mathematical Methods for Scientist and Engineer*, Mc-Graw Hill (1978).
- [53] K. Hagiwara et al. (Particle Data Group), *Phys. Rev. D* **66**, 010001 (2002) [URL: <http://pdg.lbl.gov>].
- [54] G. F. Giudice, A. Riotto, I. Tkachev and M. Peloso, *JHEP* **8**, 14 (1999) and references therein.
- [55] G. 't Hooft, *Nucl. Phys. B* **72** (1974) 461.
- [56] L. N. Lipatov, *Sov. Phys. JETP* **63**, 904 (1986) [*Zh. Eksp. Teor. Fiz.* **90**, 1536 (1986)].
- [57] J. Bartels, L. N. Lipatov and G. P. Vacca, *Nucl. Phys. B* **706** (2005) 391 [arXiv:hep-ph/0404110];
J. Bartels, L. N. Lipatov, M. Salvadore and G. P. Vacca, *Nucl. Phys. B* **726** (2005) 53 [arXiv:hep-ph/0506235].

- [58] L.N. Lipatov, *Pomeron in quantum chromodynamics*, in “Perturbative QCD”, pp. 411-489, ed. A. H. Mueller, World Scientific, Singapore, 1989; Phys. Rep. **286** (1997) 131.
- [59] R.A. Janik and J. Wosiek, Phys. Rev. Lett. **82** (1999) 1092.
- [60] J. Bartels, L. N. Lipatov and G. P. Vacca, Phys. Lett. B **477**, 178 (2000) [arXiv:hep-ph/9912423].
- [61] L. Łukaszuk and B. Nicolescu, Nuovo Cimento Lett. **8** (1973) 405.
- [62] J. Bartels, M. A. Braun, D. Colferai and G. P. Vacca, Eur. Phys. J. C **20**, 323 (2001) [arXiv:hep-ph/0102221].
- [63] L. N. Lipatov, arXiv:hep-th/9311037.
- [64] L. N. Lipatov, JETP Lett. **59** (1994) 596 [Pisma Zh. Eksp. Teor. Fiz. **59** (1994) 571].
- [65] L. D. Faddeev and G. P. Korchemsky, Phys. Lett. B **342**, 311 (1995) [arXiv:hep-th/9404173].
- [66] S. E. Derkachov, G. P. Korchemsky and A. N. Manashov, Nucl. Phys. B **617**, 375 (2001) [arXiv:hep-th/0107193].
- [67] H. J. De Vega and L. N. Lipatov, Phys. Rev. D **64**, 114019 (2001) [arXiv:hep-ph/0107225].
- [68] S. E. Derkachov, G. P. Korchemsky, J. Kotanski and A. N. Manashov, Nucl. Phys. B **645**, 237 (2002) [arXiv:hep-th/0204124].
- [69] H. J. de Vega and L. N. Lipatov, Phys. Rev. D **66**, 074013 (2002) [arXiv:hep-ph/0204245].
- [70] G. P. Vacca, Phys. Lett. B **489**, 337 (2000) [arXiv:hep-ph/0007067].
- [71] J. Kotanski, arXiv:hep-th/0511279.
- [72] J. Bartels, Z. Phys. C **60** (1993) 471.
- [73] J. Bartels and M. Wusthoff, Z. Phys. C **66** (1995) 157.

- [74] M. A. Braun and G. P. Vacca, *Eur. Phys. J. C* **6** (1999) 147 [arXiv:hep-ph/9711486];
G. P. Vacca, arXiv:hep-ph/9803283.
- [75] L. D. Faddeev, Les Houches 1995, "Relativistic gravitation and gravitational radiation" pp. 149-219, arXiv:hep-th/9605187.
- [76] M. Karbach and G. Müller, *Computer in Physics* **11** (1997) 36, arXiv:cond-mat/9809162.
- [77] C. Rebbi and R. Slansky, *Rev. Mod. Phys.* **42** (1970) 68.
- [78] P. Cvitanovic, "Group Theory: Lie's, Tracks and Exceptional Groups", Web Book, <http://www.nbi.dk/GroupTheory/>.
- [79] N. N. Nikolaev, W. Schafer and B. G. Zakharov, *Phys. Rev. D* **72** (2005) 114018 [arXiv:hep-ph/0508310].
- [80] Yu. L. Dokshitzer and G. Marchesini, *JHEP* **0601** (2006) 007 [arXiv:hep-ph/0509078].
- [81] A. Kovner and M. Lublinsky, *JHEP* **0702** (2007) 058 [arXiv:hep-ph/0512316].
- [82] R. L. Jaffe, *Phys. Rev. D* **15** (1977) 281.
- [83] C. Itzykson and M. Nauenberg, *Rev. Mod. Phys.* **38** (1966) 95.
- [84] M. Greiter and S. Rachel, *Phys. Rev. B* **75**, (2007) 184441.
- [85] M. R. Douglas and G. W. Moore, arXiv:hep-th/9603167.
- [86] T. Blazek, S. F. King and J. K. Parry, *JHEP* **0305** (2003) 016 [arXiv:hep-ph/0303192].
- [87] S.L. Glashow, in *Proceedings of the Fifth Workshop on Grand Unification*, Editors: K.Kang, H. Fried and P.H. Frampton, World Scientific (1984). pages 88-94.
- [88] S. Mandelstam, *Nucl. Phys. B* **213**, 149 (1983).
- [89] Z. Kakushadze, *Phys. Lett. B* **491** (2000) 317 [arXiv:hep-th/0008041].
- [90] L. J. Dixon, J. A. Harvey, C. Vafa and E. Witten, *Nucl. Phys. B* **274** (1986) 285.

-
- [91] L. J. Dixon, J. A. Harvey, C. Vafa and E. Witten, Nucl. Phys. B **261** (1985) 678.
- [92] Z. Kakushadze and S. H. H. Tye, Phys. Lett. B **392** (1997) 335 [arXiv:hep-th/9609027].
- [93] A. M. Uranga, JHEP **9901** (1999) 022 [arXiv:hep-th/9811004].
- [94] K. Oh and R. Tatar, JHEP **9910** (1999) 031 [arXiv:hep-th/9906012].
- [95] I. R. Klebanov and M. J. Strassler, JHEP **0008** (2000) 052 [arXiv:hep-th/0007191].
- [96] A. Hebecker and M. Ratz, Nucl. Phys. B **670** (2003) 3 [arXiv:hep-ph/0306049].
- [97] S. Benvenuti and A. Hanany, JHEP **0508** (2005) 024 [arXiv:hep-th/0502043].
- [98] Z. Kakushadze, Nucl. Phys. B **544** (1999) 265 [arXiv:hep-th/9808048].
- [99] Z. Kakushadze, Phys. Rev. D **59** (1999) 045007 [arXiv:hep-th/9806091].
- [100] A. Fayyazuddin and M. Spalinski, Nucl. Phys. B **535** (1998) 219 [arXiv:hep-th/9805096].
- [101] Z. Kakushadze, Phys. Rev. D **58** (1998) 106003 [arXiv:hep-th/9804184].
- [102] Z. Kakushadze, Nucl. Phys. B **529** (1998) 157 [arXiv:hep-th/9803214].
- [103] Z. Kakushadze, JHEP **0110** (2001) 031 [arXiv:hep-th/0109054].
- [104] K. S. Babu, T. W. Kephart and H. Pas, arXiv:0709.0765 [hep-ph].
- [105] P. H. Frampton and T. W. Kephart, Int. J. Mod. Phys. A **19** (2004) 593 [arXiv:hep-th/0306207].
- [106] P. H. Frampton, Phys. Rev. D **60**, 121901 (1999) [arXiv:hep-th/9907051].
- [107] T. W. Kephart and H. Pas, Phys. Lett. B **522**, 315 (2001) [arXiv:hep-ph/0109111].
- [108] T. W. Kephart and H. Pas, Phys. Rev. D **70**, 086009 (2004) [arXiv:hep-ph/0402228].

- [109] J. B. Dent and T. W. Kephart, arXiv:0705.1995 [hep-ph].
- [110] T. W. Kephart and Q. Shafi, Phys. Lett. B **520**, 313 (2001) [arXiv:hep-ph/0105237].
- [111] T. W. Kephart, C. A. Lee and Q. Shafi, JHEP **0701**, 088 (2007) [arXiv:hep-ph/0602055].
- [112] R. Slansky, Phys. Rept. **79**, 1 (1981).
- [113] M. E. Machacek and M. T. Vaughn, Nucl. Phys. B **222**, 83 (1983).
- [114] T. P. Cheng, E. Eichten and L. F. Li,
- [115] P. H. Frampton, R. N. Mohapatra and S. Suh, Phys. Lett. B **520** (2001) 331 [arXiv:hep-ph/0104211].
- [116] J. B. Dent, P. L. Iafelice and T. W. Kephart, In preparation.
- [117] J. T. Giedt, arXiv:hep-ph/0204315.